Università degli Studi di Padova

Dipartimento di Ingegneria Industriale

CORSO DI LAUREA MAGISTRALE IN INGEGNERIA ENERGETICA

Tesi di Laurea Magistrale in Ingegneria Energetica

Application of a model for assessing the infection risk from COVID-19 in indoor environment

Relatore
Prof. Michele De Carli
Correlatore
Prof. Angelo Zarrella

Laureando
Giacomo Tognon

Academic Year 2020-2021

Abstract

Nowadays, one of the most important issues worldwide concerns the COVID-19 pandemic, caused by the spread of the new virus called SARS-CoV-2. The scientific research is making an effort to acquire more knowledge on the transmission modalities of this virus and provide effective solutions to mitigate the infection rate.

In this thesis work, the topic of airborne transmission of SARS-CoV-2 in indoor environment is taken on and a model is presented for the assessment of infection risk to which a susceptible subject is submitted. It was developed starting from an accurate review of the existent risk models proposed by scientific literature. This model is built coupling a zonal ventilation model with infection risk calculation. The former enables the definition of the air movements within the indoor space. The latter applies a risk equation derived from the well-known Wells-Riley model and based on a hypothetical dose unit of pathogens named "quantum". The objective is investigating the importance of relative position of susceptible individuals and infected source on infection probability, as well as the influence of other parameters, such as ventilation rate (*ACH*), room volume, use of masks.

The model was firstly applied to a typical office room, and then, to a fourfold volume room. For both case-studies, the outdoor air is supplied and distributed through a mixing ventilation system. A four-cells discretization grid was adopted, each cell constituting a well-mixed zone. The simulation results show that infection probability is almost uniform within the spaces, suggesting that increasing the number of cells could be suitable to describe the spatial variation of risk. Concerning ventilation rates and volume, higher values of both parameters increase the dilution of infectious material, lowering the overall risk. Finally, wearing protective devices is strongly recommended to mitigate airborne transmission and FFP2 respirators proved to be better than surgical masks.

Future developments consist of validation of the results and model improvements in order to make it applicable to various real cases. In this way, it will be possible carrying out risk assessment analyses for different ventilation concepts and for more voluminous spaces.

Table of contents

Figure Index

Table Index

Introduction

Epidemics have always been one of the most important issues the world has faced in history and the ongoing COVID-19 pandemic, a respiratory disease caused by a new type of coronavirus, is generating a dramatic situation globally. The difficulty in containing the infection cases lies in the high transmissibility of the virus and the potential lack of symptoms by infected people. These aspects place a problem for national governments regarding the organisation of the public life, which became deeply different compared to that communities were used to.

There is still much discussion on the possibility that SARS-CoV-2 may spread and cause infection though the air. Given the shortage of scientific proofs concerning that point, the maximum caution must be maintained. The airborne transmission of coronavirus becomes relevant in the case of indoor environments. Therefore, it is necessary to quantify the airborne infection risk within enclosed space and investigate how adequate control measures could reduce it.

In this thesis, a mathematical model for the assessment of the airborne transmission risk is developed and presented. The objective of the model is quantifying the infection risk for specific case-studies under different boundary conditions and examining the importance of some influential parameters, especially the relative position of susceptible and infected people, ventilation rate, ventilation plant configuration and terminals layout, room volume, and use of personal protective equipment. The work is organised into four chapters.

Chapter 1 deals with the description of the framework related to the COVID-19 international issue. The transmission routes of typical respiratory diseases are illustrated highlighting the main differences. Particular attention is paid to the airborne infection cycle and the description of its phases is provided in detail. Furthermore, the existent countermeasures to mitigate the infection rate are illustrated.

Chapter 2 explains how it can be mathematically modelled the airborne infection risk from common respiratory diseases in enclosed environments. A systematic review of the scientific literature has been carried out to understand how existent risk models were built and applied. The simplest risk formulations derived from the well-known Wells-Riley equation and the more complex dose-response models are reported. The former are based on the concept of infectious “quantum”, whose definition is specified later on. Moreover, it is underlined the importance of experimental tests and CFD modelling in determining the dispersion of pathogens in the indoor air.

In Chapter 3, an infection risk model is proposed. It is based on the idea of dividing the analysed geometrical domain into different zones. Through a ventilation zonal model (POMA), the interzonal flowrates can be calculated which drive the spread of infectious material within the room volume. In this way, the spatial variation of infection risk can be defined and the importance of different positions for susceptible and infected subjects can

be investigated. In the chapter, the construction of the model and the coupling of the zonal part with the infection risk calculation are discussed and shown. Zonal model basis concepts are described accurately, as well as adopted simplification and assumptions made in the modelling approach. At the end of the section, the explanation of how to insert the use of masks is provided. The model has been developed as a MATLAB a code.

Chapter 4 shows the applications of the model for two case-studies. The first one regards a typical single office room, whereas the second one is an open space office with a fourfold volume compared to the previous case. The main results coming from the simulations are reported, and the importance of different parameters affecting the infection risk level is discussed. As to this last aspect, particular attention is given to ventilation rate, room volume, masks properties and relative positions of individuals and ventilation plant terminals.

Finally, the main limitations of the developed model are listed, and some future improvements are proposed in order to broaden its feasibility to more complicated real case-studies. In fact, the idea is to implement the model for evaluation of airborne infection risk within very voluminous indoor environments.

Chapter 1

Covid-19: an international issue

Nowadays, the entire world must cope with the new COVID-19 pandemic, a respiratory infection caused by the SARS-CoV-2[1] virus, whose existence was first reported to the WHO[2] Country Office in China on 31st December 2019 [1]. Because of the international traffic concerning the global markets and tourism, this virus has rapidly spread all over the world at the beginning of 2020.

Governments rapidly took adequate countermeasures to contain the infections. The administrative institutions provided behavioural rules to be applied in the everyday life by people, through guidelines and ordinances. However, these procedures are continuously updated, because the scientific community still has a weak knowledge about several aspects of this novel disease. The more we learn about COVID-19 features, the more effective will be the applied control measures by the governmental regulations.

One of the most important aspects is understanding the transmission routes of the SARS-CoV-2. If the infection pathways are clear, then the correct strategies could be implemented to target the specific transmission mode. This is an international issue, and the scientific research is employing all possible resources to give us answers on how to mitigate the spread of infections.

In this chapter an overview of the problem is provided. It is focused on a review of the transmission routes of respiratory diseases, with particular attention to COVID-19. Moreover, the main control measures adopted worldwide will be briefly discussed.

1.1 The transmission routes

Respiratory diseases spread among humans when a susceptible person comes in contact with infectious secretions released by an infected person. In fact, mucous or saliva secretions can carry pathogen material that could transmit the infection. Susceptible subjects are those that cannot count on any sort of protection against the pathogen of interest (i.e., people without genetic immunity and not vaccinated).

Nowadays, it is considered that both viral and bacterial respiratory diseases transmission could occur through 3 routes [1]–[4]:

1. Contact route
2. Large droplets route
3. Airborne route

---

[1] Severe Acute Respiratory Syndrome Coronavirus 2

[2] World Health Organization

Whatever the pathway, the transport vectors for the pathogens are saliva, mucous particles or any type of organic fluid that is expelled from the infected subject in the form of infectious droplets. Viral or bacterial microorganisms concentration in the human respiratory tract strongly depends on the course of the disease (i.e., people in the acute phase of illness will have higher viral/bacterial load). For viral respiratory diseases, the viral load is expressed in *viral RNA copies/ml*. Thanks to the advancements in molecular diagnostics, the viral load can be determined using nasal, nasopharyngeal, mouth, and throat swabs: a mucous sample is extracted from the upper respiratory tract (URT), which is an easily accessible site, and then it is analysed through RT-PCR[3] molecular method [5]. These biological instruments proved to be effective in the detection of positive subjects during the current COVID-19 pandemic. In Italy, for example, that has been one of the first countries where the virus was detected other than China, the public bodies make extensive use of swabs as a screening procedure for the disease.

The viral load of an ill person represents the pathogenic material that is available to be expelled in the surrounding environment and, potentially, towards a sensible subject. The subsequent infection derives from one of the 3 above-mentioned pathways. Figure 1.1 gives a representation of these infective routes [6].

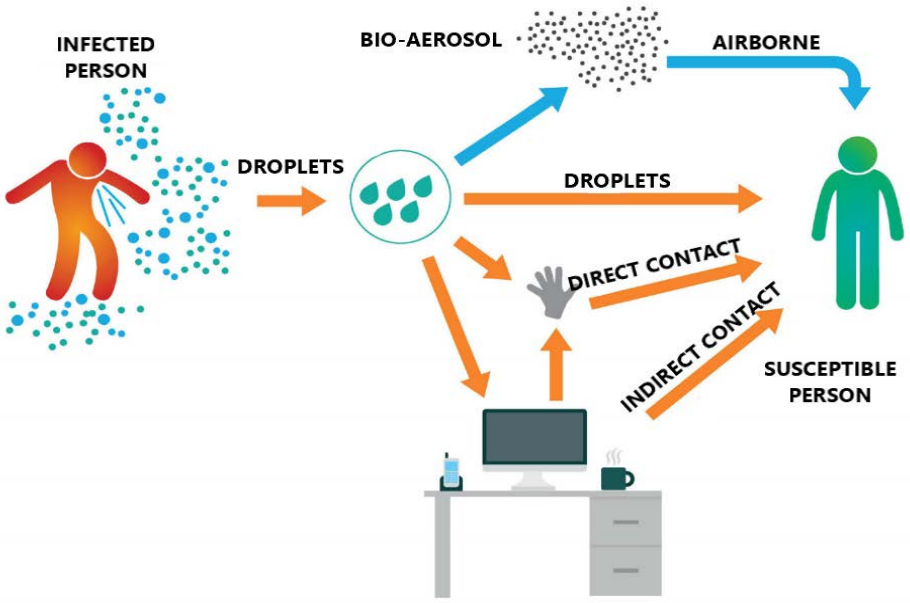

Figure 1.1 The transmission routes of respiratory diseases.
Source: adapted from [6, p. 1]

The following paragraphs illustrate each infection mode individually. Contact and droplets routes are shown briefly, while greater relevance is given to the airborne (or aerosol) route. In fact, the latter is the core of several research studies and it will be the central topic of the modelling part of this document.

[3] Reverse Transcriptase-Polymerase Chain Reaction

1.1.1 Contact transmission

The contact route of infection occurs when the susceptible person directly comes in physical contact with the infected subject's mucous secretion or saliva. This infection pathway can be divided into two subcategories in dependence on the contact site: direct contact mode and indirect contact mode.

Recurring actions like kissing, hugging, and shaking hands are typical examples of direct contacts. In these situations, the contact site is the infected source itself. The susceptible person directly touches potentially contaminated body of the infected subject. Direct transfer of infectious material and consequent infection are very likely to occur.

On the other hand, the vehicles of the second pathway are intermediate contaminated objects or surfaces, where infectious droplets have previously fallen on. Contaminated objects are usually referred as *fomites*, therefore this transmission pathway is sometimes also called *fomites route*. The mitigation of the infection risk caused by indirect contact is quite difficult, because it would be necessary to trace every single object and surface that people touch. However, WHO and other healthcare organizations provide effective guidelines to avoid this transmission route (see §1.3).

1.1.2 Large droplets transmission

Both droplet and airborne infection routes are related to the exhalation of small, virus-laden droplets into the environment. Human respiratory activities, such as breathing, vocalization, singing, coughing and sneezing involve the release of tens of thousands of different-sized droplets [3], [5], [7]–[9]. The difference between these two pathways depends on the size of the droplet. This parameter affects the thermodynamic behaviour of the particle when it is submitted to various fluid dynamic interactions with air in which it is transported. The main acting forces on a such small body are the following ones:

- gravitational force
- diffusion (driven by concentration gradients)
- airflow momentum and drag force (due to ventilation systems)
- buoyancy (driven by density gradients due to spatial temperature differences).

Fluid mechanics laws determine the faith of each droplet. Although it is an extremely dynamic phenomenon, it is possible to make a distinction:

- larger, heavier droplets are mostly influenced by gravity; therefore, they rapidly settle on floor or surfaces within a distance of 1÷2 m from the generation source. These lead to the *large droplets transmission route*.
- smaller, lighter droplets have low sedimentation velocity and are mostly affected by airflow patterns (momentum, drag and buoyancy) and diffusion. For this reason, they remain suspended in the air for longer periods and dispersion occurs over greater distances. Small droplets are also referred as aerosols or *droplet nuclei*. They are responsible for the *airborne transmission route* (also called *aerosol transmission*).

Figure 1.2 shows the different gravitational settlement time as a function of the aerodynamic diameter[4] of the droplets.

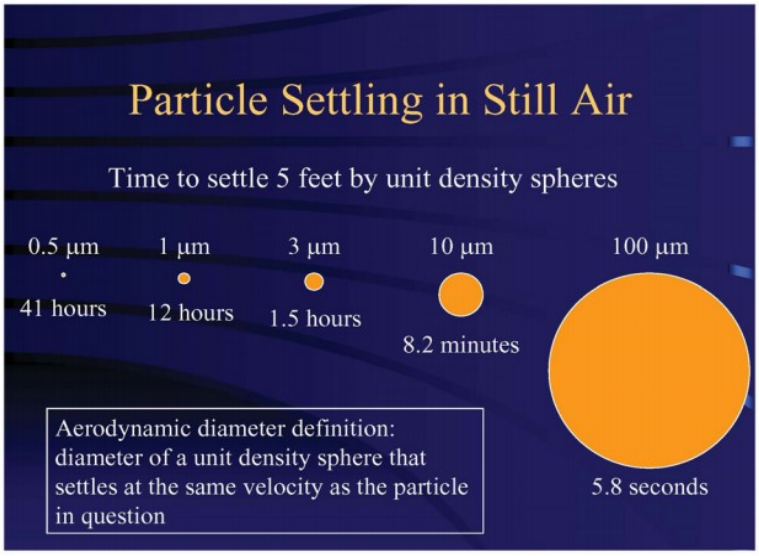

Figure 1.2 Settling of different-sized droplets.
Source: [9, p. 9]

The WHO recommends a conventional limit diameter of 5 µm to discern between droplets and droplet nuclei [4]. A lot of scientific works about airborne transmission use this value as separator (e.g., [3], [10]). Conversely, ASHRAE[5] and other researchers suggest a limit value of 10 µm [7]–[9].
Heavier droplets' movement describes a ballistic trajectory, and they could directly land on person's mucous membranes (mouth, nose, eyes). Therefore, an exposed individual is likely to contract disease through the droplet route if he stands too close to an infected one (1÷2 m). Because of the direct and quick travel of droplets from the infected to the susceptible subject, it is also defined as *direct spray route* [8]. Large droplets are also responsible for the contamination of close surfaces, so they could lead also to indirect contact infection. Also for this pathway some control measures are proposed by international guidelines (see §1.3).

1.1.3 Airborne transmission

In §1.1.2 the fluid dynamic behaviour of different-sized droplets was discussed. While larger droplets are responsible for short-range infection mode, droplet nuclei can remain suspended and be transported by air for longer distances. Therefore, they may cause the airborne transmission of respiratory diseases. Some researchers split the airborne route into short-

[4] It is defined as the diameter of a sphere that has the same settlement velocity as the real droplet.
[5] The American Society of Heating, Refrigerating and Air-Conditioning Engineers

range and long-range ways [8], where the former is related to the droplet pathway's characteristic distance (1÷2 m).

However, the infection occurs through inhalation of pathogen-containing aerosol which enters an individual's breathing zone [9]. Once inhaled, infectious particles deposit inside the human respiratory tract. If the number of inhaled infectious microorganisms reaches a threshold value for the susceptible subject, illness is likely to start. Microbiologists name infectious dose this limit number. Each respiratory disease has its own infectious dose, but its assessment is not easy, because it depends on environmental, biological, genetic and subjective factors [10].

Furthermore, droplet nuclei can also settle on distant surfaces or object causing fomite infection risk. Another possibility concerns the resuspension of deposited aerosol that could occur as a consequence of human activities (such as bed making, walking, door opening, etc.) or airflow driven by mechanical ventilation [5], [9].

Figure 1.3 shows droplet and airborne pathways.

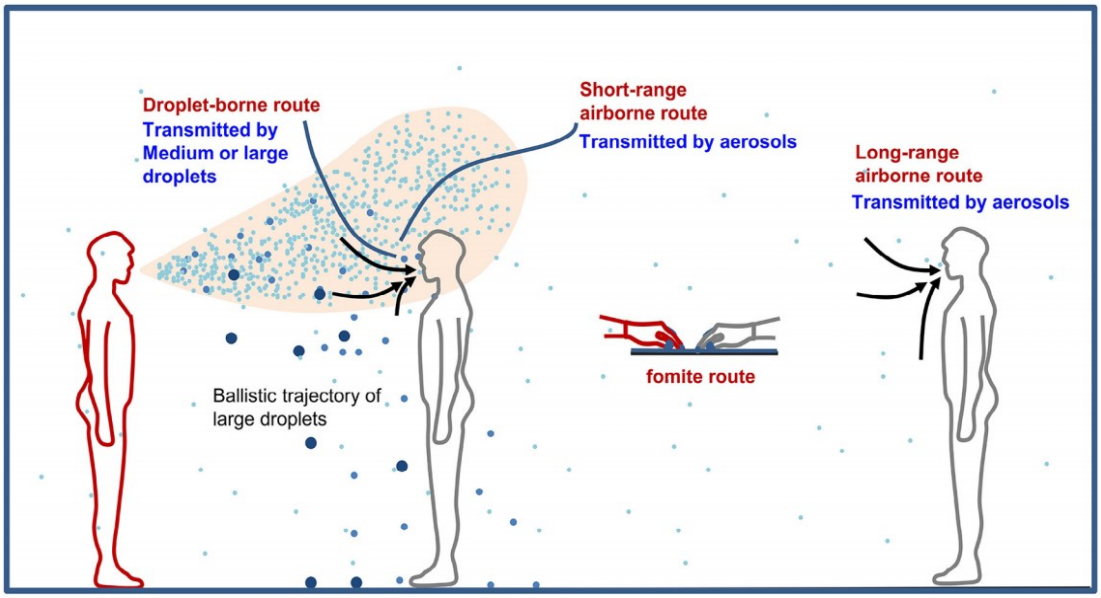

Figure 1.3 Droplets and airborne infection routes.
Source: [8, p. S106]

As stated in §1.1.2, common human respiratory activities are the source of both routes. Once exhaled, respiratory particles are supposed to face indoor environmental conditions: air temperature and relative humidity. These two parameters drive the rapid evaporation of the droplet and its decrease in size. Consequently, if a droplet shrinks sufficiently, gravity will become negligible and it would turn into a droplet nucleus [7], [9], [11]. Virus and bacteria survive if the liquid matrix does not evaporate completely, otherwise they undergo rapid inactivation. Since virus and bacteria size varies in the range from 0.02÷0.3 μm and 0.5÷10 μm respectively, it is apparent that submicrometric droplet nuclei could transport them, especially in the case of viral pathogens [3], [8].

Differently from contact and droplets route, besides the infected and susceptible subjects, airborne transmission is also affected by the behaviour of indoor air. This makes the infection pathway more complex as it includes the influence of strongly dynamic airflows. Thus, much research has been done since the last century to mathematically model this interesting transmission route. The entire airborne cycle will be presented in more detail in §1.2.
Building ventilation systems play an important role on the airborne chain, since airflow patterns affect droplet nuclei dispersion within the indoor space and their presence in the breathing zone. Indeed, airborne pathway is the only one that can be effectively controlled at engineering level (see §1.3.2). On the contrary, ventilation has a negligible effect on droplet route, because gravity is prevailing in that case.
Figure 1.4 schematically summarizes the transmission routes. It underlines the relevance of ventilation as a control measure for the airborne infection mode.

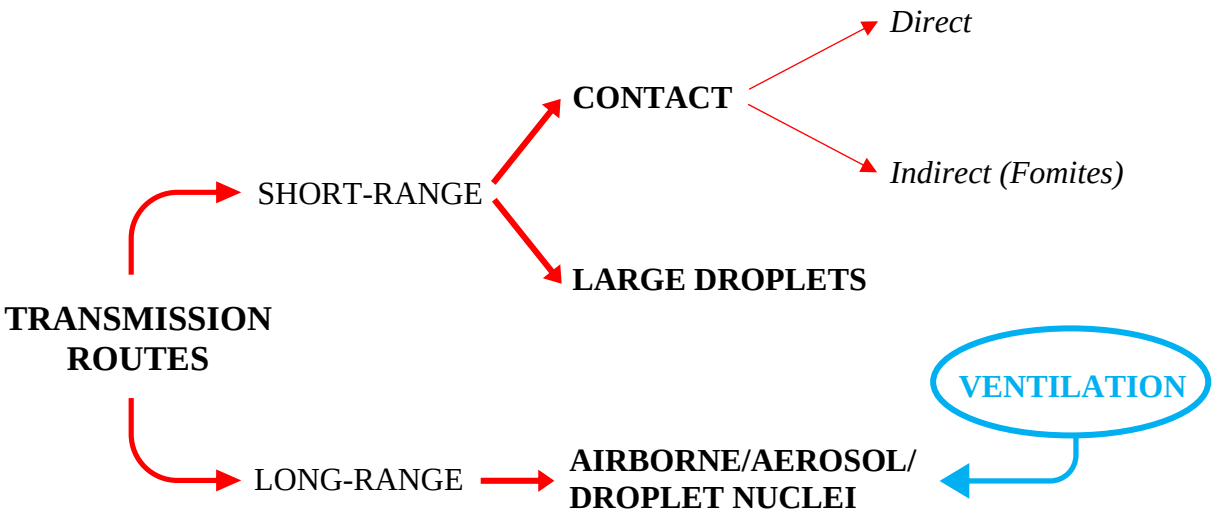

Figure 1.4 Transmission routes scheme and ventilation's role.

In conclusion, respiratory diseases can spread through three different routes. However, the relative contributions of each infection pathway depend on the analysed disease. In particular, there is still great debate on the effectiveness of the airborne route for most viral and bacterial infections [2], [4], [8]. For numerous pathogens there is enough knowledge about the predominant infection routes, whereas we do not know so much about SARS-CoV-2 since it is a recently appeared virus (see §1.4).
As the importance of the airborne pathway on the dissemination of viruses and bacteria is concerned, some scientific works classify it into three categories [4], [12]:

- *obligate* airborne: transmission occurs solely through infectious bio-aerosols
- *preferential* airborne: disease is initiated through multiple routes, but predominantly through bio-aerosols
- *opportunistic* airborne: infection occurs primarily through the other routes but may also occur in favourable circumstances through aerosols.

Special situations that could drive the opportunistic airborne transmission are called *airborne-generating procedures* (AGPs). Namely, these are especially medical activities which generates a large amount of aerosol in the vicinity of the treated patients, leading to a risky exposure for the healthcare personnel. Generally, for opportunistic airborne diseases aerosol generation from ordinary respiratory activities is not considered so problematic.

1.2 The phases of the airborne transmission cycle

Infectious droplet nuclei are also called bio-aerosols[6], since aerosols are suspensions of fine solid or liquid particles in a gaseous fluid, typically air [3]. As stated in §1.1.3, the airborne infection route is difficult to analyse because of its inherent complexity.
While contact and droplet routes entail an almost instantaneous transmission over short distances, airborne route is more effective with an increasing exposure time. In fact, the more the susceptible person remains in the confined space where the airborne pathogens are released, the more infectious material he inhales. Obviously, this increases the risk of intaking a number of pathogens that could exceed his infectious dose. Moreover, there are three actors in the airborne transmission route: the source (infected subject), the transport vector (air) and the recipient (exposed or susceptible subject). Airflow patterns play a big role in transporting small droplets over long distances. For this reason, ventilation must be considered an influential factor in the airborne route. Figure 1.5 shows these differences.

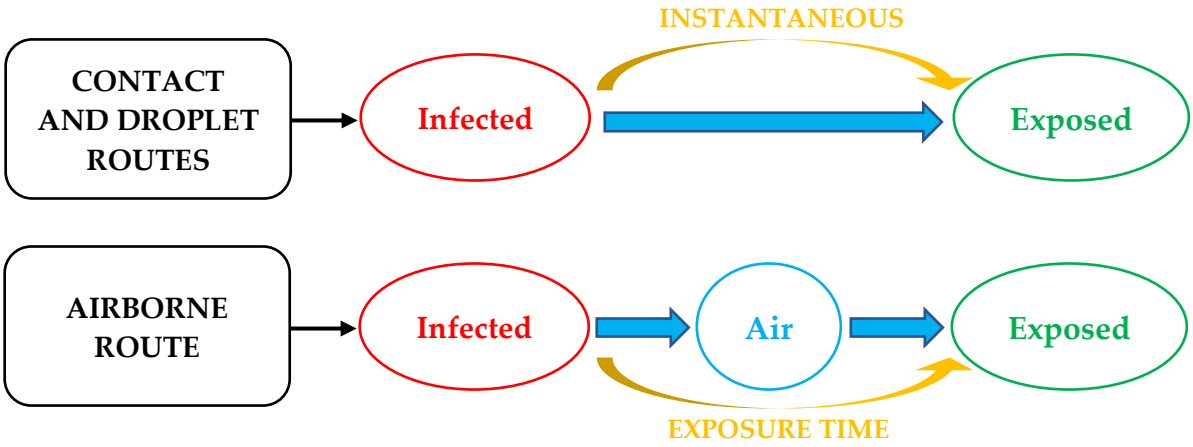

Figure 1.5 Differences between airborne and other routes.

The airborne pathway is of special interest in enclosed spaces. In the outdoors, a limitless volume is available for the dispersion of pathogens exhaled from an infected source, so airborne transmission is unlikely to occur. On the contrary, in the indoors droplet nuclei spread across a smaller volume, so they saturate indoor air after a certain time. For the rest of this work, we refer to airborne infection in indoor environments.

[6] Aerosol containing microorganisms such as viruses, bacteria, fungi, etc.

Airborne infection route can be considered as a transmission cycle consisting of a series of consecutive events. The main steps are listed hereinafter:

- generation or release of infectious aerosol
- transport and dispersion across indoor air
- exposure and subsequent inhalation and deposition
- secondary infection and the cycle restarts.

The following paragraphs explain each step of the cycle more in detail, according to what the scientific community has learnt so far [3], [5], [8], [11]. Nowadays, scientists have more knowledge about the entire airborne chain, but there is yet much to learn. Understanding each process of the pathway is fundamental for scientific community to be able to mitigate the airborne transmission and address institutions towards the correct political choices.

1.2.1 Generation of infectious aerosols

Airborne aerosols can be classified into different categories based on the generation source [3]–[5]. In airborne infection the most important mechanism of generation is constituted by common human respiratory activities such as normal breathing, talking, sneezing, and coughing. The last two are less frequent events, but they are characteristic symptoms of respiratory disease. In fact, human pulmonary dynamics are responsible for the formation and expulsion of expiratory droplets from mouth and nose. Besides, various medical procedures such as intubation, cardiopulmonary resuscitation, bronchoscopy, autopsy, and surgery are other sources of aerosols (i.e., AGPs, see §1.1.3). Finally, daily actions as walking, bed making, door and wind opening cause resuspension of deposited aerosol from surfaces.

Since we are more interested in airborne transmission in public buildings, particular attention is paid to human expiratory aerosols. Human expiration generates the smallest droplet nuclei compared to the other sources [3]. The target is the estimate of the pathogenic content of the secretions coming from each above-mentioned activity. Since breathing, talking sneezing and coughing have different dynamic behaviour, it is fundamental the definition of these parameters for each respiratory action:

- the number of generated infectious droplets and their concentration in the exhaled air volume
- the statistical size distribution of the infectious droplets
- the quantity of pathogens in each size class of aerosols

Current advanced measurement instruments and techniques such as particle image velocimetry (PIV), particle counters and other particle visualization methods [5], [7], [8], have allowed to characterized each exhalation mode in number and size of droplets. However, it remains unclear how much infectious material is present in each droplet based on its dimensions. As said in §1.1, swabs use detects the viral or bacterial load of an infected

subject. This confirms that an amount of pathogenic material is available to be expelled, but it does not mean that exhaled droplets will have the same concentration of RNA copies/ml. Wei and Li (2016) have tried to provide an explanation of the droplet formation mechanism in the human respiratory system and to link it with the content of pathogens [8]. They say that this content depends on where the droplets originate in the respiratory tract. In fact, pathogenic microorganisms are mainly found in the airways of larynx, trachea, bronchi and in the lower respiratory tract (LRT, i.e., bronchioles and alveolar region), rather than in the mouth which is the initial parts of the upper respiratory tract (URT). This means that droplets coming from the LRT are more likely to transport pathogens. Similarly, the size of the droplets depends on the origin site. The smallest ones ($\phi \leq 1$ μm) originate from bronchiolar fluid fil, the medium-sized ones (1 μm $\leq \phi \leq 100$ μm) are produced in the larynx and middle airways, and, finally, the largest ones ($\phi \geq 100$ μm) come directly from inside the oral cavity. The authors consider that two major mechanisms are possible for expiratory droplets formation inside the respiratory system. The first one is the instability caused by shear stress on the mucous-air interface in middle tract. Human respiratory airways are covered by a mucous layer and each respiratory activity imply air movements which can lead to the detachment of fluid particles. On the other hand, normal tidal breathing does not provoke instabilities on the mucous membrane, because of too weak shear forces. In this case, bronchiolar film rupture is the cause of fine droplets generation. During the expiration phase, terminal airways collapse, and their re-opening at the inhalation goes along with the burst of the viscous film with production of liquid particles. Generation mechanisms and sites within human respiratory tract are summarized in Figure 1.6.

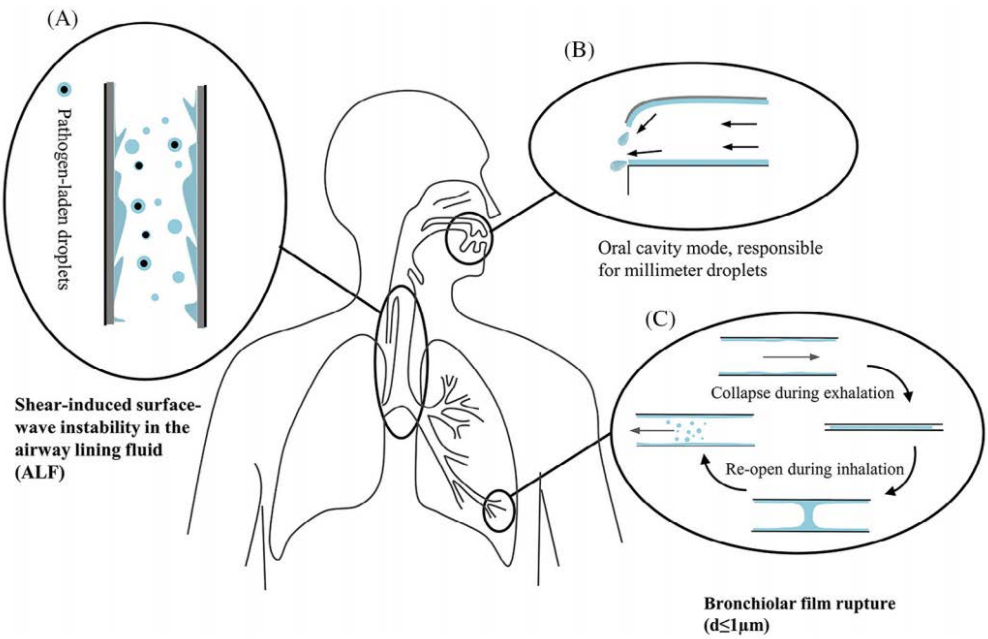

Figure 1.6 Generation mechanisms of expiratory droplets and aerosols.
Source: [8, p. S103]

Number and size of released droplets vary significantly among different pulmonary activities, because they engage distinct formation mechanisms and sites:

- normal tidal breathing entails the formation of small droplet nuclei through bronchiolar film rupture. However, some of them rapidly deposit on the airways' surface and are not expelled. In any case, breathing action does not produce many expiratory droplets.
- speaking produces an intermediate number of large droplets from oral cavity
- coughing and sneezing lead to the expulsion of a high amount of liquid secretion. These phenomena consist of strong air jets from mouth, so they induce instability in the airway lining fluid through intense shear forces. They are characterized by a large number of droplets.

As well as size and number of expired droplets, it is important to define the fluid dynamic characteristics of each respiratory activity as they affect the first interactions between the released aerosols and the indoor environment, after the exhalation. The main parameters are:

- breathing or pulmonary flow rate (mean value)
- peak exhaled flow rate and peak velocity (for strongly dynamic events)
- duration and frequency of the phenomenon
- time trend of the phenomenon (e.g., flow rate vs time)
- expiration temperature.

In general, a breathing temperature of 34°C is usually considered [3], [7].

Tidal breathing is a continuous phenomenon with an average frequency in the range of 10÷15 times/min [7]. The breathing flow rate prominently depends on the activity level; for moderate activities in sitting and standing position it ranges from 6 to 10 l/min (for other values, see §2.1.1.1). It has a peak velocity of 1÷5 m/s [8] and exhaled flow rate over time may be represented by a sinusoidal function [3], [7], [8]. Some authors suggest that a normal breathing activity could be appropriately modelled by a sinusoidal cycle consisting of 2.5 s for exhalation, 1 s break and 2.5 s for inhalation. [7]

As stated above, coughing and sneezing are characterized by respiratory flows with higher concentrations of droplets, but they are events with lower duration and lower frequency compared to ordinary breathing [7]. Peak velocities for coughing are in the range of 6÷22 m/s, with an average value higher than 10 m/s. Corresponding peak flow rates are in the range of 10÷14 L/s. For these types of phenomena, a combination of gamma probability distributions functions is suitable to represent the flow rate trend as a function of time [3], [7], [8].

Speaking frequency depends on the place where a subject is carrying out his activity. In certain situation (e.g., in public offices, shops, supermarkets, schools, etc.) it could be a recurring event. A few studies deal with this respiratory activity. However, velocity could reach a peak of 16 m/s, with an average value of 2.3÷4.1 m/s [3], [7]. Concerning the exhaled flow rate over time during speech, a constant profile can be assumed [8].

1.2.2 Airborne transport

After aerosol generation, the infection pathway proceeds through the transport phase. Infectious droplets are released by infected subject's mouth or nose into the surrounding environment. When we deal with dispersion of micrometric and smaller particles in the air, we must characterize both the aerosol from the source and the environment where the former spreads. In our case, droplets and droplet nuclei are the scattered particles, with human infected subject as the source. Furthermore, we are interested in indoor ventilated spaces as dispersion environments. Therefore, indoor air is the carrier of the infectious aerosols.
The interactions between the indoor environment and aerosols are highly dynamic. Fluid dynamics laws are able to analyse them and to determine the movements of small particles transported by indoor air. The main factors affecting this complex scenario are droplets' size (aerodynamic diameter) and thermophysical parameters of the confined space.
The transport phase of the airborne transmission route can be divided into two stages [8]. First, the expiration flow pushes the droplets from mouth and nose towards the indoor environment. In this step, the separation between larger droplets and droplet nuclei occurs. Secondly, airborne infectious material spreads via room airflow over the available volume for prolonged times. The following subparagraphs examine these steps.

1.2.2.1 Release from source to the indoor environment

Infected source pathogenic material is emitted from mouth and nose into the indoor environment through the above-mentioned respiratory actions. As said in §1.2.1, these activities generate a certain number of different-sized droplets. So, the pathogenic matrix is a mixture of both droplets and droplet nuclei.
This is a dynamic step as it involves rapid physical interactions between the initial expiratory flows, human thermal plume, and indoor environment.
The exhaled flow momentum determines how far droplets are dragged into the indoor space. The strength of the expiratory flux is related to the performed respiratory action. Tidal breathing produces a weak exhalation, so droplets are pushed within a maximum distance of 1÷2 m. On the contrary, cough and sneezes have properties similar to a starting jet or puff [8]. They yield turbulent aerosol-laden jets that can penetrate the indoor environment for distances higher than 2 m, before aerosol mixes with air.
In the second instance, body thermal plume has an influence on weak expiratory jets. Human subjects are heat sources and bodies are a sort of heat exchangers that dissipates metabolic heat flux into the surrounding environment. In other words, there is a continuous heat exchange between human, at a temperature of about 37 °C, and the indoor environment. This process generates the so-called convective boundary layer (CBL) around the body. It has different velocity and thickness along skin or clothing surface since it starts as a laminar, thin flow from the feet, and it grows and speeds up going upward. The turbulent terminal part is also named thermal plume. The latter rises from the chest up to a meter above the head [8]. CBL and thermal plumes are a function of several factors (e.g., surrounding air

temperature, furniture design and location, clothing, body posture, metabolic rate and consequent heat flux, etc.) [7]. Clearly, a rising thermal plume can pull upward small particles coming from a weak exhalation flow, avoiding a direct spray towards a susceptible person face. On the other hand, coughing or sneezing jets are strong enough to break the boundary layer and to penetrate the indoor environment horizontally. In the latter situation, the protective function of the plume is impaired, but it is rapidly restored.

Finally, expired droplets are submitted to a rapid evaporation (as asserted in §1.1.3). More precisely, a heat and mass transfer occurs. Therefore, droplets change both in temperature and mass. Neglecting radiation, the exchange mechanisms are convection and evaporation [3]. The process depends on indoor temperature (T_{ind}) and relative humidity (RH_{ind}). The latter is particularly important, because it defines the size reduction rate of the droplet and the equilibrium point of the mass transport phenomenon. Indeed, low relative humidity values bring about a fast and prolonged evaporation of larger droplets, that transform into droplet nuclei before falling on a surface [9]. Some droplets remain big enough to be drawn on floor or surfaces by gravity, whereas the other shrink until they reach aerosol size and remain suspended in the air. Wells in 1934 studied the thermodynamic behaviour of droplets and found a relationship between droplet size, evaporating and falling rate. His studies have encouraged successive researches that lead to the construction of the so-called Wells evaporating-falling curves of droplets [11], [13]. These curves are shown in Figure 1.7.

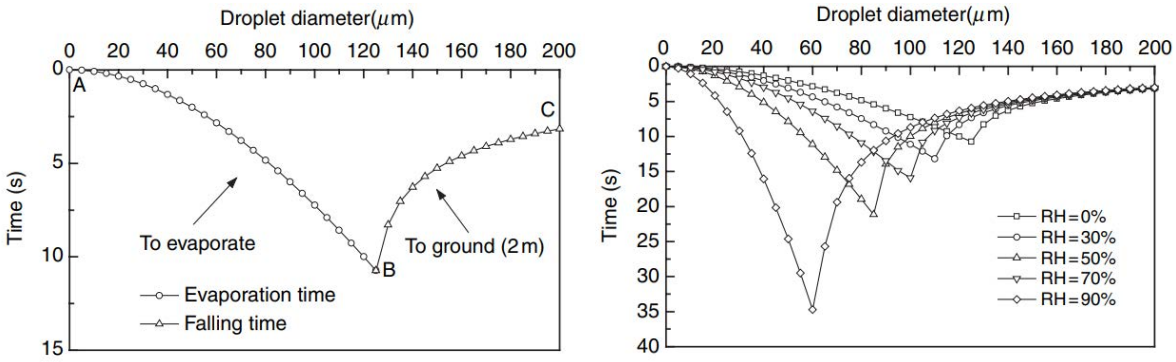

Figure 1.7 Evaporating-falling curve of droplets. Evaporating-falling curve for a temperature of 33 °C for the droplet, and indoor air temperature and relative humidity of 18 °C and 0%, respectively (a). Evaporating-falling curves for different RH values (b).
Source: [13, p. 218]

Figure 1.7(a) shows a curve for fixed environmental conditions (T_{ind}=18 °C, RH_{ind}=0 %), while different trends for variable RH_{ind} are represented by Figure 1.7(b). Droplet diameter refers to the initial value at the ejection moment from the source. From this graph we can identify the limit size that distinguishes droplets which become aerosol from those that settle on a surface.

Most of expiratory droplets are generally smaller than 100 μm, so they easily transform into droplet nuclei through evaporation [11]. When a sort of equilibrium in heat and mass transfer

process is reached between them and the environment, the residual aerosol is transported away by indoor airflow.

1.2.2.2 Droplet nuclei spread in the indoor environment

The dispersion phase on a larger spatial scale follows the transient and dynamic phase of exhalation moment. Heat and mass transfers still occur, but at a smaller rate. Droplet nuclei are free to move through indoor air in the whole available volume. Actually, this is another dynamic step in the airborne transport. In fact, the pathogen-laden aerosol movements are governed by a series of fluid dynamic interactions with different airflows [7], [8], [11]:

- ventilation plant and air distribution system (engineering aspect)
- residual wake and vortexes of exhalation flows
- occupants' inhalation flows
- thermal plumes of human bodies and other heat sources (e.g., electrical equipment)
- wake flow behind walking people
- human movements and activities inside the space (e.g., turbulence from bed making)
- doors and windows opening
- room interior design and furniture position (i.e., room layout)

The main flows between these ones are illustrated in Figure 1.8.

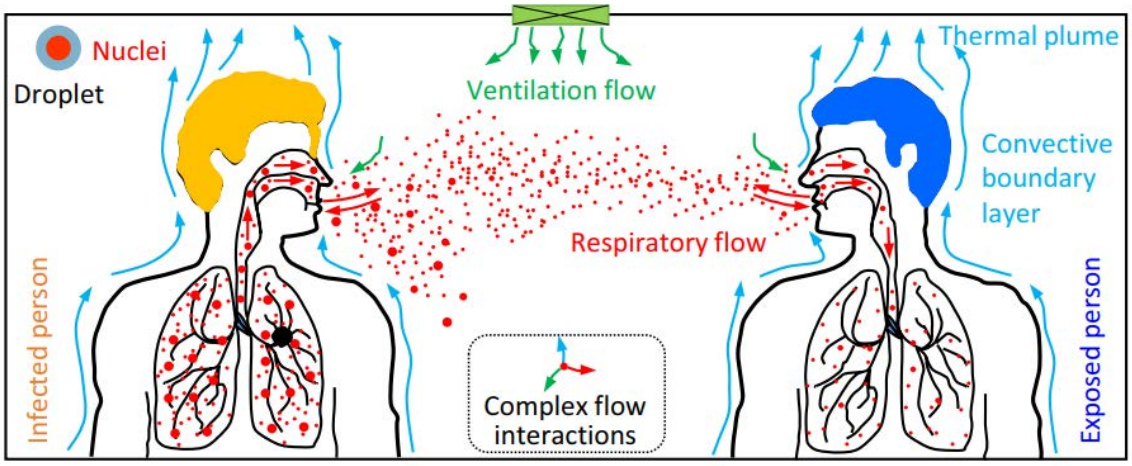

Figure 1.8 Interactions affecting droplet nuclei dispersion.
Source: [7, p. 501]

Therefore, fluid dynamic behaviour of indoor air transporting aerosol is a hard issue. Moreover, continuous variations are likely to present both spatially and temporally and the achievement of a steady-state indoor airflow is almost impossible. Aerosol transport is driven by air streamlines whose configuration is strongly variable over time.

Nevertheless, modelling the dispersion of particles in an environment means considering both air and infectious droplet nuclei, as the carrier and the suspended material, respectively. Indoor air is a continuum phase, and its fluid dynamic behaviour is defined by the resolution of the Navier-Stoke equations (mass, momentum, and energy balances equations). Instead,

aerosols are a discrete phase. Several studies affirm that submicrometric droplet nuclei behaviour is very similar to that of gases in ventilated environments and their dispersion is mainly affected by diffusive motions driven by concentration gradients. Conversely, other interactions including gravity, airflow momentum and drag force have a higher influence on larger droplet nuclei [3], [7].
Among all the above-listed airflows, the ventilation and distribution system have a great importance from an engineering point of view. Through ventilation, the pathogens dispersion can be controlled; for this reason, an appropriate design of the ventilation plant could reduce infection risk and make the indoor environment healthier (see §1.3.2).
However, the transport phase is what differentiates the airborne transmission route from the other two. It defines the motion field and, above all, the concentration of the infectious aerosols in different points of the indoor environment, based on the spatial resolution we can achieve. The latter parameter is essential since the infection risk assessment is founded on it, so, it will be of special interest in the modelling part of this work.

1.2.3 Survivability and infectivity of pathogens

A measure of airborne pathogens' strength lies in their viability and infectivity. Viability refers to the capacity to survive in a given set of environmental conditions. Instead, infectivity is related to the ability to attack host cells, reproduce, and cause disease. All infective microorganisms are inevitably viable, but not vice versa [3]. These two parameters determine if a certain respiratory disease can spread through the airborne route or not. When a pathogen is not viable and infective anymore, it is said to be inactivated.
Survivability is not an independent phase of the airborne cycle, but it evolves alongside dispersion step in the indoor air (see §1.2.2).
A pathogen cannot remain viable in the air indefinitely. First, during aerosolization, the expiratory flow can provoke shear forces that can inactivate some microorganisms. Second, viability is also function of the environmental conditions, both biochemical and physical. These include indoor temperature, relative humidity, oxygen and ozone concentration, atmospheric pollutants, UV radiation [3], [10], [11]. Finally, residence time is another influencing aspect, especially in the case of viral pathogens: the more a virus remains airborne without finding a host cell, the more likely is its inactivation.
The combination of the environmental parameters defines pathogens stability. Indoor temperature and relative humidity cause the evaporation of the liquid carrier. If the protective matrix totally evaporates, pathogens will rapidly inactivate. Loss of water is the main stressor causing loss of viability [3]. Moreover, both temperature and humidity can affect the lipid envelope and protein coat destroying the pathogen [11]. Viruses present a minimal survival for a relative humidity range of 40÷70 % and increasing temperatures enhance their inactivation [3].

The period of survival is also influenced by air composition. Chemical pollutants and other chemical species, including ozone and oxygen, are effective in destroying various pathogens [3], [11]. Aliabadi et al. (2011) highlight that outdoor air seems to be more unfavourable to pathogen survivability than indoor air [3]. The authors link this fact to the concentrations of air ions and the above-mentioned chemical compounds. They define a parameter called *open air factor* (OAF) to justify this effect.

Electromagnetic radiation has a variable effectiveness against infectious microorganism, based on the wavelength. UV radiation proved to have a high destructive power on any sort of pathogen. Outdoors, it is provided by the sunlight, so pathogens have short viability time out there [3], [10], [11]. On the other hand, air quality engineers take advantage of this discovery to design special UV devices for the indoor inactivation (see §1.3.2).

Viability is necessary but not sufficient condition for infectivity. The latter establishes if a pathogen is capable to overcome physical and immunological barriers in the attacked host, in this way it can multiply and initiate disease [3]. It depends on biological characteristic of both the pathogen (i.e., its virulence) and the susceptible subject (i.e., immune response). Moreover, the infective power is linked to some inhalation phase aspects (see §1.2.4).

Despite their importance in the airborne infection risk evaluations, viability and infectivity determination turns out to be difficult for most of respiratory diseases. Infectivity remains the most problematic as it is a function not only of the disease, but also of the host; considering the biological heterogeneity among the global population, it is clearly a big issue.

However, the scientific literature points out that current techniques and measure instruments have allowed to learn more about the matter. Tang (2015) affirms that advancements in pathogen detection and diagnostic methods permitted to reveal the presence of potentially transmissible organisms in the airborne environment through air sampling procedures. Although shear stress at the air-sampler suction unit could lead to viability losses, the author informs that infectious agents are present in the air [5]. Aliabadi et al. (2011) review the current techniques adopted to realize if a certain respiratory disease can be transmitted through the airborne route. The authors identify four major categories: *animal tests*, *culture methods*, *molecular methods*, and *plaque assay methods* [3]. As regards the animal tests, Nalca et al. (2011) noticed that rabbitpox virus in rabbits shows features similar to smallpox in human beings, that is recognized to be airborne transmissible [14]. Each method has its own advantages and disadvantages, so uncertainty on viability and infectivity is still substantial.

An exponential decay trend is often considered to mathematically model the viability function over time of some pathogens, even if it is an approximation [3]. Anyway, the presence of viable pathogenic material in the air highlights a potential airborne infection risk. The more viable organisms are detected, the more aggressive that disease is, since it is capable to face and withstand the environmental stressors.

In conclusion, the transport phase, and the survival of airborne pathogens have an outstanding importance. The interplay between air and droplets gives information about the spatial concentration of viable pathogens.

1.2.4 Inhalation and restart of the cycle

After generation and transport, the final step of the airborne transmission is the inhalation by the exposed subject. During normal breathing cycle, a susceptible person inhales a certain number of airborne pathogens, according to their concentration in the indoor air. This number defines the intake dose. Nevertheless, before considering what happens inside human respiratory tract, it is important to analyse what affects the inhalation airflows towards nose and mouth.

The main influence comes from the thermal plume of susceptible subject's body. It has two opposing effect: on one hand it operates as a sort of natural air curtain that protects the person from exhaled flows coming from a close infected occupant; on the other side, its ascending motion could bring pollutants and pathogens from the floor or trunk region towards the breathing zone. For these reasons, the thermal plume outlines the inhalation streamlines and their pathogenic load [5], [7], [8].

Human respiratory system consists of three regions: the upper respiratory tract (URT), including nasopharynx and mouth; the middle airways, i.e., larynx, trachea, and bronchi; the lower respiratory tract (LRT), with bronchioles, the terminal airways and the alveolar region where oxygen-carbon dioxide exchange takes place [3].

Once pathogen-laden droplet nuclei enter human respiratory tract, they are submitted to a turbulent airflow and settle on the airway surfaces. Deposition is driven by different mechanisms, including Brownian diffusion for aerosols with a diameter lower than 0.1 μm, a combination of diffusion and impaction for aerosols between 0.1 μm and 1 μm, gravitational sedimentation for aerosols larger than 1 μm [3]. However, the penetration into deeper sites of the system depends on their size and on the morphology of the host respiratory airways. Generally, droplet nuclei (i.e., small and medium droplets up to 5 μm in diameter) settle predominantly in the central airways and in the alveoli, while larger droplets (relative to droplet route) stop at the upper part [10].

When the inhaled pathogenic agents reach a sufficiently high number to overwhelm the immune defences of the susceptible host, they are able to cause infection and disease could begin. As stated in §1.1.3, scientists call *infectious dose* this threshold value [3], [8]. It has a characteristic value for each respiratory disease, and it specifies its aggressiveness. However, its evaluation is not simple since it is function of different aspect [3], [5], [8], [10], [11]. It depends on:

- the number of inhaled pathogens
- the size of the droplet nuclei that transport these pathogens, because this determines the final deposition site within the respiratory tract

- the distribution of the specific receptors, required by the analysed pathogen to successfully start the infection, within the respiratory tracts
- host immune responses and immunological history

The third point only refers to viral respiratory diseases. In fact, bacteria and fungi can multiply without a host cell, a favourable environment is sufficient. On the other hand, viruses need to bond to specific target cells, and these follow a certain distribution pattern inside human respiratory system [11].
Clearly, the precise infectious dose of a respiratory disease is not simple due to mankind heterogeneity. For example, each ethnic group has fought its own battle against different diseases and developed its own genetic immunity. Moreover, morphology, receptors distribution, and immune defence may differ among individuals [11]. Finally, the turbulent airflow inside human respiratory tract is not well understood, which is why infectivity evaluation of a pathogen is even more complicate than its viability (as said in §1.2.3).
The uncertainty around the values of infectious doses is the reason why we talk about *airborne infection risk in terms of probability*.
Once inhalation leads to successful infection, the respiratory disease starts, and it can amplify from the initial deposition site to peripheral tissues. Based on the advancement status of the disease, the host could develop symptoms and become a new infected source; secondary infections may occur and human airborne transmission cycle restarts [10].

Scientific research has done a lot of progresses in the comprehension of the airborne route mechanism, so far. In any case, there are also unknown aspects that need to be investigated in the future. Although current knowledge lacks quantification of some essential aspects including viability and infectious doses for several respiratory diseases, the airborne pathway continues to fascinate many researchers, especially those that deal with mathematical modelling and infection risk calculation.
However, understanding the entire airborne cycle from a qualitative point of view is fundamental because it guides international institutions towards the correct choices to reduce infection cases, to safeguard people lives and to improve salubrity in the indoor environments.

1.3 Countermeasures to minimise infection risk

For most respiratory diseases, it is generally difficult to quantify the relative contributions of different routes. Since there is great debate on the significance of airborne transmission of pathogen, international organisms, including WHO and CDC[7], focus on the other two routes. Anyway, they provide universal precautions through international guidelines. These recommendations are effective in mitigating all routes. On the other hand, if a transmission

[7] US Centers for Disease Control and Prevention

path proves to be predominant for a certain disease, then precise transmission-based measures could be considered to mitigate it [4].
Countries apply the directives on national land to slow down the infection rate, especially when a pandemic risk arises as in the case of COVID-19. Whatever the measure, the target is always blocking each potential transmission mode. Controls can be subdivided into three categories: administrative, personal, and environmental and engineering [2], [3], [11].
Administrative controls are imposed by public authorities though political ordinances. They consist of obligations and restrictions in the everyday life of all citizens with the purpose of containing the infection cases. These measures are listed below considering four action levels:

- individual behaviour: avoiding overcrowding in enclosed spaces; social distancing of 1 o 2 m; hand hygiene when visiting a public building.
- social organization: contact tracing; isolation and quarantine observance for ill people; lockdown in case of extreme necessity.
- public life and workplaces management: frequent cleaning and disinfection of the environment (potentially contaminated surfaces or objects); activity scheduling, including distance learning, smart working, reduction of the occupation density in public buildings, obligation of queuing at the supermarket for all customers.
- medical field: vaccination campaign; herd immunity.

Personal control strategies include handwashing, reducing physical contact, and use of personal protective equipment (PPE[8]). PPE are a set of protective clothing or devices, the most important being latex gloves and masks. Wearing masks or respirators proved to be effective in the mitigation of infection spread. National administrations can make the use of masks mandatory in public buildings.
Environmental and engineering control techniques are developed to strike specifically the airborne route, so they can be considered like transmission-based precautions. They are continuously improved and updated as knowledge about airborne infection progresses. Engineering control measures focus on indoor ventilation, and air distribution and treatment. In the following paragraphs, the effectiveness of these countermeasures in weakening the transmission routes is analysed.

1.3.1 Contact and droplet route mitigation

Infection control is effective if it blocks any stage of the infection pathways. Contact and droplet route characteristics are well-known from §1.1.1 and §1.1.2. Administrative and personal protective strategies seem to be suitable for their mitigation.
The best way to impair direct contact infections is avoiding any type of physical contact and segregation of human sources through quarantine and isolation policies. Lockdown may be

[8] In Italy DPI (*Dispositivi di Protezione Individuale*)

necessary if a disease becomes an epidemic threat, as this provision reduces contacts at the maximum level.

As regards the fomites route, hand hygiene must be observed to prevent surface contamination. However only accurate disinfection and cleaning of the indoor environment guarantee a substantial mitigation. In public places, each surface or object that a person may have come in contact with, must be sanitised.

Eventually, large droplets infection can be impaired maintaining social distancing and wearing masks. A minimum threshold distance of 2 m is worldwide accepted, according to falling motions of large droplets. The relationship between cross-infection risk and distance from the infected source, in indoor environments, is shown in Figure 1.9. As we can see, risk infection is substantial in the region within 1÷1.5 m. Whereas, for longer distances it assumes a low, but constant value, because of aerosol dispersion and potential inhalation [7]. Certainly, for close contact, there is airborne route contribution, too.

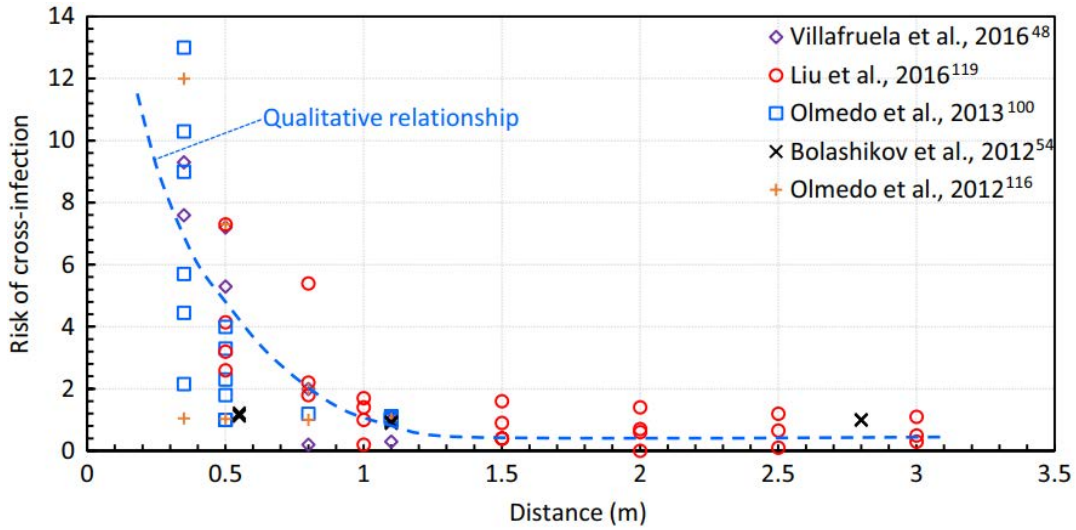

Figure 1.9 Risk of infection vs distance from the source.
Source: [7, p. 505]

Respirators and masks provide filtration of exhalation flows stopping larger droplets. Moreover, they weaken the expiration jets, so, even if some droplets managed to cross the filter, they would reach a shorter horizontal distance. Therefore, masks permit an effective control of the generation source, rather than protecting the susceptible person droplet infection [8]. People around the world use surgical masks and special respirators such as N95, in America, and FFP2, in Europe (N95 and FFP2 has the same filtration level).

In any case, gathering prohibition and public activity programming are the best possible choices for both contact and droplet route because they prevent frequent close encounters and reduce potential surface contaminations.

1.3.2 Airborne route mitigation strategies

Airborne infection risk can be mitigated through some of the previous measures.
Aerosol dispersion occurs over wider spaces than droplet falling, so a threshold distance of 2 m is not adequate anymore (airborne cross-infection risk persists over long distances in indoor environments, see Figure 1.9). However, keeping suitable distance remains a good measure, because aerosol concentration is higher in close proximity to the source.
Surgical masks and respirators filter the exhaled air from droplets and droplet nuclei, therefore the former cannot evaporate. As fine aerosols are regard, these personal devices have a filtration efficiency that varies with their size. Generally, respirators have higher filtration capacity compared to surgical mask, especially for very fine particles, but some studies suggest that they have not so different performance in protection against respiratory infections [4], [12].
As we said in §1.2, airborne infection develops over longer distances and periods and it is characterized by a transmission cycle with three main phases: generation, air transport and inhalation. Hitting one of these stages, the chain can be broken reducing the infection risk.
Avoiding overcrowding is a suitable measure that works on both the generation and exposure, reducing infected sources and exposed individuals sharing the same environment at the same time.
Masks, in this case, prove to be effective also for inhalation. Contrary to large droplets, aerosols remain suspended in air and could reach the breathing zone of a susceptible individual which, through a mask, could protect himself from infectious particles coming from the air. Wei et al. (2016), however, affirm that surgical mask are better in supressing exhalation, rather than inhalation, as shown in Figure 1.10 [8].

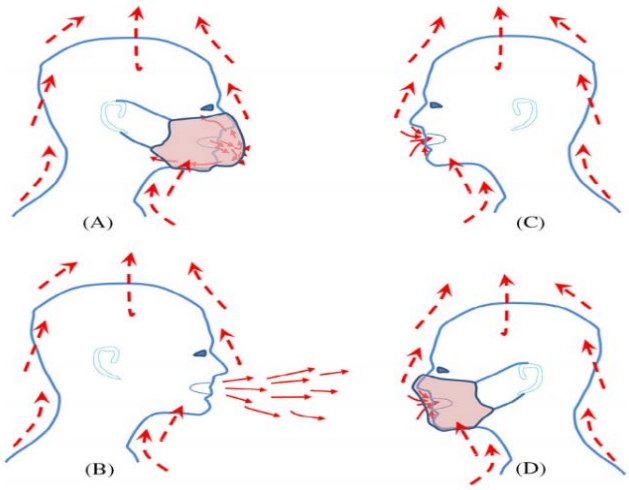

Figure 1.10 Use of masks for airborne control. Exhaled aerosol from an infected person with (A) and without mask (B). Inhalation flows for a nearby exposed individual with (D) and without (C) mask.
Source: [8, p. S104]

Administrative and personal control measures are effective in the management of source and exposure phases. However, airborne infection risk has a non-zero value until aerosol remains in the indoor air. Therefore, these precautions are necessary, but not sufficient in mitigating the airborne route.

The reduction of pathogen concentration in indoor air leads to a lower infection risk. Therefore, it is possible to work directly on the air transport phase, which is the objective of *engineering* or *environmental strategies*.

Figure 1.11 shows the hierarchy in the control measures for the mitigation of airborne infection risk in indoor environments. As it can be seen, elimination through physical removal of the pathogen from air would be the best strategy as it would reset the risk. Since this ideal outcome is not really possible, engineering control level is the most effective.

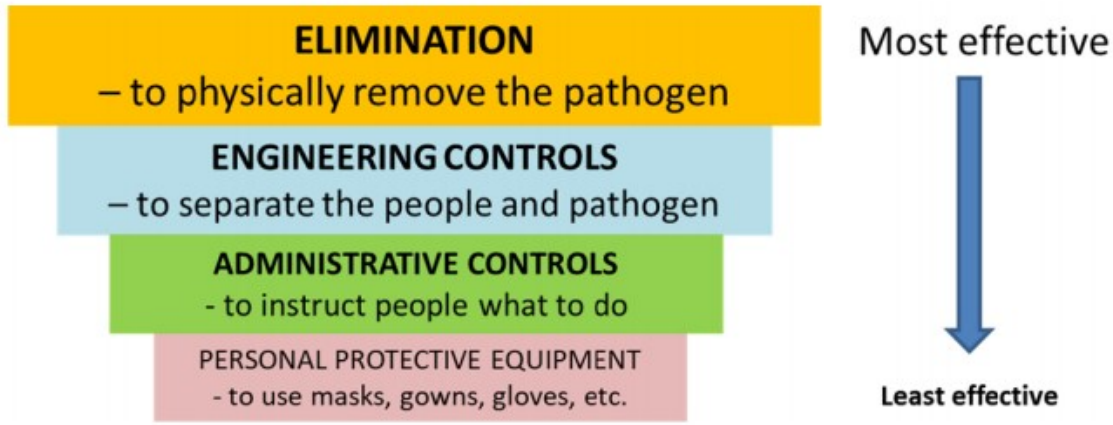

Figure 1.11 Airborne infection control pyramid.
Source: [2, p. 2]

In the following paragraphs, current engineering measures that deal with ventilation and air distribution features, air disinfection and cleaning devices, HVAC system management, and suitable thermophysical parameters for indoor air will be discussed.

1.3.2.1 Ventilation and air distribution role

Considering that infectious aerosols are constantly released by the infection source through respiratory activities, ventilation is the only way to decrease their concentration in an enclosed space. For this reason, ventilation and air distribution plants play a crucial role in removing infectious particles.

Ventilation systems are fundamental to insert fresh air into occupied zones. They are classified according to the mechanism driving airflows [3]. *Mechanical ventilation* consists of fan-driven airflows. In this case, a duct system is installed in the building to bring the air to the target place.

Natural ventilation is based on natural pressure differences between indoor and outdoor air, caused by natural forces including wind intensity and density-generated buoyancy effects. This type of ventilation can be achieved though properly designed openings in the building envelope or frequent opening of windows (aeration).
Mechanical ventilation is more energy consuming than natural ventilation since the latter does not rely on fans. However, the ventilation rate provided by natural forces is usually unpredictable as it depends on many factors (opening size and orientation, climatic and weather conditions, etc.). That is why, *hybrid ventilation* has been conceived to exploit both natural and mechanical ventilation advantages. Hybrid systems guarantee lower energy use than mechanical ones, but they require an accurate design.
Another classification is relative to air distribution strategy [3], [7]. Ventilation brings air to the indoor space, while air distribution determines the airflow pattern in the room. *Mixing ventilation* (MV) aims to create perfectly mixed indoor air with low concentration of pollutants. Effective mixing is achieved through high turbulent supply flow from the ceiling. Air is subsequently extracted through an exhaust grille at the top of the room.
Displacement ventilation (DV) systems, on the other hand, supply fresh cool air from a bottom diffuser and extract it from an upper exhaust grille. The airflows are driven by density difference in the indoor air (i.e., buoyancy) due to internal heat sources that warm up the supplied air; so, an upward flow regime is established. This motion creates a thermal stratification and a vertical gradient for pollutants concentration. In this way, noxious substances are propelled towards the ceiling, out of the breathing zone, where they accumulate and pour out though the exhaust vent. Displacement ventilation shows better energetic performances than mixing ventilation, since air can be supplied at a lower velocity.
Another ventilation concept is *Downward ventilation* (DnV), in which cool air is introduced from the top of the room, while exhaust removal occurs at the bottom.
As regards infection control, ventilation contributes directly to the airborne spread of pathogens. The principle is based on reducing the infection risk through the replacement of contaminated air with fresh outdoor air, which is supposed to be clean. The mechanism consists of two physical principles: dilution and subsequent mechanical removal of pathogens [2], [3], [11]. Fresh outdoor air dilutes the aerosols and carries them towards the exhaust grilles. Two parameters must be considered to achieve this goal:

- **Air Changes per Hour (*ACH*)**: it represents the amount of outdoor air that is supplied to the space. It is the ratio of the volumetric flow rate of outdoor air divided by the volume of the ventilated space. Higher *ACH* values mean increasing dilution of infectious agents and promoting their removal. Therefore, risk will decrease.
- **Airflow distribution patterns**: these depends on the adopted distribution strategy and the relative position of supply diffusers, exhaust vents and people. They define the overall airflow direction and the airflow structure (i.e., the air streamlines) that determine the dispersion of pathogens across the available volume.

Outdoor clean air is fundamental for the dilution of pathogens. That is why in the outdoors airborne infection risk is supposed to be negligible: infectious aerosol undergoes an exceptional dilution over an unlimited volume.
Natural ventilation can reach 50 *ACH* or more under favourable climatic conditions, but outdoor air flow rate is usually changeable and unpredictable. Mechanical systems, instead, provide lower nominal supply flow rate, but keep them constant over time [2], [3].
However, increasing ventilation rate is not sufficient to mitigate infection risk, but it must be accompanied by the control of pathogens movements through indoor airflows. Higher *ACH* lead to augmented mixing and dispersion towards previously clean zones if a suitable removal airflow is not planned [7]. So, an appropriate design of the air distribution system has an outstanding importance.
Many researches have analysed the importance of a certain air distribution strategy and arrangement of inlet and outlet openings on the infection risk, as indicated in an exhaustive review article [7]. Design choices depend on the final use of the building. For example, displacement ventilation, despite its energetic efficiency, seems to be unsuitable for healthcare facilities [3], [8]: for the moderate height of hospital rooms, pollutants and pathogens could be trapped in the breathing zone because of thermal stratification (*lock-up phenomenon*), increasing the airborne infection risk.
On the other hand, downward ventilation would be appropriate, but its performance is affected by the mixing effect caused by the counteraction of opposing flows coming from the diffuser and thermal plume of heat sources, respectively [3], [7].
Recently, advanced air distribution techniques have been proposed as infection control measures: *personalized ventilation* (PV) and *personalized exhaust* (PE) [7]–[9], [11]. These systems are designed to generate local airflows that should reduce the exposure risk. They cannot provide a suitable flow rate for whole air volume, so they are always coupled with a traditional ventilation and air distribution plant. Personalized ventilation consists of high-momentum air jets directed towards a person face to give a cleaning effect in his breathing zone. Conversely, personalized exhaust is based on air extractions through outlet openings nearby a person. In this way, potentially infected aerosol would not spread in the room.
We could say that PV controls the inhalation stage, whereas PE controls the source. These two methods proved to be really effective in the reduction of airborne infection risk, especially when they are combined. However, they are useful only if individuals remain in their positions.

1.3.2.2 Air disinfection and cleaning

Airborne infection risk would become zero if it would be possible to remove every single pathogen in the air (see Figure 1.11). Since sterilisation is not possible, there are some air

cleaning or disinfection devices of which air filters and UVGI[9]-units are the main ones [2], [3], [9], whose purpose is the decontamination of indoor air.

Air filters function is the mechanical removal of pathogens from air. They can be portable stand-alone units or be installed in the air ducts of the AHU[10] of the building's HVAC[11] system. The former are installed inside the ventilated space where they do not disturb human activities. Suction and purification of the indoor air is performed continuously.

The filtration efficiency is strongly dependant on the particle size. The worst performance occurs for removal of aerosols between 0.1 and 0.3 μm. In fact very fine droplet nuclei (below 0.1 μm) are captured by diffusional forces, while the larger ones are captured by impaction [3]. In healthcare settings, where an optimal salubrity is required, highly efficient particle air filters (HEPA) are used in place of normal devices; these filters have enhanced filtration power over a wide spectrum of sizes.

A problem related to filters installed in the supply and recirculation ducts of an AHU, is the energy need for air pumping. These devices introduce additional pressure drops that must be compensated from auxiliary fans. Moreover, pressure drops increase alongside increasing filtration efficiencies.

UVGI-units constitute another interesting technology. As already expressed in §1.2.3, electromagnetic radiation has a variable inactivation power on microorganisms based on its wavelength. The entire UV spectrum proved to have a remarkable germicidal effect, with 265 nm being the optimum wavelength (UV-C range). Most UV devices generate energy at a wavelength of 254 nm. Depending on the sensitivity of the microorganism to UV and the UV dose it receives, this radiation can inactivate the pathogen by wrecking its protein-based envelope and the genetic material [9].

As for filters, UV equipment can be placed either inside the ventilated space or upstream of air supply system [2], [3], [9]. In the first case we talk about *upper-room* systems, such as UV-lamps located close to the ceiling directing radiation into the upper zone in order to minimise human exposure. In the second case we talk about *in-duct* systems operating inactivation on recirculated infectious air. A combination of filters and UVGI in the ventilation ducts would guarantee an even higher air disinfection effectiveness.

Recently, another technology is catching on in air disinfection, that is *non thermal plasma* (NTP) technique. Plasma is a mixture of ionised gases that is composed of many charged particles, including ions, electrons, excited molecules and atoms, free radicals, but it remains electrically neutral. It can be generated providing the ionisation energy to gas through an electrical discharge. The term non-thermal refers to the fact that this plasma is not in thermodynamic equilibrium: electrons are free to move after ionisation and, because of their small mass, they can be accelerated by an electric field reaching higher temperatures, while other larger particles remain at room temperature. Free radicals, in presence of oxygen,

[9] UltraViolet Germicidal Irradiation

[10] Air Handling Unit

[11] Heating, Ventilation and Air Conditioning

generate special chemical reactive species called ROS (*Reactive Oxygen Species*). These species give oxidative power to the gaseous flux, that can demolish a large number of pollutants and microorganisms such as viruses, bacteria, fungi, VOCs (*Volatile Organic Compounds*), some chemical substances, etc.
This technology finds an effective application as air disinfection method for infection risk mitigation. In this case, the indoor air is ionised, and, thanks to the oxygen presence, free radicals generate ROS and destroy airborne pathogens with excellent removal performances. Some NTP-based devices have been conceived in the last years. Like filters and UV, both portable NTP air cleaners and in-duct installations exists. The former recirculate self-purifying air inside the room. The latter are located upstream of air supply system, especially in the recirculation duct, so decontaminated air is directly introduced into the room. To obtain an almost perfect disinfection effect, filter, UV-lamp and NTP device could be combined all together in AHU ducts.
The beneficial species of ionised air can also contribute to decontaminate surfaces, reducing fomite infection risk. Normally, cleaning operations are carried out scattering nebulized (aerosolised) liquid disinfectant onto the surface. But NTP ionizers present some advantages compared to traditional nebulization: their activity can be automated implementing suitable duty cycles; they do not require human presence; disinfection through gas guarantees an isotropic effect as it can also reach point in the volume inaccessible for manual operations.
Jonix S.r.l, an Italian society dealing with indoor air quality (IAQ), has developed NTP devices. These have special actuators that ionise air through *dielectric barrier discharge* (DBD) principle explained above [15], [16].

1.3.2.3 HVAC plant management

HVAC plant is integral part of the building. Its purpose is to provide thermal comfort and optimal indoor air quality (IAQ) in the indoor environment guaranteeing people health and productivity in their daily activities. This goal is achieved through heating in winter, cooling in summer and adequate ventilation with outdoor air.
HVAC systems are different in size and configuration according to what type of building they are serving. For example, healthcare facilities require special plants, public buildings rely on mechanical ventilation, while most residential building on aeration.
As we have said so far, these plants have great importance relatively to pathogens dispersion and airborne infection risk control. For this reason, in this period of COVID-19 pandemic, national organisations dealing with indoor environments control have published documents with recommendations on HVAC systems management and maintenance. This is the case of ASHRAE, in the United States [9], and AiCARR[12], in Italy [6], [17]–[21]. Thus, companies and public institutions are instructed about how planning their activities in a safe way. The main hints are summarized below.

[12] *Associazione Italiana Condizionamento dell'Aria, Riscaldamento e Refrigerazione*

First, ventilation rate with outdoor air must be increased as much as possible. For aeration-based buildings, windows must be opened frequently. As stated in §1.3.2.1, this will enhance dilution and removal of contaminated air. If possible, the ventilation system should work continuously, also during non-occupancy hours when infectious aerosol could be present.
Another recommendation is avoiding air recirculation, as it can carry pathogens from a space with an infected source, towards areas that would not have been contaminated. This is the case of centralised AHUs serving multiple zones of a building. This possibility depends on how the plant has been originally designed. If possible, it should run providing 100% of external air, with outdoor air dampers completely opened, whereas recirculation ones should be closed. Otherwise, outdoor air flow rate must be maximised [2].
If recirculation ducts are equipped with filters or disinfection devices (see §1.3.2.2), the infectious risk connected to recirculating pathogens would be contained and the nominal configuration does not need modifications. This is important from an energetic point of view, since recirculation permits to lower the energy use.
At room (decentral) level, split-conditioning units may be installed for cooling. They should not be turned off, otherwise thermal comfort would be compromised. In this case, the ventilation function is entrusted to windows opening [2].
Figure 1.12 encompasses all the above-mentioned engineering strategies to be implemented to reduce pathogens concentration in the air and the resulting airborne infection risk.

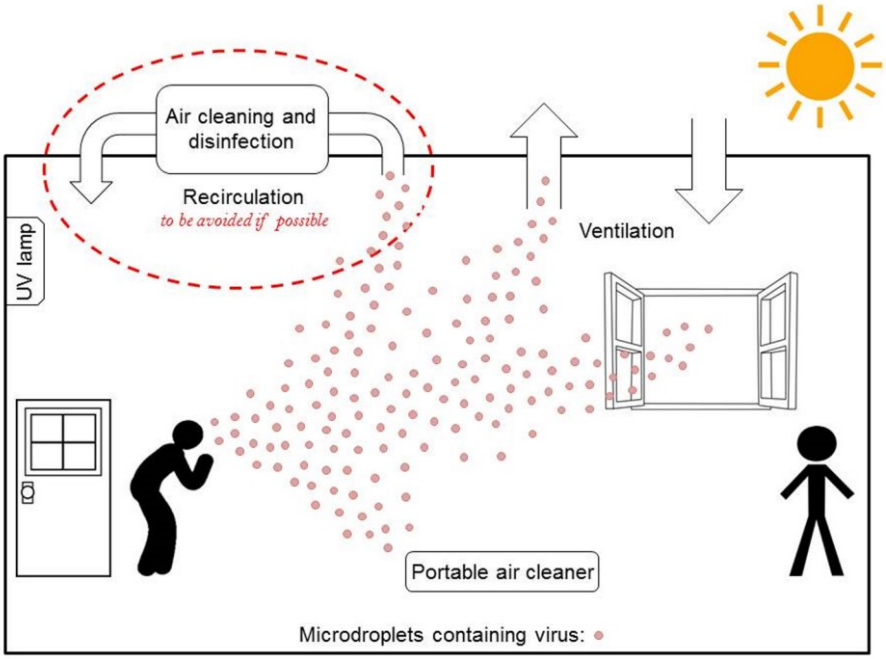

Figure 1.12 Engineering level controls to reduce the airborne infection risk indoors. Source [2, p. 5]

Furthermore, HVAC system must appropriately control the thermophysical parameters of indoor air, namely temperature and relative humidity. It was shown in §1.2.3 that these two affect the survivability of airborne pathogens. Higher temperature easily inactivates viruses,

but, for comfort matter, it is not possible to increase excessively this parameter. Conversely, relative humidity can be regulated maintaining its value between 40 and 60 %, that is a range in which viruses present the minimum viability. In fact, lower RHs cause mucous desiccating weakening their barrier function against extraneous microorganisms. Moreover, droplet nuclei formation by evaporation would be intensified. On the other hand, higher RHs undermine environmental salubrity and promote mould proliferation.

In previous paragraphs, strategies adopted worldwide for reducing the spread of respiratory disease among the communities have been shown. If the main transmission route of a certain disease is known, then the most suitable control measures can be applied (transmission-based precautions). As regards airborne infection mitigation, ventilation and air distribution system play a big role (engineering level control).
Even if they provide guidelines with recommendations on ventilation system management, national organisations point out that current standards dealing with indoor environments control establish ventilation parameters only to achieve comfort and adequate indoor air quality (IAQ) for general wellness and productivity. They do not provide specific requirements for airborne infection risk reduction. Optimal values of *ACH*, indoor temperature and relative humidity to face the spread of a respiratory diseases are not known at the moment [3], [9], [11]. Engineers and designers must rely on present buildings codes, but these should be updated considering such critical situations as the one we are experiencing today with the COVID-19 pandemic.

1.4 What is known about COVID-19 and other diseases

In the previous paragraphs it was explained how cross-infection can occur (i.e., the transmission routes) for respiratory diseases and how its risk can be reduced. In this paragraph, it is presented what is known about the characteristics of common pathogens and what scientific community has discovered about SARS-CoV-2 so far. If enough information about a disease features is available, then countermeasures focused on its preferential transmission route can be applied [4].
Only three diseases are classified as airborne transmissible in the international guidelines from international health organisations such as WHO: tuberculosis, measles, and chickenpox. Tuberculosis is a respiratory disease caused by a bacterium, and it is recognized as an obligate airborne infection. Instead, measles and chickenpox, which have viral origin, are preferential airborne infections (see §1.1.3) [2], [12].
Seasonal influenza and zoonotic influenza (like the avian one) are thought to spread mainly through contact and droplet route, but there is still a great debate on the importance of the airborne route. Morawska et al. (2020) argue that the long-range transmission through fine virus-laden aerosol is possible [2], and that viral genome copies were detected in the air [4].

Conversely, Seto (2015) considers this viral disease is an opportunistic airborne infection, that only occur under special situations of plentiful aerosol generation [12].
Respiratory syncytial virus (RSV), which is a cause of bronchiolitis in infants, is commonly contact and droplet transmissible, but outcomes from Knibbs and Sly (2016) suggest that airborne infection is strongly feasible, too [22]. Shiu et al. (2019) confirm this line of thought as RSV viral RNA was recovered in the air [4].
Norovirus causes symptoms as nausea and vomit. It is strongly believed that infectious aerosols generated by human secretions lead to cross-infection. Eames et al. (2009) think that the airborne route was the reason for several nosocomial outbreaks and that this virus is difficult to contain [11].
Rhinovirus (common cold) has limited data regarding its transmission routes, but it seems that pathogens are present in airborne particles [4].
Smallpox transmission could contemplate the airborne mode and tests on rabbits were carried out by some scientist to study possible countermeasures, as rabbitpox showed similar characteristic to human one [14].
The uncertainty behind the airborne infection relevance for the above-listed diseases lies in the difficulty to give a clear quantification of the viability and infectivity of the material detected in the air. Moreover, historical outbreaks support the propensity to spread through the other two routes. Conversely, measles, tuberculosis, and chickenpox have been studied for years and many nosocomial and public outbreaks confirm their airborne aggressiveness. However, a common issue encompasses all these pathologies: the assessment of the airborne infectious doses remains not simple.
SARS-CoV-2 is a novel respiratory virus, so current knowledge is scarce, but scientist are deploying a lot of resources to bridge the gaps. First, past epidemics caused by coronaviruses can be taken on as starting point. These viruses were SARS-CoV-1 and MERS-CoV[13]. Generally, they are considered to spread through contact and droplet route, and precautions targeting these two pathways proved to be effective [12]. However, infectious MERS-CoV was detected in the air [4] and many documented outbreaks report airborne infection cases for SARS-CoV-1 [1]. Therefore, for coronaviruses airborne transmission seems possible, at least at an opportunistic level (see §1.1.3).
As regards COVID-19, WHO still officially consider that human-to-human transmission occurs via contact and droplets [1], [6]. It recognises airborne infection as possible, but unlikely. For this reason, the guidelines focus on providing countermeasures for the first two routes. To the contrary, many scientists pled for the formal acknowledgement of the airborne transmission route and the implementation of suitable engineering control strategies. They argue that there is plenty of supporting proofs.
First, as we said before, SARS-CoV-1 is likely to spread also through air and novel coronavirus has many similarities with it [1].

[13] Middle East Respiratory Syndrome coronavirus

In second instance, several studies have found positive air samples for SARS-CoV-2 genome (RNA), demonstrating that the virus is present in the air and a potential airborne infection risk arises [2]. SARS-CoV-2 has shown to be stable in air with a half-life of 1.1 h [23], [24]. This datum gives us information about the viability of the virus in air, which follow an exponential decay. Obviously, the infectious dose is not known at the moment.

Finally, in 2020, there were two documented outbreaks that would justify the airborne transmission for COVID-19. The first one took place at a restaurant in Guangzhou, China, on 23rd January 2020, caused by an infected subject coming from Wuhan [23]. The second one burst out at a choir rehearsal in Mount Vernon, Skagit County (Washington State, USA) on 10th March 2020, where 33 members out of 61 attendees became sick and other 20 were suspected to have been infected, too. A symptomatic subject was the trigger [23], [24]. The dynamics of the activity at the restaurant and the observance of restrictions at the choir cause to think that infections occurred through the airborne route, rather than contact and droplets.

Other than transmission routes, another problem related to COVID-19 is the disease development. Firstly, it has an incubation period ranging from 2 to 14 days, so contact tracing and spread containment get complicated.

Furthermore, the phase of illness is characterized by a variety of symptoms so that it can be confused with other diseases.

Finally, and most importantly, once infection occur the ill subject may not present symptoms. In this case, he remains asymptomatic. The problem is that among all the infected people in the world, a significant percentage is asymptomatic. These people, unaware of having contacted the virus, continue their habitual activities, attending public spaces and meeting other people. In this way, coronavirus can easily spread inside a community.

The fact that SARS-CoV-2 may be airborne transmissible and the potential presence of asymptomatic individuals in public facilities push researchers to pay attention to the transport and dispersion of fine, virus-laden aerosols. That is why mathematical modelling of the airborne infection risk has an outstanding importance to analyse the indoor environment safety and to verify the suitability of different engineering control techniques. The following chapter deals with risk models.

Chapter 2

Airborne infection risk modelling

The research on the airborne infection route in indoor environments can be structured in this logical manner:

- understanding how the airborne transmission phenomenon works, and which environmental and biological parameters affect the travel of pathogenic aerosol from the infected source towards the susceptible receptor
- development of theoretical models in the form of mathematical equations that quantify the airborne infection risk
- use of these models to predict the risk under different environmental conditions (parametric or sensitivity analysis) and to evaluate the effectiveness of control measures (above all personal and engineering ones, see §1.3).

The first point is what already treated in detail in §1.2: the airborne pathway consists of subsequent phases, going from infectious aerosol generation to inhalation by the susceptible person. Each phase is affected by specific influential factors, many of which are not yet well-understood. For example, biological parameters such as viability, infectivity and pathogen-host interaction remain unclear, whereas physical mechanisms, including indoor dispersion and respiratory deposition of pathogens, are governed by air turbulence, which is still a controversial topic in fluid dynamics field. For this reason, the airborne infection cycle is characterized by a high complexity level. In this chapter, two more steps of the research path are treated. Infection risk models take into consideration the entire airborne route from the infected to the exposed individual, so the developed mathematical equations contain parameters that characterize the different transmission phases. Since exposure level is affected by many complexities, infection is a random event. For this reason, quantitative infection risk assessment is based on statistical and probabilistic calculations. Therefore, risk models output is a probability of infection ranging from 0 to 1.

The interest in epidemiological studies has increasingly grown during the last century, and many risk models have been developed and employed. Aliabadi et al. (2011) and Sze and Chao (2010) describe current models in detail in their review works [3], [25].

The principle on which all models are based is that infection probability depends on the intake dose of pathogenic aerosol by the susceptible receptor. The greater the dose, the higher is the risk of contracting the disease. The intake dose is the amount of infectious agents reaching the target infection site in the human respiratory tract. It is determined by the concentration of pathogens in the air close to the susceptible person (i.e., the exposure level), pulmonary ventilation rate, exposure time and respiratory depositions of particles. On the basis of the intake dose, the probability of infection is calculated by a mathematical equation.

Risk models can be classified as *deterministic* or *stochastic*. In deterministic models, it is assumed that each subject has an inherent tolerance dose for a certain pathogen. Infection occurs when the intake dose matches or exceeds his tolerance level. So, the model, in this case, determines with certainty whether the individual will get sick or not. On the other hand, stochastic models assume that any intake dose, even a single pathogen, could initiate infection in the host organism. However, both categories give as output a probability, since tolerance dose differs between individuals in a random way, depending on their immunological defences.

Risk models can also be classified as *threshold* and *non-threshold*. The former are based on the threshold dose concept which is the minimum amount of pathogens required to start infection within an entire community: when a population intakes a dose lower than this threshold value, nobody will be infected. So, it is different from tolerance dose, which is an inherent minimum dose characteristic of each individual.

The most important distinction, however, is related to the definition of intake dose. Two approaches have taken shape in quantifying the airborne infection risk: models based on the concept of "quantum of infection", and models which consider the actual quantity of pathogen in terms of DNA/RNA copies. Quantum or quanta constitute a hypothetical infectious dose unit, while genetic copies of pathogens express the actual number of inhaled infectious microorganisms. The former models derive from the Wells-Riley equation, the first formula based on quanta, whereas the latter are called dose-response models. In the following paragraphs, these two approaches are discussed.

Figure 2.1 represents the different approach of Wells-Riley model and dose-response models.

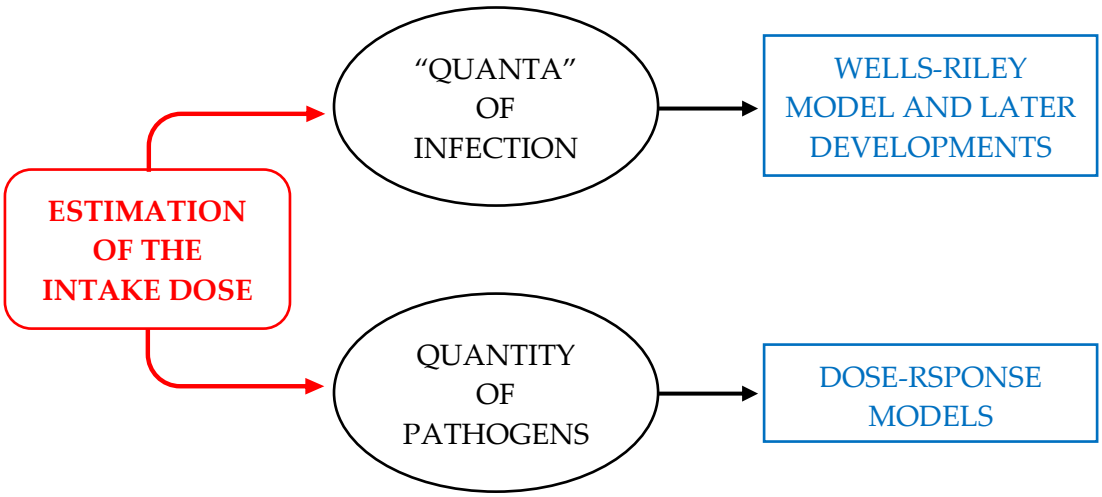

Figure 2.1 Wells-Riley and dose-response approaches.

Both types of model require an estimation of the intake dose and give as output the infection probability.

2.1 Simple models based on "quanta" of infection

The first simple models derive from studies carried out by Wells and Riley during the middle of the last century [25], [26]. They are based on the concept of "quantum of infection", proposed by Wells (1955). A quantum is defined as the number of infectious airborne particles required to infect a person [3], [25]. Originally, Wells gave another definition for this fictitious dose. During his epidemiological studies on airborne infection, he noticed that the number of subjects becoming sick followed a Poisson probability distribution in relation to the number of infective droplet nuclei they had inhaled. He established that one quantum was the infectious dose needed to transmit the disease to 63,2% of susceptible people [26], [27]. Whatever the used definition, quanta can be considered just like "packets" of infectious particles which constitute hypothetical dose units. A quantum could be a single or more airborne particles, depending on the considered respiratory disease. Quanta of more virulent diseases would consist of a small number of droplet nuclei, but a precise quantification of the number of particles is still too complicated.
The first model on this concept was developed by Wells and Riley. Successive modifications were introduced to overcome some limitations of the original formulation, arising from its initial assumptions. The main characteristics of these models are:

- the indoor environment is well-mixed, i.e., air properties and quanta concentration are uniform over the available space. This is the main assumption for these quanta-based simple models. Therefore, a balance equation of quanta concentration in the room can be written as follows:

$$V\frac{\mathrm{d}C}{\mathrm{d}t} = qI - QC \tag{2.1}$$

- based on quanta concentration, the intake dose by the susceptible receptor can be determined. The relationship between dosages and infections is described by a Poisson distribution, thus, infection risk is expressed through an exponential probability equation:

$$P_I = \frac{NC}{S} = 1 - \mathrm{e}^{-dose} = 1 - \mathrm{e}^{-p\int_0^{t_{exp}} C(t)\mathrm{d}t} \tag{2.2}$$

Equation (4.6) expresses the balance of quanta in the indoor environment. The left-side term is the accumulation of quanta over time, which is equal to the generation rate by the sources (q^*I) minus the rate of quanta removed by ventilation (Q^*C). This is the meaning of the employed symbols:

- V is the volume of the indoor space [m^3]
- C is the quanta concentration in the indoor air [quanta/m^3]
- t is the time variable [h]

- q is the quanta generation rate per infected person [quanta/h]
- I is the number of infected people in the room [-]
- Q is the ventilation rate [m^3/h]

The removal rate by ventilation refers only to the fraction of outdoor supplied air, if any recirculation is present. Q is equal to the product between volume V and air exchanges per hour ACH, expressed in [h^{-1}].

The quanta generation rate parameter q is characteristic of each respiratory disease. It represents the infectivity of a pathogen and the infectious source strength in a given situation. Infectivity depends on the aggressiveness of the microorganism. The infectious source strength is also a function of the activity level, since heavy exercise leads to more intense breathing rates accompanied by higher production of infectious droplet nuclei. Moreover, special medical procedures (i.e., AGPs, see §1.1.3) are responsible for a huge generation of aerosols, so in these situations quanta generation rate would be higher.

Equation (2.2) calculates the individual probability of airborne infection. The risk is a function of the intake dose, which, in turn, depends on the quanta concentration C, as shown in the third and fourth members of the equation. The used symbols represent these parameters:

- P_I is the infection probability [-]
- NC is the number of new infection cases among the susceptible population [-]
- S is the number of susceptible individuals [-]
- $dose$ is the intake dose, i.e., the number of inhaled quanta [quanta]
- p is the pulmonary ventilation rate or breathing rate [m^3/h]
- t_{exp} is the exposure time interval [h]

The infection probability P_I can also be expressed as a percentage. The number of inhaled quanta depends on the breathing rate p, which is function of the activity level of the susceptible subject.

The most important and controversial parameter is the quanta generation rate q. It cannot be directly obtained, but it is estimated through epidemiological retrospective analysis of actual documented outbreaks of specific respiratory diseases (see §2.1.1.2). The reliability of these backward calculations lies on the completeness of information concerning environmental and geometrical data of the indoor space, as well as the potential presence and operating conditions of ventilation systems. Since different outbreaks are related to different human activities, estimations of q for the same respiratory disease could give different values. As stated above, the activity level strongly affects the rate of production and exhalation of the infectious quanta by the infected people.

Equations (4.6) and (2.2) take different shapes according to the applied model and its assumptions. In the following paragraphs, a brief overview will be carried out: starting from the simplest and oldest model (Wells-Riley), the derived models that bring some modifications to the original one will be presented.

2.1.1 Wells-Riley model

As we said, this is the first and simplest model developed for assessing the airborne infection risk indoors. It considers the balance of quanta concentration, described by Equation (4.6), under the following assumptions:

- the room is considered well- mixed, so quanta are distributed uniformly and there are not concentration gradients
- the model works in steady-state conditions, so quanta concentration reaches the saturation level instantaneously, even at initial instants from infected person entry in the room
- quanta generation rate q from the infected individual is constant over time
- the incubation period of the disease is longer than the considered exposure time, so the number of infective subjects remains constant. In other words, no susceptible becomes an infectious source over the time scale of the model
- quanta are removed only by fresh air ventilation. Biological decay of the airborne pathogens, gravitational deposition rate of bigger droplet nuclei, filtration, and disinfection of air, are not considered in the removal of infectious quanta.

With these hypotheses, steady-state quanta concentration can be derived from the balance:

$$C_{ss} = \frac{qI}{Q} = \frac{qI}{V * ACH} \tag{2.3}$$

Where ACH are the air changes per hour [h^{-1}], and C_{ss} represents the steady-state concentration of quanta. Since C_{ss} remains constant over the exposure time, unless ventilation rate Q changes, the integral in Equation (2.2) becomes a simple product between this concentration and total exposure time t_{exp}. The well-known Wells-Riley equation for infection risk prediction is the following:

$$P_{I_{W-R}} = \frac{NC}{S} = 1 - \mathrm{e}^{-\frac{Iqpt_{exp}}{Q}} \tag{2.4}$$

Where each symbol has the same meaning as above. Equation (4.6) is the simplest relationship which gives the infection risk under steady-state conditions.

Another parameter that can be derived from Wells-Riley model is the reproduction number R_{A0}, i.e., the number of secondary infection cases that arise when a single infected subject is introduced into a population where everyone is susceptible, in an indoor environment [7], [28]. In other words, it is the ratio between new infections and infected individuals, as expressed by the equation:

$$R_{A0} = \frac{NC}{I} \tag{2.5}$$

This index expresses the disease spreading rate inside a community. An R_{A0}>1 means that the disease can successfully propagate among the susceptible population, and the larger the value the more likely the spread could result in an epidemic. Therefore, the interest of epidemiologists and scientific community is to keep this parameter under the unitary value. Dealing with indoor spaces where a single infected spends time with a certain number of susceptibles (i.e., I=1), the reproduction number is equal to the number of new cases, and Equation (4.6) becomes:

$$R_{A0} = (N - 1) * P_{I_{W-R}} \tag{2.6}$$

Where N is the total number of people sharing the ventilated space (i.e., N=S+I), and P_I is the individual infection probability from Equation (2.4).
From the Equation (2.4), it can be seen that Wells-Riley model considers the whole airborne transmission route. First of all, quanta generation rate q is related to the phase of infectious droplet nuclei production. It represents the rate at which these hypothetical infectious packets are exhaled into the indoor environment by the infected subject. Then, ventilation rate Q characterizes the phase of particles transport and dispersion in the indoor air. Its value quantifies dilution and removal rate of quanta. Finally, breathing flowrate p indicates the phase of inhalation and accumulation of quanta in the respiratory tract. The intake dose is the overall outcome of the entire process.
Parameters such as ventilation flowrate Q and exposure time t_{exp} depend on the considered place and situation. Usually in airborne infection risk assessments, a single infected person is considered sharing the indoor environment with other susceptibles. This is consistent with typical situation in healthcare settings, where health personnel treats isolated patients. For COVID-19 this assumption may not be verified in real situations, due to potential presence of several asymptomatic subjects. As regards q and p, they are related to personal factors, above all the activity level. These last two parameters are presented in the following sub-paragraphs.

2.1.1.1 Pulmonary ventilation rate (p)

Pulmonary ventilation rate p is the parameter which characterizes the inhalation phase by the vulnerable receptor. It is the air volume flowrate that an average individual inhales during his breathing activity. Usually, inspiration and expiration are considered to have similar flow dynamics, for this reason we generally talk about breathing flowrate. It is the product of tidal volume V_{br}, i.e., the volume of exhaled/inhaled air at each breath (m^3), times breathing frequency N_{br}, i.e., the number of breaths in an hour (breaths/h) [29].
In the matter of risk assessment, the exhalation process is implicitly included in quanta generation rate q. On the other hand, the inhalation phase is very important from the exposed subject point of view. In fact, continuous breathing cycles during exposure to a certain

quanta level in an enclosed space, lead to accumulation of virus-laden particles in the respiratory tract. Inhalation determines the overall intake dose and the consequent airborne infection risk.
The values of this parameter are well-known and are a function of the subject activity level. As said in §1.2.1, generally, for sedentary activities or standing position, p ranges between 6 l/min and 10 l/min (i.e., equivalently, from 0.36 m^3/h to 0.60 m^3/h) [7]. Average values for different activity levels are reported in Table 2.1.

Table 2.1 Pulmonary ventilation rate for different activity levels.
Source: adapted from [29]

PERFORMED ACTIVITY	Inhalation rate p [m^3/h]
Resting	0.49
Sedentary activity/Standing	0.54
Light exercise	1.38
Moderate exercise	2.35
Heavy exercise/Sport activity	3.30

The aforementioned breathing flowrates are mean values between male and female individuals [29]. For activities that lie between the indicated levels, the average of two subsequent values can be considered (e.g., a mean value between 0.54 and 1.38 m^3/h for very light exercise).

2.1.1.2 Quanta generation rate (q)

This parameter represents quanta emission rate from the infected source by exhalation. Being a hypothetical dose unit, it cannot be determined with direct methods, but it must be calculated through a backward use of Equation (2.4) on real documented outbreak cases, for a specific respiratory disease. This epidemiological method is called *retrospective* analysis [23], [30]. This calculation can be carried out only with complete information about the real indoor environment where the outbreak burst, such as:

- volume and dimensions of the space (V)
- total number of involved people (N), especially how many were infected sources (I) and how many susceptibles (S)
- type of ventilation system and outdoor air change rate (ACH)
- type of performed activity, which defines the inhalation flowrate (p)
- total exposure time (t_{exp})
- number of new infection cases (NC) among the susceptible population.

The ratio between new infections (NC) and initial number of susceptible people (S) is defined as the *attack rate* of the considered outbreak. It is substituted into the infection probability P_I and quanta generation rate q of the disease is easily calculated from Equation (2.4) [25].

The backward calculated *q* considers implicitly many complexities of the airborne transmission pathway, that were mentioned at the beginning of the chapter: gravitational settlement of larger droplet nuclei; biological decay of airborne pathogens (i.e., viability loss); infectivity and host-microorganism interaction; respiratory deposition of the infectious particles. All these controversial aspects are someway included in the parameter [3], [25]. Nevertheless, if, for example, biological decay or gravitational deposition rate are explicitly considered in the backward evaluation of *q*, the latter will not contain that information. In this case, infection risk assessments should take it into account (see §2.1.4).
For most well-known respiratory diseases, many historic outbreaks are available for evaluating the quanta generation rate *q* of the specific pathogen. Table 2.2 shows *q* ranges for viruses and bacteria that are or are believed to be airborne transmissible (also mentioned in §1.4).

Table 2.2 Range of quanta emission rates for different respiratory diseases.
Source: adapted from [30]

RESPIRATORY DISEASE	**Quanta generation rate *q* [quanta/h]**	***Notes***
Rhinovirus	1÷10	-
Influenza	0.029÷630	-
Measles	~90÷8640	-
SARS-CoV-1	10÷300	-
Tuberculosis	1.25÷226	*Normal respiratory activities*
	250÷30840	*Aerosol-generating procedures*

The previous table is taken from a manual about an airborne infection risk calculation tool developed by some researchers during the last year [30]. The authors made an accurate review of previous published risk modelling studies and got possible values of *q* for the most important airborne pathogens. The reported range goes from the minimum to the maximum values found in different works. The lower part of the interval is related to light respiratory activities (tidal breathing, speaking normally, etc.), while the higher part refers to more intense exercises (speaking loudly, singing, heavy breathing, etc.).
Parameter *q* expresses the aggressiveness of a certain disease and the strength of the infected source. For example, measles is a really aggressive pathogen, since it has the largest quanta production rate for normal breathing activities. This means that, if an infected subject shares an indoor space with susceptible people, measles may easily spread causing secondary infections. On the other hand, rhinovirus appears to be a weak airborne pathogen. However, in the case of tuberculosis, Table 2.2 reveals that special medical procedures, applied during patients treatment, can lead to higher quanta emission rate from the source, due to elevated generation of aerosol. These situations are called *superspreading events*.

As regards SARS-CoV-2, there have not been many available documented outbreaks so far, since it is a novel virus. Buonanno et al. (2020) propose a forward emission approach in two subsequent works [23], [29]. In the first paper, the authors explain the method to determine *q* for novel coronavirus [29]. Starting from the viral load in the sputum (expressed in viral RNA copies per ml) and knowing the concentration of different-sized droplets from various respiratory activities, the quanta generation rate can be determined through a corrective coefficient of infectivity that allows the conversion from viral RNA copies to quanta. This factor is not currently known for SARS-CoV-2, but the authors claim that values for SARS-CoV-1 can be used, thanks to the similarity between these two pathogens. In the later publication, the authors applied the method with a Monte Carlo simulation, taking into account the variations of input data [23]. In this way, they obtained a probability density function (*pdf*) for quanta emission rate *q*, concerning different respiratory activities. The outcomes are log-normal distributions for SARS-CoV-2 characteristic emission rates. Therefore, they point out that parameter *q* should be considered as a range of values for a given exhalation mode, rather than a certain value. However, in case a scenario of exposure to a "certain emission rate" should be simulated, they suggest considering the 66th percentile of these density functions.

From low-emission to high-emission activities, *q* ranges between ~0.02 and 1500 quanta/h. Table 2.3 shows *q* values for SARS-CoV-2. Only recommended noteworthy points of log-normal distributions are considered. Emission scenarios are subdivided according to the type of respiratory activity and activity level.

Table 2.3 Quanta generation rates for SARS-CoV-2.
Source: adapted from [30, p. 17]

Activity Level	Respiratory activity	$\log_{10}(q)$		Median *q* [quanta/h]	66th perc. [quanta/h]	90th perc. [quanta/h]
		Avg.	Std. Dev.			
Resting	Oral breathing	-0.43	0.72	0.37	0.74	3.11
Standing		-0.37	0.72	0.43	0.85	3.57
Light exercise		0.02	0.72	1.05	2.07	8.76
Heavy exercise		0.40	0.72	2.51	4.97	21.0
Resting	Speaking	0.24	0.72	1.74	3.46	14.6
Standing		0.33	0.72	2.11	4.19	17.7
Light exercise		0.70	0.72	4.99	9.88	41.8
Heavy exercise		1.07	0.72	11.7	23.2	97.9
Resting	Speaking loudly	1.05	0.72	11.2	22.2	93.9
Standing		1.08	0.72	12.1	23.9	101
Light exercise		1.50	0.72	31.6	62.7	265
Heavy exercise		1.88	0.72	75.0	149	628

Observing Table 2.2 and Table 2.3, a comparison of the infectious strength based on the emitted quanta can be carried out, which shows that SARS-CoV-2 has lower airborne infectivity than measles and tuberculosis, while it is more aggressive than rhinovirus, SARS-CoV-1, and influenza.
In order to validate their method, in the second paper [23], Buonanno et al. (2020) carried out a backward calculation of *q* through a retrospective analysis of two outbreak cases, one at a restaurant in Guangzhou (China), the other at a choir rehearsal in Skagit (USA). For the first case, a quanta emission rate of 61 quanta/h was obtained, and it falls between 90th and 95th percentile of the probability density function of *q* characteristic of speaking during light activity level, typical of having a meal at restaurant. For the second case, the resulting value of 341 quanta/h falls between 90th and 95th percentile of the probability density function of *q* for singing or speaking loudly during light exercise; it can be seen that these values are consistent with those calculated.

Once *q*, *p*, and the features of the considered exposure scenario in an indoor space have been defined, airborne infection probability can be easily determined through Wells-Riley model (Equation (2.4)). Anyway, it is a very simple model, which rarely gives satisfactory results. For this reason, later works tried to improve the model, overcoming some inherent limitations related to initial hypotheses.

2.1.2 Gammaitoni-Nucci model

The first modification to Wells-Riley model was proposed by Gammaitoni and Nucci in 1997 [25], [27]. In their model, the assumption of well-mixed room air is still applied, but the differential Equation (2.1) on quanta concentration balance is solved under non-steady state conditions. A time-variable quanta concentration is determined rather than assuming it instantaneously reaches the saturation level, i.e., the steady-state condition. This global expression was obtained for concentration of quanta in transient state:

$$C_{ts}(t) = \frac{qI}{\lambda V} + \left(C_0 - \frac{qI}{\lambda V}\right) * \mathrm{e}^{-\lambda t} \tag{2.7}$$

Where C_{ts} is quanta concentration under time-variant regime [quanta/m^3], q is quanta generation rate [quanta/h], I is the number of infected subjects, V is the volume of the indoor space [m^3], C_0 represents the initial quanta concentration in the room at time t=0 [quanta/m^3], t is the exposure time [h], λ is infectious quanta removal rate or air disinfection rate [h^{-1}]. In this last parameter lies another difference between Gammaitoni-Nucci and Wells-Riley approaches. Gammaitoni-Nucci model consider that quanta removal is achieved not only through the ventilation rate, represented by air change per hour (*ACH*), but also with other mechanisms or control measures such as biological decay, gravitational deposition,

ultraviolet irradiation, particle filtration (see §2.1.4). This advanced model is more realistic than Wells-Riley model, because, when the infected person start emitting quanta at time t=0, it will take some time to reach quanta concentration at the saturation level.
Considering the time weighted average quanta concentration in the room, the airborne infection probability is calculated through Gammaitoni-Nucci equation:

$$P_{I_{G-N}} = \frac{NC}{S} = 1 - \mathrm{e}^{\left(-\frac{pqI}{V} * \frac{\lambda t + \mathrm{e}^{-\lambda t} - 1 - \left(\frac{\lambda V C_0}{qI}\right) * \mathrm{e}^{-\lambda t} + \left(\frac{\lambda V C_0}{qI}\right)}{\lambda^2} \right)} \quad (2.8)$$

Where P_I is the infection probability (it can be expressed by percentage value) and the other symbols have the same meaning as in Equation (2.7). Equation (4.6) shows that the intake dose in the exponential term is correlated to a quanta concentration variable over time.
Gammaitoni-Nucci model can be used to calculate the reproduction number R_{A0}. It is sufficient to substitute the probability term in Equation (2.6) with the expression in Equation (4.6), for the case with a single infected in the room.
Retrospective analysis for the backward calculation of quanta emission rate q can be done also employing this model. Especially for outbreak cases characterized by short exposure times, Gammaitoni-Nucci equation should be used to make an accurate evaluation of q. In fact, Wells-Riley model considers steady-state quanta concentration, which remains higher than values given by Equation (2.7), above all in the first exposure period. This means that Wells-Riley equation underestimates the actual quanta emission rate of the analysed situation.
On the other hand, in infection risk prediction (*prospective* analyses of exposure scenarios), Wells-Riley model is conservative, namely it will overestimate the probability of infection compared to Gammaitoni-Nucci one. This approach has been considered for these assessments in various researches [23], [27], [29], [31]. For example, Knibbs et al. used this model to calculate airborne infection risk for different diseases, in typical healthcare settings within a large teaching hospital [31].
Despite the improvements on time variability of infection probability, Gammaitoni-Nucci model keeps the assumption of well-mixed environment, so it does not adequately evaluate the risk on spatial basis.

2.1.3 Rudnick-Milton model

Rudnick and Milton proposed a modified Wells-Riley equation in 2003 [25], [28]. They refined two weak points of the original model: steady-state conditions and the necessity to know the outdoor air supply rates. The latter are usually difficult to measure and often vary during the exposure time. Their model works both in steady-state and transient condition

like Gammaitoni-Nucci one. Moreover, it does not require the measurement of the air exchange rate. However, Rudnick and Milton maintained some assumption of the original model: well-mixed indoor environment and quanta removal rate driven only by fresh air flowrate, neglecting other mechanisms and engineering techniques.
The principle on which this model is based is that a susceptible individual must inhale air that has been previously exhaled by an infected subject, sharing the same environment, to contract the disease. Exhaled breath is the vehicle of infectious particles, as it contains a certain quanta concentration. The fraction of inhaled air previously exhaled by another individual, is called *rebreathed fraction*.
Their strategy is to determine this fraction by monitoring continuously the CO_2 concentration in the environment. Human exhaled breath contains almost a concentration of 40000 ppm of CO_2, while outdoor air has a concentration value of 400 ppm. Without other CO_2 sources than human subjects, it can be considered a marker of exhaled breath. Therefore, the rebreathed fraction can be determined with CO_2 level measurements in the enclosed space, assuming well-mixed air, as shown by the following equation:

$$f = \frac{V_e}{V} = \frac{C_{CO_2} - C_{outd,CO_2}}{C_a} \tag{2.9}$$

Where f is the rebreathed fraction [-], V_e is the equivalent volume of expired air contained in the whole environment [m^3], V is the volume of the room [m^3], C_{CO2} is the measured concentration of CO_2 in the environment [ppm], $C_{outd,CO2}$ is the volume fraction of CO_2 in the outdoor air [ppm], C_a is the volume fraction of CO_2 added to exhaled breath [ppm].
In infection risk assessments a certain exposure time is considered: the time-weighted average rebreathed fraction ($\bar{f}$), can be computed easily by integrating f over time and dividing by the elapsed time [28]. In this way, it is possible to perform probability calculation under non-steady-state conditions.
The susceptibles intake dose over the exposure time can be calculated through the time-weighted average infectious quanta concentration in the ventilated space:

$$\bar{C} = \frac{\bar{f} I q}{N p} \tag{2.10}$$

Where $\bar{C}$ is average quanta concentration [quanta/m^3], $\bar{f}$ is the average rebreathed fraction, I is the number of infected sources, N is the total number of people in the space, q is quanta emission rate [quanta/h], p is the breathing rate [m^3/h]. As it can be seen from Equation (2.10), quanta concentration is equal to the concentration of quanta in the exhaled breath of infectors (q/p) multiplied by the volume fraction of air in the space that was exhaled by infectors ($\bar{f}I/N$) [28].

Finally, we can obtain the intake dose and calculate the infection probability through Rudnick-Milton equation:

$$P_{I_{R-M}} = \frac{NC}{S} = 1 - \mathrm{e}^{\left(-\frac{\bar{f}Iqt_{exp}}{N}\right)} \tag{2.11}$$

Where P_I is the infection risk, t_{exp} is the total exposure time [h], and the other symbols have the same meaning as before. Equation (4.6) can be used in retrospective analyses to calculate q, and to determine the reproduction number R_{A0} substituting it into Equation (2.6).
The main advantage of Rudnick-Milton model is that it simply relies on measurements of CO_2 concentration in the indoor space, rather than outdoor air ventilation rate. Actually, continuous monitoring of CO_2 level corresponds somehow to indirectly measure the time-variable amount of outdoor air sent to the indoor space. Anyway, the required measure instruments are relatively cheap, so this approach seems to be winning. The model has been applied in some works [28], [32].
Despite these good aspects, Rudnick-Milton model presents the same weakness as Wells-Riley and Gammaitoni-Nucci models: since it assumes well-mix air, it does not give heterogeneous infection probability with an accurate spatial resolution.

2.1.4 Risk models: masks and engineering control measures

Quanta-based model can be modified considering the contributions given by the use of masks and other control measures in reducing the airborne infection risk. In this paragraph, it will be explained how these two aspects can be incorporated in the risk equations.
As regards surgical masks and respirators, in §1.3.2 the possibility of reducing both the emission and inhalation of infectious particles through their use has been described. The wearing of these devices is modelled through the application of a corrective scaling factor both on the infected person generation rate q, and on susceptibles breathing rate p [25], [27]. The overall result is the decrease of the intake dose and infection probability. Considering that personal protective devices have a filter efficiency X [%] and a face-seal leakage factor Y [%], it is possible to determine their actual filter efficiency Z [%] using this relationship:

$$Z = X - \frac{X * Y}{100} \tag{2.12}$$

Then, the mask scaling factor f_{mask} [%] is defined as:

$$f_{mask} = 100 - Z \tag{2.13}$$

This is the corrective factor that must be applied to q and p in the infection probability equations (i.e., Equations (2.2), (2.4), (2.8), (2.11)).
Some masks and respirators have different filtration efficiencies X depending on the flow direction. For example, surgical masks are better at reducing quanta emission rather than quanta inhaled. In these cases, two global efficiencies, one in generation phase Z_{ext} (i.e., from mouth towards the environment), the other in inhalation phase Z_{int} (i.e., from indoor environment towards the mouth), can be defined, by obtaining two corrective factor $f_{mask,ext}$ and $f_{mask,int}$ to be applied to q and p, respectively.
As biological and fluid dynamic behaviour of infectious droplet nuclei are concerned, as well as the role of engineering and environmental controls, all these aspects contribute to quanta removal in the indoor space and to subsequent reduction of their concentration in the air. Therefore, they can be included in quanta removal rate term of the infection risk equations [25], [27]. Wells-Riley model considers only ventilation rate Q as a removal driver, while Gammaitoni-Nucci model integrates all types of mechanisms that lead to a reduction of quanta concentration, whether natural or engineering (see §2.1.1 and §2.1.2). The major mechanisms contributing to quanta removal are:

- ventilation rate with outdoor air (engineering)
- biological decay or viability loss in the airborne state (natural)
- gravitational deposition (natural)
- UV germicidal irradiation (engineering)
- filtration (engineering)

The removal efficiencies of these processes or devices are all expressed in term of *equivalent air changes per hour*, and the global air disinfection rate is given by this relationship:

$$\lambda = \lambda_{vent} + \lambda_{viab} + \lambda_{dep} + \lambda_{UV} + \lambda_{filt} \tag{2.14}$$

Parameter λ is the global removal rate [h^{-1}], λ_{vent} is the removal rate from ventilation [h^{-1}], λ_{viab} is the inactivation rate from viability losses [h^{-1}], λ_{dep} is the removal rate from gravitational deposition [h^{-1}], λ_{UV} is the removal rate associated to UV irradiation [h^{-1}], λ_{filt} is the removal rate from filters [h^{-1}].
The deposition rate depends on droplet nuclei size, while airborne viability loss is characteristic of the considered pathogen. On the other hand, we can give an expression to the equivalent air changes for the engineering controls. For ventilation, λ_{vent} corresponds to the actual air changes per hour ACH. For filtration devices in the space, or in the air handling unit, λ_{filt} can be defined as:

$$\lambda_{filt} = \frac{Q_{filt} * \eta_{filt}}{V} \tag{2.15}$$

Where Q_{filt} is the air flow rate across the filter [m^3/h], V is the room volume [m^3], η_{filt} is the filtration efficiency [-].
For UVGI devices, the formulation is almost identical:

$$\lambda_{UV} = \frac{Q_{UV} * \eta_{UV}}{V} \tag{2.16}$$

Where Q_{UV} is the air flow rate across the UV lamp [m^3/h], V is the room volume [m^3], η_{UV} is the germicidal efficiency [-].
The global removal rate λ can be used directly in Gammaitoni-Nucci model, i.e., Equation (2.8), while in Wells-Riley model it must be multiplied by V to obtain an equivalent ventilation rate Q to be inserted in Equation (2.4).
A particular aspect is worthy of being highlighted regarding viability loss and deposition rate in retrospective analysis for the back-calculation of quanta emission term q. If these mechanisms are not considered explicitly in the evaluation, then q value implicitly contains this information. Conversely, if they are explicitly integrated in the risk equation, q does not include them. This difference must be considered in risk prediction calculations.

The risk models presented above, allow quick, simple assessment of infection probability for different exposure scenarios in indoor environments. However, they present some limitations [25]:

- they are based on "quantum" concept, a hypothetical dose unit. Quanta emission rate q is backward calculated from documented outbreaks and it consider implicitly many complexities that characterize the airborne transmission route, especially pathogen infectivity, pathogen-host interaction, and respiratory deposition of particles. This retrospective evaluation does not consider the diversity between individuals, so quanta generation rate gives an average image of the pathogen and human being behaviour. This means that q calculated from a certain case, may not be really suitable for other exposure scenarios, causing implicit errors in risk assessment.
- they consider only the airborne route. In fact, q is determined from outbreaks for which only airborne infections are thought to have happened.
- they do not consider the spatial heterogeneity of infection risk, since they assume well-mixed room. In reality, spatial distribution of infectious particles (or quanta, for these models) is of outstanding importance in risk assessments. Susceptible people close to the infected source are more exposed to exhaled quanta than people far away. Anyway, the quanta generation rate q is calculated considering well-mixed air, so it already contains this type of error.

In the following paragraph, newer risk models called dose-response models are presented, which can be used in place of quanta-based ones.

2.2 Dose-response models

Dose-response models are risk formulations built from experimental infectious dose data [3], [25]. A susceptible population is exposed to different doses of the considered pathogen, and individual responses is then registered (i.e., observing what fraction of population becomes infected). In this way, a relationship for pathogen-population interaction can be constructed through data interpolation, obtaining specific fitting parameters. The empirical infection tests are usually conducted on animals (i.e., *animal test*), rarely on human subjects. Human tests, on this matter, are difficult to execute for ethical issues, and because some pathogens are too dangerous to be aerosolized (e.g., SARS coronaviruses).

The inhaled doses refer to the actual quantity of pathogens rather than hypothetical units as quanta [26]. This means that, when an infectious dose is administered to the experimental population, microbiologists exactly know the quantity of "infectious particles", i.e., number of microorganisms or number of acid nuclei copies (DNA/RNA copies). These experimental settings are nowadays available thanks to the advancements in molecular diagnostics field.

The procedure of the epidemiological experiments consists of undergoing the tested susceptibles to increasing infectious doses of aerosolized pathogens. The fraction of population becoming infected is registered and the current dose is given a name related to this fraction. For example, the infectious dose that cause infection to half of the population, is called ID_{50}.

Dose-response models can be divided into deterministic and stochastic [25]. Deterministic models are purely empirical and are based on the tolerance dose concept. Through experimental data, the frequency distribution of the tolerance dose of the tested subjects is sketched. The derived cumulative distribution describes the dose-response relationship between pathogen and population, and it also represents the infection risk. Figure 2.2 shows an example of tolerance dose distribution in deterministic dose-response models.

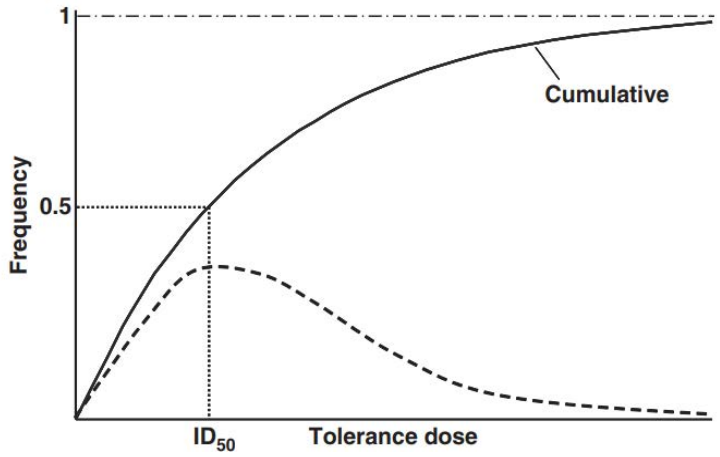

Figure 2.2 Frequency distribution of tolerance dose and cumulative infection risk
Source: [25, p. 5]

The tolerance dose concept allows to consider the variability in the immunological status and sensitivity to pathogen between different tested individuals. Therefore, many complexities of the airborne route, including pathogen infectivity and pathogen-host interaction, are considered explicitly in these experimental studies. The most known deterministic models use lognormal, log-logistic and Weibull distributions.
On the other hand, stochastic models are semi-empirical. The main principle is that any intake dose may cause illness in a susceptible individual, if pathogens manage to reach the favourable infection site in the respiratory tract. Deterministic models consider the intake dose as an exact value, equal to the aerosolized quantity of pathogens provided to the tested population. Stochastic models involve a double probability: the aerosolize dose of pathogens is randomly distributed in the air, and the actual intake dose depends on successful respiratory deposition. The first probability gives an estimation of the exposure level of a subject (i.e., infectious material available in the breathing zone), the second conditional probability gives an estimation of the intake dose. Based on these ideas, some stochastic models have been developed. The following one is the *exponential dose-response model*:

$$P_I = 1 - \mathrm{e}^{-rD} \tag{2.17}$$

Where P_I is the infection risk, D is the intake dose, r is a constant that expresses the chance of a pathogen to survive inside host respiratory tract and initiate infection. In other words, r represents the infectivity of the pathogen.
Exponential model does not consider the variability in host sensitivity to pathogen as r is a constant value. Another model was developed providing a beta-distribution to r values to compensate for this shortcoming. It is the *beta-Poisson dose-response model*:

$$P_I = 1 - \left(1 + \frac{D}{\beta}\right)^{-\alpha} \tag{2.18}$$

Where P_I is the infection risk, D is the intake dose, α and β represent pathogen infectivity, pathogen-host interaction, and variability in immune status of susceptibles.
Equation (2.17) and (4.6) are empirical relationships, where r, α and β are the fitting parameters. They express pathogen infectivity and its capacity to overcome host defences.
Dose-response models present some advantages compared to quanta-base models:

- they rely on actual quantities of pathogens, expressed in nucleic acid copies concentration, not a hypothetical dose unit such as infective quanta.
- more accuracy in infection risk evaluation, since they are based on real experimental data on infections caused by a specific pathogen. In this case, the fitting parameters characterise the pathogen, rather than quanta generation rate q. Each respiratory disease has its own dose-response model.

- many complexities of the airborne transmission route are considered explicitly in the equations. For example, infectivity and pathogen-host interaction are represented by the fitting parameters. In this way, the intake dose *D* is distinct from the infectivity term. Conversely, in the models presented in §2.1, the inhaled dose is expressed in quanta, which, in turn, implicitly contain the information on infectivity, host sensitivity and interaction between organisms.
- they can also be used to calculate the infectious source strength of an outbreak in terms of the quantity of pathogen, rather than the number of quanta, in retrospective analysis.
- the other infection transmission routes, i.e., droplet and fomite route, can be included in a dose-response model. To assess the combined effect of multiple exposure pathways, the sum of all the corresponding intake doses can be substituted into the dose-response model.

Dose-response models seem to be far more powerful than quanta-based models in predicting infection risk accurately, especially for the possibility to distinguish the different transmission routes. However, dose-response approach has also some defects that penalise their use in quick risk assessment studies:

- their construction requires a rich infectious dose database for the interested pathogen.
- for many respiratory diseases, data come from animal tests. Therefore, an interspecies extrapolation of infectivity data is necessary for subsequent application to human beings. Unfortunately, immune responses and host-pathogen interactions often differ between species.
- the accurate estimation of the intake dose *D* is possible only if the different sizes of droplet nuclei are considered. We should know the volume density of expiratory droplets at a given point of the room and the concentration of pathogens in the respiratory fluid. Moreover, viability loss rate must be considered in the transport phase. In this way, estimated exposure level and intake dose will be more reliable.

The last point highlights that dose-response models can be correctly used only if aerosols different size is considered, and infection risk is evaluated with a certain spatial and temporal resolution. Risk assessors often assume well-mixed environment even for these models. They consider a single size for droplet nuclei, which are uniformly distributed in the air transporting a constant nucleic acid copies concentration. In this way, intake dose is a rough estimation. Furthermore, the biological decay of airborne pathogen remains an important issue also for dose-response models.

However, both quanta-based models and dose-response models under well-mixed air assumption do not provide the infection risk with a high spatial resolution, so they are far from producing realistic outcomes. In the following paragraphs, the developments of other techniques in this direction are presented.

2.3 CFD modelling and experimental measurements

In the previous paragraphs we have seen that assuming a well-mixed environment leads to inaccurate infection risk predictions. A good risk model should provide different infection probabilities according to the position in the room, with infection risk depending on the proximity to the infective source.

In real situations, infectious particles are not distributed uniformly in the indoor air, but there are concentration gradients. The knowledge of the spatial distribution of the aerosols is important to give an adequate spatial resolution to risk calculation. The aim is to determine the concentration of pathogens in different points of the room volume. Two methods are available for this purpose: experimental measurements and *computational fluid dynamics* (CFD) modelling [5], [7], [25]. Both strategies permit to detect particles concentration in different positions in the analysed domain. They can be employed alone or in combination with risk models hereinabove.

Experimental tests, related to human infection issues, are nowadays a powerful technique thanks to the availability of high-resolution particle capture/visualization methods (e.g., particle image velocimetry PIV, smoke particles visualization, Schlieren imaging technique, etc.) and advanced air samplers [5], [7]. The improvement in the measurement instruments makes the outcomes reliable.

Experiments are set up to simulate the dispersion of airborne pathogen in the enclosed space. Obviously, aerosolized pathogens must be substituted by a surrogate. Smaller virus-laden droplet nuclei behave like a gas, so a tracer gas is used as dispersed phase in the air. On the other hand, larger droplet nuclei are replaced by aerosols produced by special nebulizers. These machines allows the user to generate monodispersed particles, i.e., particle of uniform, desired aerodynamic diameter. Several consecutive tests are required to analyse the influence of particle size on spatial distribution of pathogens. Tracer gas or aerosol are released into the space, where they spread over the available volume, and, finally, concentrations are measured and registered by instruments located in different points of the room.

CFD modelling is carried out through software on calculators with high computational power [5], [7], [25]. CFD models allow to characterize the motion field of a fluid in a given domain, solving the well-known Navier-Stokes equations numerically (i.e., mass, energy, and momentum balances). CFD programs work with high temporal and spatial resolution, since the geometrical domain is discretized into thousands, or even millions, of infinitesimal cells. CFD and experiments are not worlds apart: in fact, experimental measurements are usually performed to validate CFD results and verify the correct definition of the model.

As regards the airborne infection matter, air is the continuum phase that transports the aerosolized pathogens, constituting the dispersed phase. In CFD models, pathogens are substituted by tracer gases. The user must define the geometrical domain and the boundary conditions of the analysed scenario. Results are obtained running the simulation on the software. At the end, the motion field is solved, that is the thermophysical properties of the

fluid are calculated at each point of the room volume. These properties can be temperature, pressure, density, air velocity, gas concentration. The last represents pathogens concentration in real situations.
Both experiments and CFD models have the advantage of providing realistic results regarding the spatial distribution of infectious particles in actual exposure situations. CFD provide higher spatial resolution than experiments, since the latter rely on a limited number of instruments placed in some key points of the room. Nevertheless, these techniques present some drawbacks.
Experimental tests are time-consuming. Time is required to locate the measurement instruments and devices, and the experiment session itself may last for prolonged periods. In addition, measurement instruments are expensive.
CFD models require huge computational effort, according to the desired set resolution. This implicates that days or weeks may be necessary to conclude a simulation. Moreover, the user must have a good knowledge to define properly the boundary conditions of the problem. Finally, the accuracy of CFD results depends also on the applied turbulence model [3]. Turbulent regime still remains research matter for fluid dynamics. More sophisticated, accurate turbulence model means higher computational effort and time.
Once spatial concentration of pathogens surrogate is known, the infection risk can be evaluated in two ways. The first possibility is to directly calculate the *intake fraction*, i.e., the proportion of exhaled pathogen mass from the infected individual that is inhaled by the exposed individual [7]. This parameter is equivalent to the *rebreathed fraction* (*f*), used in Rudnick-Milton model (see §2.1.3). Intake fraction is defined as:

$$IF = \frac{\int_0^{t_{inh}} y_{inh}(t)\dot{m}_{inh}\mathrm{d}t}{\int_0^{t_{exh}} y_{exh}(t)\dot{m}_{exh}\mathrm{d}t} \tag{2.19}$$

Where *IF* is the intake fraction, y_{inh} is the inhaled pollutant mass fraction [ppm], y_{exh} is the exhaled pollutant mass fraction [ppm] by the infected source, $\dot{m}_{inh}$ is the mass flow rate of inhaled air [kg/h], $\dot{m}_{exh}$ is the mass flow rate of exhaled air [kg/h], t is time [h], with t_{inh} exposure or total inhalation time of the susceptible individual and t_{exh} total release time of the infected individual. If t_{inh} and t_{exh} are equal, i.e., infected and susceptible individuals enter and exit the room at the same moment, we can simply take a global exposure time t_{exp}.
Equation (4.6) shows that intake fraction compares total inhaled pathogens with total released pathogen in the exposure scenario. Considering susceptible individuals located at different distances from the infected source in the indoor environment, those with higher *IF* will be more likely to get sick. So, *IF* values give an idea of the spatial heterogeneity of infection risk within an enclosed space, but it does not quantify the infection probability.
To obviate this problem, another possibility is to integrate CFD or experimental results with an infection risk model. The equivalent intake dose of pathogens is calculated based on the

registered concentrations of tracer gas or aerosol. Both dose-response and quanta-based models can be used. Although quanta are theoretical packets of infectious particles, in CFD analyses they can be replaced by tracer gas which is released by the source at an emission rate equal to q (boundary condition). Then the intake dose is evaluated in terms of quanta and infection risk is obtained with Wells-Riley or Gammaitoni-Nucci model. The best combination to do a perfect risk assessment lies on integrating CFD with a dose-response model for the specific pathogen, better still if the biological decay law was known. In this case the infection probability derives from actual intake doses, not hypothetical ones.

As regards airborne infection risk in the general topic of indoor air quality (IAQ), in scientific literature there are many research works founded on CFD modelling and experimental measurements. Villafruela et al. [33] constructed a CFD model and gathered experimental data to verify the suitability of displacement ventilation system in hospital rooms with bedded patients, at different air change rates (6 h^{-1}, 9 h^{-1}, 12 h^{-1}). They calculated intake fraction based on particles spatial distribution, and observed lock-up phenomenon, with high pathogen concentration at the breathing zone of the healthcare worker. Therefore, they concluded that for healthcare facilities, displacement ventilation should be avoided, in favour of mixing ventilation. Zhu et al. [34] proposed an integration between CFD modelling and Wells-Riley equation to numerically assess the risk of airborne influenza transmission in bus microenvironment. They replaced quanta of influenza with computational droplet nuclei with an aerodynamic diameter of 5 μm, considering a generation rate q of 67 quanta/h (typical value used for influenza). The purpose of the research was determining the influence of the airflow patterns on the infection risk, comparing 3 scenarios for mixing ventilation, with different positions of air diffusers and exhaust vents, and a scenario for displacement ventilation. They proved that displacement ventilation system is suitable in containing infection risk in buses. They also analysed the role of recirculation and concluded that good filtration on the recirculated air has the same effect of supplying 100% of outdoor air. Another interesting study was done by Hathway et al. [35]. They did not directly assess the infection risk in indoor environments. First, experimental data were elaborated to verify their CFD model on the dispersion of pollutants or pathogens. Then, they introduced the concept of zonal source. It is fictitious representation of transient emitting source that moves inside the room over the exposure time. The transient source movements describe an action field, so they thought to replace this time and space variable behaviour with an average pathogen release performed by a zonal source that occupies this entire field. CFD simulations were run to validate this new depiction of an infected source in enclosed spaces. The results confirmed the suitability of their idea.

It is clear that CFD and experiments are the best way to observe the actual spatial distribution of airborne pathogens, but the above-mentioned disadvantages make them unsuitable for rapid risk assessments.

2.4 An intermediate approach: zonal risk model

As already explained in the previous paragraphs, simple risk models are based on the assumption of well-mixed environment, leading to homogeneous pathogens concentration throughout the available volume. Consequently, each susceptible individual undergoes the same infection probability, regardless of his proximity or distance from the infective source, and of airflow patterns. Nevertheless, the impossibility of reaching a perfect mixing in real environments leads to spatial variation of infection risk. CFD modelling is a strategy to calculate pathogens concentrations in detail at different positions of the room. However, it requires a significant computational effort.

Therefore, an intermediate approach is necessary to determine the infection risk accounting for the relative position of infected and susceptible people, and indoor airflows, which convey pathogens, or pollutants in general, across their preferential directions (effect of streamlines). The idea is to subdivide the environment into multiple zones (or cells), to achieve a spatial discretization of the domain. Each zone is considered as well-mixed, with a homogeneous concentration of infectious material [25]. Therefore, there is a single value for infection risk in a given zone, determined by risk equations shown in the previous paragraphs. The overall criterion can be called *zonal risk model*.

The zonal method can be applied with both quanta-based models and dose-response models. From here on, only concentration of infectious material in terms of quanta will be considered. There are some examples of zonal risk models in literature. Cavallini et al. [36] used a zonal model, called *segregated model* in the paper, to calculate infection risk in a multi-room office building. In this study, the premise is divided into 12 zones: 10 offices and 2 common areas, i.e., corridor and service rooms. The authors set a quanta concentration balance in each zone, considering the interzonal flowrates as vehicle of pathogens from one zone to the other.

The worthiest example of zonal risk modelling is offered by some researchers of the university of Leeds [37]. They propose to divide the entire environment into multiple zones and to couple Wells-Riley model with a zonal ventilation model. The discretization of the domain allows to evaluate the spatial variation of infection risk, while the zonal ventilation model is used to calculate interzonal airflow rates. These flows constitute the connection between different zones and carry quanta from one cell to the other. Figure 2.3 shows a schematic representation of the applied method.

As stated before, each zone is considered as well-mixed and a quanta concentration balance is established considering generation, ventilation removal and interzonal transfers. The balance is expressed in this way for the *i*-th zone:

$$V_i * \frac{\mathrm{d}C_i}{\mathrm{d}t} = q_i I_i - Q_{oi} C_i - \sum_k Q_{ik} C_i + \sum_k Q_{ki} C_k \qquad (2.20)$$

Where V_i is the volume of the zone [m^3], C_i is quanta concentration of the zone [quanta/m^3], q_iI_i is quanta generation rate in the zone [quanta/h], based on the number of infected people in the zone I_i, Q_{oi} is the exhaust airflow rate from the zone which removes quanta [m^3/h], Q_{ik} and Q_{ki} are the volume flow rates to and from adjacent zone k [m^3/h], respectively, and C_k is quanta concentration of the adjacent zone k [quanta/m^3].

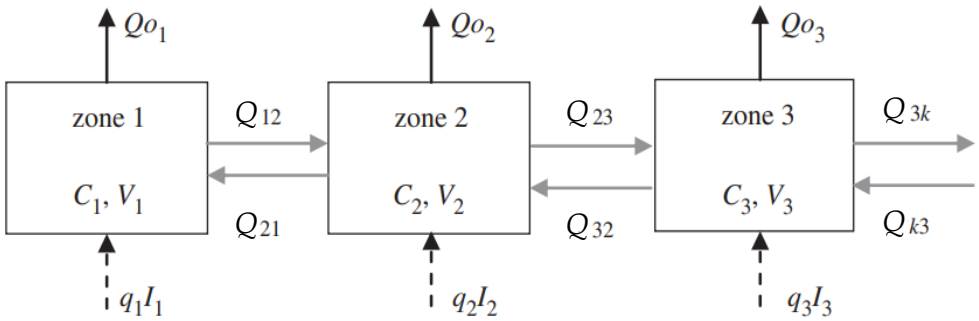

Figure 2.3 Schematic representation of zonal risk modelling.
Source: adapted from [37, p. S795]

The key parameters of this approach are represented by the interzonal flowrates Q_{ik} and Q_{ki}, and zonal ventilation model is necessary to calculate them. Once these flowrates are defined, quanta concentration in the zone can be calculated through the Equation (4.6), both under steady-state or transient condition. Finally, a homogeneous infection risk for susceptibles in the zone, is computed trough general Equation (2.2).
The method presented in this paragraph is really interesting as it gives more accurate outcomes compared to models based on well-mixed assumption, and, at the same time, requires less computational resources than CFD simulations. Assuming well-mixed environment, some information about the influence of proximity to the infective source and airflow patterns could be lost. Conversely, zonal risk models permit to consider these aspects. This is really important, because some observations may be done on air distribution system design (i.e., position of air diffusers and exhaust grills, which determine the airflow patterns).

In this thesis work, a zonal risk model is constructed starting from literature material [37]. The output of the model is the airborne infection risk from COVID-19, in a given indoor space. It was decided to use a quanta-based equation for the estimation of infection probability. This choice is consistent with the lack of dose-response relationships for SARS-CoV-2, since it is a novel pathogen. Secondly, the interzonal flowrates will be calculated through a specific zonal ventilation model developed by some researchers (see §3).
The following chapter will present the construction of the overall model, with great attention to the zonal ventilation model.

Chapter 3

Development of a zonal risk model

In this chapter the development of a zonal risk model is described. Its purpose is the evaluation of the airborne infection risk from COVID-19 in indoor environment, therefore the final output consists of the probability of becoming infected for a susceptible person which is in the same space of an infected source for a certain time.
The approach presented in §2.4 is followed. The indoor space of interest is partitioned into multiple zones or cells, and the airborne infection risk is calculated within each of them. The single zone is considered as well-mixed, so pathogen concentration is uniform in the sub-volume. In this way, the model enables to examine the spatial distribution of risk. These zones are not independent: two adjacent cells are in continuous communication, as there are interzonal airflows crossing the boundary surfaces, which are the drivers of the transfer of infectious particles from one zone to the other.
The model presented below, is split into two separate parts:

- application of ventilation zonal model. Based upon the applied discretization of the geometrical domain, this first step is implemented to calculate the interzonal airflow rates between the different zones.
- application of infection risk model. This second step is implemented to calculate the airborne infection probability. Pathogen concentration within each zone is evaluated through a balance equation, where the airflows calculated in the first part, are integrated. Finally, calculation is performed by a risk equation.

In the following paragraphs, the structure of each part is illustrated in detail.

3.1 The ventilation zonal model: POMA

A zonal model is used in the analysis of airflow and temperature distribution as an intermediate approach between multi-room models and CFD simulations.
Multi-room or nodal modelling is the simplest method. It considers perfect mixing for each room of a building, with homogeneous temperature, pressure, and density for room air. In this sense, a single room constitutes a node which is connected to the other rooms and to the outdoor environment by internal openings (internal doors), and openings in the envelope (doors and windows), respectively. This approach has the advantage to be user friendly in the problem definition and calculation procedure. However, it only provides bulk airflows between different rooms of the whole building. It does not give detailed information on temperature distribution and airflow patterns within a single room.
Conversely, CFD software allows the accurate definition of temperature distribution and interzonal airflows within a single room. This degree of detail is achieved through the

numerical resolution of Navier-Stokes equations for fluids motion. Nevertheless, this method requires user effort in terms of problem definition, and it is time-consuming from a computational point of view. Therefore, its application is restricted to single spaces with fixed boundary conditions over a limited time interval; its integration for problem with time-variable conditions with voluminous spatial domains, remains complicated.
A zonal model exploits the advantages of these extreme approaches. It provides more accurate results than nodal modelling, and it involves fewer computational resources than CFD. A macro-discretization of the domain through the partition of a room into different cells is the core of the method. A critical review describes the features and differences between zonal models developed in the last decades [38]. Figure 3.1 illustrates how partition of a room is performed by a ventilation zonal model. Figure 3.1(b) shows how different cells interact through the airflows crossing the boundary surfaces.

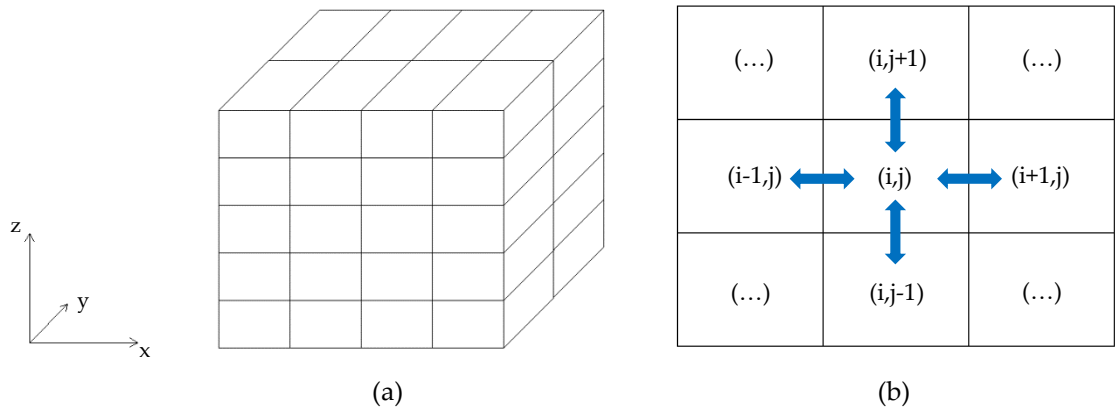

Figure 3.1 Zonal modelling approach. Example of a 3D-discretization of a room (a). Discretization shown on a plane (e.g., horizontal x-y, vertical x-z, etc.), with indication of interactions between cells, i.e., the airflow rates crossing the separation surfaces (blue double arrows) (b).

In this thesis work, the motion field of air in a confined space is determined starting from a ventilation zonal model called POMA (**Pr**essurized Z**O**nal **M**odel with **A**ir Diffuser) [39], [40]. This model is developed to deal with mechanically ventilated spaces. The basic assumption of the model are the following:

- the analysed volume is divided into parallelepiped or cube-shaped zones, and the discretization is coherent with a classical Cartesian coordinates system (see Figure 3.1). This means that the boundary surfaces separating one cell from the other, are all vertical or horizontal.
- the air is considered inviscid. The drag force at the boundary layer along the wall surfaces, is neglected. Consequently, the airflow rates are not affected by interaction between air and wall surfaces.

- air pressure is not uniform within each zone. A reference pressure P_{ref} is applied at the bottom, and then it is hydrostatically distributed, decreasing towards the top of the cell. Figure 3.2 shows this assumption.

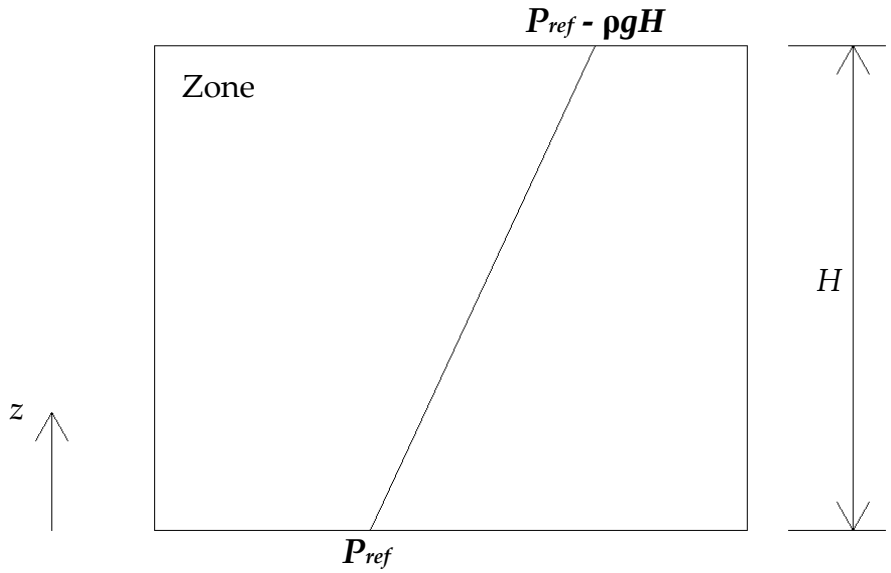

Figure 3.2 Pressure distribution of a zone.

Thus, at a generic height *z*, the pressure value can be determined by:

$$P_z = P_{ref} - \rho g z \tag{3.1}$$

Where *z* is the considered height [m], ρ is the density of air in the zone [kg/m^3], *g* is the gravitational acceleration [m/s^2], P_{ref} is the reference pressure of the zone [Pa], and P_z is the pressure at the considered point [Pa].

- air temperature (*T*) and density (ρ) are assumed to be well-mixed within each zone. Considering air as an ideal gas, pressure, temperature, and density are linked by the ideal gas law:

$$\frac{P_{ref}}{\rho} = R_{air} T \tag{3.2}$$

Where P_{ref} is the reference pressure of the zone [Pa], ρ is the density of air in the zone [kg/m^3], R_{air} is gas constant for air [J/(kg K)], and *T* is the absolute temperature of the air in the zone [K]. Equation (4.6) shows that density and temperature are assumed to be related to the reference value of the pressure hydrostatic distribution of the zone.

The parameter R_{air} is calculated as follow:

$$R_{air} = \frac{R}{MM_{air}} \tag{3.3}$$

Where R is the ideal gas constant equal to 8314 J/(kmol K), and MM_{air} is the air molar mass equal to 28.97 kg/kmol.

In each zone i, the mass and energy conservation are described by Equation (3.4) and (4.6):

$$\frac{\mathrm{d}M_i}{\mathrm{d}t} = \sum_{j=1}^{n_{zon}} \dot{m}_{ij} + \dot{m}_{sup} - \dot{m}_{rem} \tag{3.4}$$

$$\frac{\mathrm{d}E_i}{\mathrm{d}t} = \sum_{j=1}^{n_{zon}} q_{h_{ij}} + q_{h_{sup}} - q_{h_{rem}} \tag{3.5}$$

For both equations, n_{zon} represents the total number of zones in which the room is divided.
For the mass balance (Equation (3.4)), M_i is the air mass of the zone i [kg], t is time [s], $\dot{m}_{ij}$ are the mass flowrates crossing the boundary surface between zone i and j [kg/s], $\dot{m}_{sup}$ is the mass flowrate supplied to the zone [kg/s], and $\dot{m}_{rem}$ is the mass flowrate extracted from the zone [kg/s].
Regarding the energy balance (Equation (4.6)), E_i is the energy in zone i [J], t is time [s], $q_{h,ij}$ are the heat fluxes between zone i and j [W], $q_{h,sup}$ is the heat flux supplied to the zone [W], and $q_{h,rem}$ is the heat removed from the zone [W].
The aim of the model is the definition of the mass and heat exchanges between adjacent zones, represented by $\dot{m}_{ij}$ and $q_{h,ij}$, respectively. Their formulation depends on the type of boundary surfaces they cross.

3.1.1 Types of boundary surfaces

There are different types of boundary surfaces, according to how airflows and heat fluxes are modelled within the room. In this work, some simplifications are made, regarding particular airflows:

- thermal plumes from internal heat sources, like human bodies and electrical devices, are neglected.
- air jets from air diffusers are not modelled. We only consider supplied air term $\dot{m}_{sup}$ in the zones with air diffusers, while extracted air term $\dot{m}_{rem}$ in the zones where exhaust grilles are located.
- the drag force at the wall surfaces is ignored.

Based on the previous hypothesis, no *special* zones are present. The simple cells are called *normal* or *current* zones. Two types of boundary surfaces are identified:

- *normal boundaries*: they are crossed by airflows, with mass and heat transfer.
- *wall surface boundaries*: they are the portions of wall that delimit the outer zones. These surfaces are interested only by heat exchanges, no mass transfer occurs across them.

In the following paragraphs, the modelling of mass and heat transfer is shown, depending on the type of boundary.

3.1.2 Normal boundary: modelling of the airflows

Normal boundaries are air-to-air interfaces. The modelling of the interzonal airflows is based on the so-called *Power Law*. It could be considered as a simplification of the Navier-Stokes momentum equation which characterizes the fluid motion within the spatial domain.
According to this law, the mass flow is a function of the static pressure difference between two points located at opposite sides of the interface. This formulation is described by the following relationship:

$$\dot{m} = \rho k A \Delta P^n \tag{3.6}$$

Where $\dot{m}$ is the mass flow rate crossing the boundary [kg/s], ρ is the density of the airflow [kg/m^3], A is the area of the boundary surface [m^2], ΔP is the static pressure difference [Pa]. Power law equation is characterized by two constant parameters k and n. The former is the *flow coefficient*, representing the permeability of the surface to air mass transfer, and it is usually set at a value of 0.83 m/(s Pa^n). The latter is the *flow exponent* with a value of 0.5 for turbulent regime and 1 for laminar. In this work, turbulent airflows is assumed.
Equation (4.6) is a general relationship. It takes different shapes depending on the orientation of the normal boundary. The following sub-paragraphs illustrate the formulations for horizontal and vertical interfaces, respectively.

3.1.2.1 Airflow across horizontal boundary

The objective is the calculation of mass flows across the horizontal interface separating two zones one above the other. The pressure difference between zones, at the height of the boundary, must be known to employ the Power Law (Equation (4.6)). Considering the hydrostatic distribution of air pressure within a cell, the reference pressure of the upper zone must be compared to the pressure at the summit of the lower one. This situation is shown in Figure 3.3. Each zone has its own reference system with origin at the bottom level. Indexes 1 and 2 to name the zones are arbitrary chosen to show an example.

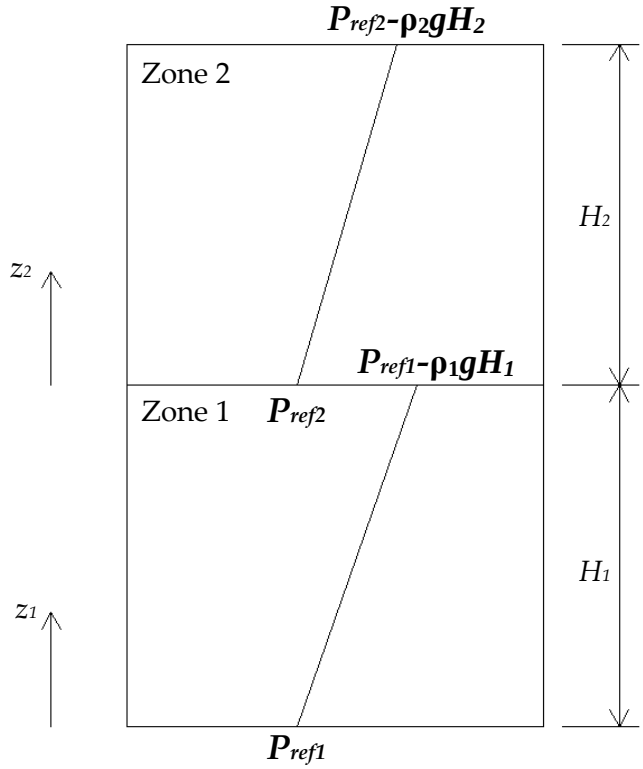

Figure 3.3 Horizontal normal boundary modelling.

The pressure difference across the horizontal boundary is given by:

$$\Delta P_{12} = P_{ref_2} - \left(P_{ref_1} - \rho_1 g H_1\right) \tag{3.7}$$

Where ΔP_{12} is the pressure difference across the interface[Pa], P_{ref} are the reference pressures [Pa], ρ_1 is the density of air of zone 1 [kg/m^3], g is the gravitational acceleration [m/s^2], and H_1 is the height of the lower zone [m].
And the mass flow can be determined using the Power Law:

$$\dot{m}_{12} = \rho k A_{horiz} \left|P_{ref_2} - \left(P_{ref_1} - \rho_1 g H_1\right)\right|^n \tag{3.8}$$

Where $\dot{m}_{12}$ is the mass flow across the boundary [kg/s], ρ is the density of air of the zone from which the flowrate comes, A_{horiz} is the area of the horizontal boundary [m^2], k is the flow coefficient [m/(s Pa^n)], and n is the flow exponent.
The airflow could have two different directions: ascending or descending, depending on which side of the boundary has the higher pressure. These two possible configurations are shown in Figure 3.4.

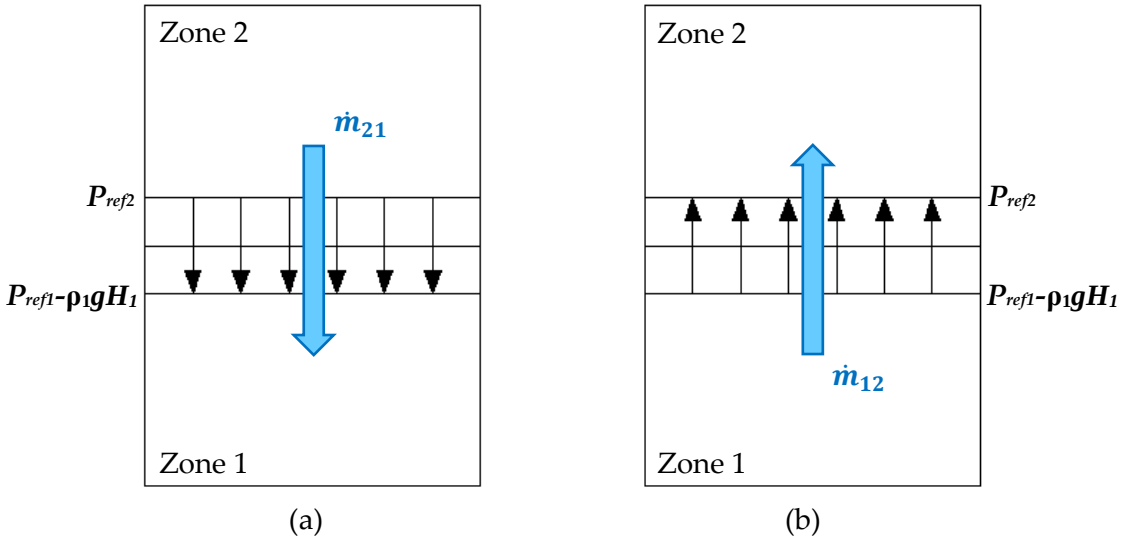

Figure 3.4 Airflow configurations for horizontal normal boundary. Descending flow (a). Ascending flow (b).

A descending airflow occurs when the reference pressure of the upper cell outcomes the pressure at the top of the lower cell. In this case, the mass flows can be modelled as follows:

CONDITION: $P_{ref1} - \rho g H_1 < P_{ref2}$

$$\dot{m}_{12} = 0 \tag{3.9}$$

$$\dot{m}_{21} = \rho_2 k A_{horiz} \left(P_{ref_2} - \left(P_{ref_1} - \rho_1 g H_1 \right) \right)^n \tag{3.10}$$

Where the symbols have the same meaning as before. All the mass flowrate goes from the upper zone to the lower zone, so the considered air density is equal to ρ_2.
On the other hand, an ascending airflow arises if the pressure at the bottom is higher than the pressure at the top. The mass flows will be given by:

CONDITION: $P_{ref1} - \rho g H_1 \geq P_{ref2}$

$$\dot{m}_{12} = \rho_1 k A_{horiz} \left(\left(P_{ref_1} - \rho_1 g H_1 \right) - P_{ref_2} \right)^n \tag{3.11}$$

$$\dot{m}_{21} = 0 \tag{3.12}$$

All the flowrate goes from the lower to the upper zone, so the air density is set equal to ρ_1.
Equations (3.9)-(4.6) are formulated in order to obtain always positive mass flowrates.

3.1.2.2 Airflow across vertical boundary

For vertical interfaces separating two adjacent zones the calculation of the airflows is more complex. Differently from horizontal surfaces, the pressure difference across the vertical boundary varies along the height of the cells (*z* coordinate), due to the hydrostatic distributions of pressure on both sides. The trend and slope of pressure profiles are determined by air reference pressure and air density values within the zone. At a certain height *z*, these profiles intersect, highlighting a null pressure difference. This point is called *neutral plane* Z_n. There is no horizontal airflow across this plane. The general situation for a vertical normal boundary is shown in Figure 3.5.

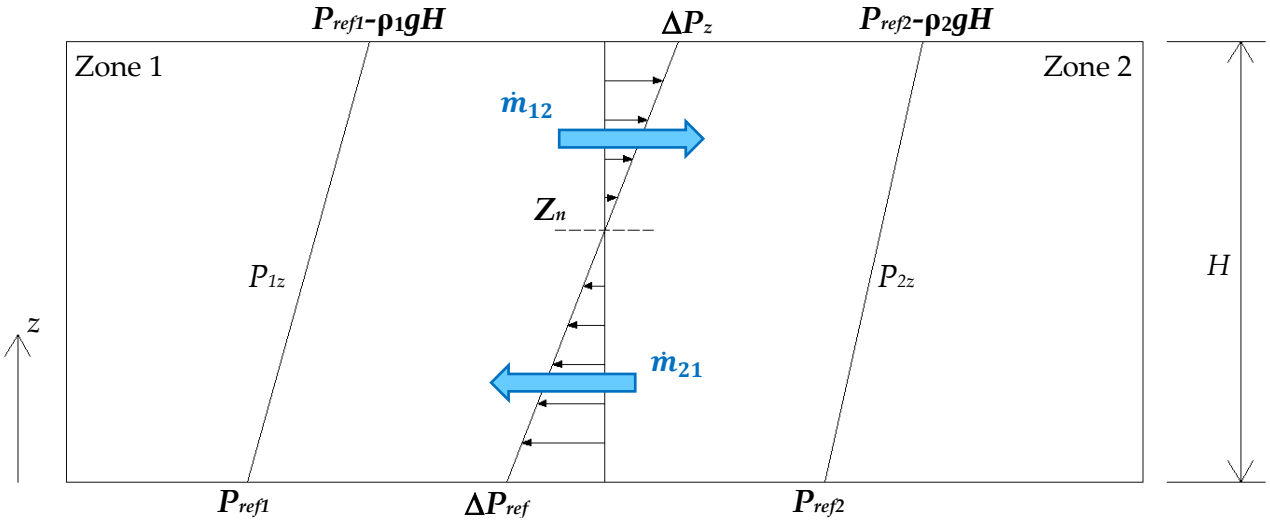

Figure 3.5 Vertical normal boundary modelling.

As shown in the figure above, passing through the neutral plane, the airflow reverses its direction. The net flowrate is obtained subtracting the opposite flows.
The height of the neutral plane is given by this relationship:

$$Z_n = \frac{\Delta P_{ref}}{g\Delta\rho} \tag{3.13}$$

Where Z_n is the height of the neutral plane [m], ΔP_{ref} is the reference pressure difference [Pa] and $\Delta\rho$ is air density difference [kg/m^3] between two adjacent zones, g is the gravitational acceleration [m/s^2].
The pressure difference along *z* coordinate (ΔP_z in Figure 3.5) can be written as:

$$\Delta P_z = P_{1z} - P_{2z} = \left(P_{ref_1} - \rho_1 g z\right) - \left(P_{ref_2} - \rho_2 g z\right) = \Delta P_{ref} - \Delta\rho g z = \Delta\rho g (Z_n - z) \tag{3.14}$$

Where *z* is the height of the considered point [m].

Substituting the last expression of Equation (4.6) into the Power Law (Equation (4.6)), and integrating along *z*, the formulations for mass flow rates below and above the neutral plane are obtained:

$$\dot{m}_{0-Z_n} = \rho_{0-Z_n} kL|\Delta\rho g|^n \frac{|Z_n|^{n+1}}{n+1} \tag{3.15}$$

$$\dot{m}_{Z_n-H} = \rho_{Z_n-H} kL|\Delta\rho g|^n \frac{|Z_n - H|^{n+1}}{n+1} \tag{3.16}$$

Where L is the depth of the vertical interface [m] and the other symbols have the same meaning as in the previous equations. $\dot{m}_{0-Z_n}$ is the mass flowrate crossing the interface portion from 0 to Z_n, and it corresponds to $\dot{m}_{21}$ in Figure 3.5. Conversely, $\dot{m}_{Z_n-H}$ is the mass flowrate crossing the interface portion from Z_n to H, and it corresponds to $\dot{m}_{12}$ in Figure 3.5. Equations (3.15) and (4.6) depict the generic situation displayed in Figure 3.5. However, there are eight different configurations for airflows across a vertical boundary. This multiplicity depends on where the neutral plane is located. In fact, it could fall out of the range 0-H. Ultimately, flow configuration is established by reference pressure and density values. Each configuration has its own relationship as presented below.
Figure 3.6 shows the situations when the density of zone 1 is higher than zone 2.

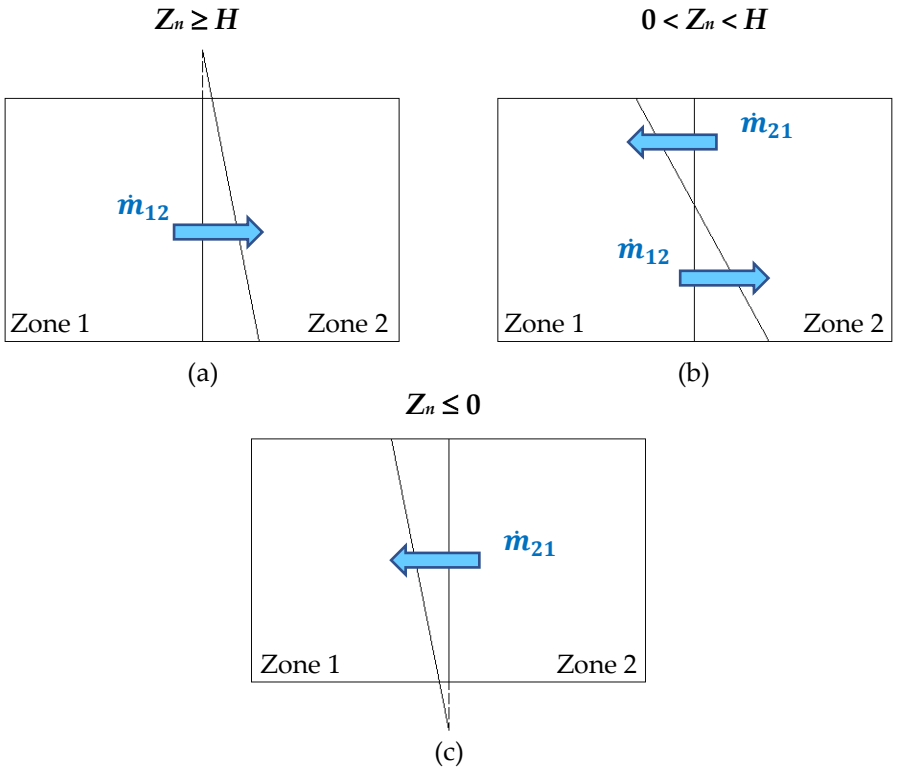

Figure 3.6 Airflow configurations for vertical normal boundary with $\rho_1 > \rho_2$. Case $Z_n \geq H$ (a). Case $0 < Z_n < H$ (b). Case $Z_n \leq 0$ (c).

The mass flowrates of Figure 3.6(a) are modelled in this way:

CONDITIONS: $P_{ref1} > P_{ref2}$; $\rho_1 > \rho_2$; $Z_n \geq H$

$$\dot{m}_{12} = \rho_1 kL\big((\rho_1 - \rho_2)g\big)^n \left(\frac{{Z_n}^{n+1}}{n+1} - \frac{(Z_n - H)^{n+1}}{n+1}\right) \tag{3.17}$$

$$\dot{m}_{21} = 0 \tag{3.18}$$

The mass flowrates of Figure 3.6(b) are modelled as follows:

CONDITIONS: $P_{ref1} > P_{ref2}$; $\rho_1 > \rho_2$; $0 < Z_n < H$

$$\dot{m}_{12} = \rho_1 kL\big((\rho_1 - \rho_2)g\big)^n \left(\frac{{Z_n}^{n+1}}{n+1}\right) \tag{3.19}$$

$$\dot{m}_{21} = \rho_2 kL\big((\rho_1 - \rho_2)g\big)^n \left(\frac{(H - Z_n)^{n+1}}{n+1}\right) \tag{3.20}$$

Finally, the mass flowrates of Figure 3.6© are given by:

CONDITIONS: $P_{ref1} < P_{ref2}$; $\rho_1 > \rho_2$

$$\dot{m}_{12} = 0 \tag{3.21}$$

$$\dot{m}_{21} = \rho_2 kL\big((\rho_1 - \rho_2)g\big)^n \left(\frac{(H - Z_n)^{n+1}}{n+1} - \frac{(-Z_n)^{n+1}}{n+1}\right) \tag{3.22}$$

Other three possible configurations arise if density in zone 2 is higher than zone 1, as shown in Figure 3.7. The computation of mass flow rates is carried out in the same way.
The mass flowrates of Figure 3.7(a) are modelled as:

CONDITIONS: $P_{ref2} > P_{ref1}$; $\rho_2 > \rho_1$; $Z_n \geq H$

$$\dot{m}_{12} = 0 \tag{3.23}$$

$$\dot{m}_{21} = \rho_2 kL\left((\rho_2 - \rho_1)g\right)^n \left(\frac{{Z_n}^{n+1}}{n+1} - \frac{(Z_n - H)^{n+1}}{n+1}\right) \tag{3.24}$$

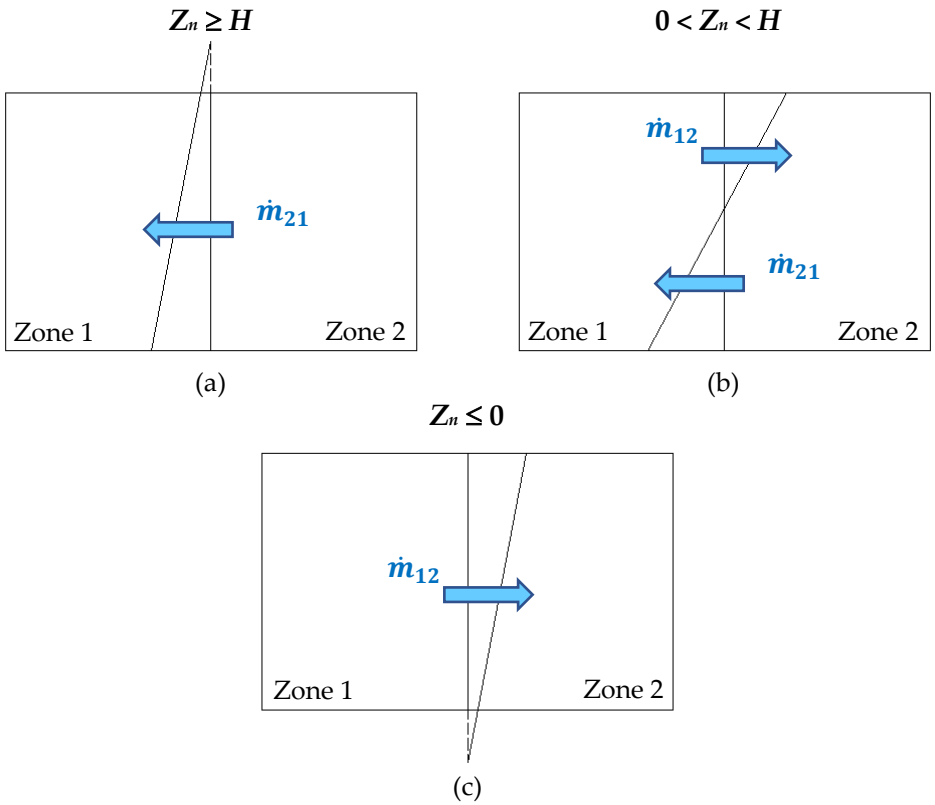

Figure 3.7 Airflow configurations for vertical normal boundary with $\rho_2 > \rho_1$. Case $Z_n \geq H$ (a). Case $0 < Z_n < H$ (b). Case $Z_n \leq 0$ (c).

The mass flowrates of Figure 3.7(b) are modelled as:

CONDITIONS: $P_{ref2} > P_{ref1}$; $\rho_2 > \rho_1$; $0 < Z_n < H$

$$\dot{m}_{12} = \rho_1 kL\left((\rho_2 - \rho_1)g\right)^n \left(\frac{(H - Z_n)^{n+1}}{n+1}\right) \tag{3.25}$$

$$\dot{m}_{21} = \rho_2 kL\left((\rho_2 - \rho_1)g\right)^n \left(\frac{{Z_n}^{n+1}}{n+1}\right) \tag{3.26}$$

Finally, the mass flowrates of Figure 3.7(c) are given by:

CONDITIONS: $P_{ref2} < P_{ref1}$; $\rho_2 > \rho_1$

$$\dot{m}_{12} = \rho_1 kL\left((\rho_2 - \rho_1)g\right)^n \left(\frac{(H - Z_n)^{n+1}}{n+1} - \frac{(-Z_n)^{n+1}}{n+1}\right) \tag{3.27}$$

$$\dot{m}_{21} = 0 \tag{3.28}$$

Lastly, if air densities of the two zones are equal, there is not a neutral plane. The pressure difference across the vertical boundary remains constant along *z*, and it is equal to the difference between the reference values. The resulting airflow can follow two directions, as shown in Figure 3.8.

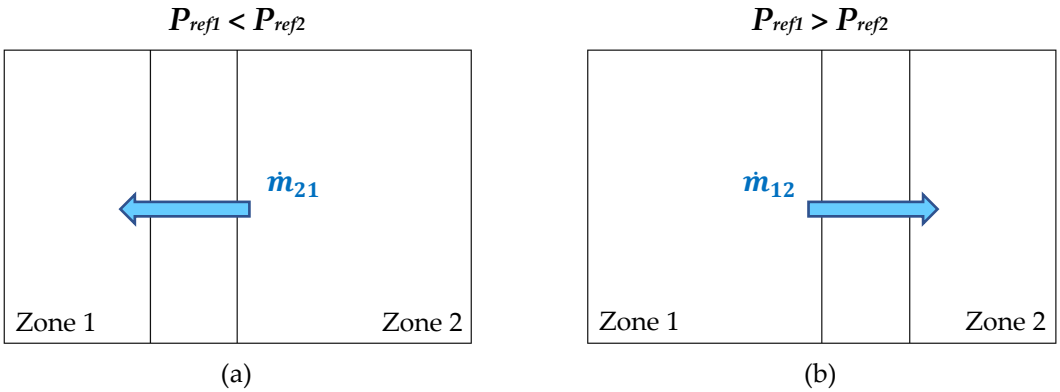

Figure 3.8 Airflow configurations for vertical normal boundary with $\rho_1 = \rho_2$. Case $P_{ref1}<P_{ref2}$ (a). Case $P_{ref1}>P_{ref2}$ (b).

The mass flowrates of Figure 3.8(a) are modelled as follows:

CONDITIONS: $\rho_1 = \rho_1$; $P_{ref1} < P_{ref2}$

$$\dot{m}_{12} = 0 \tag{3.29}$$

$$\dot{m}_{21} = \rho_2 k A_{vert} \left(P_{ref_2} - P_{ref_1}\right)^n \tag{3.30}$$

Figure 3.8(b) illustrates the opposite situation:

CONDITIONS: $\rho_1 = \rho_1$; $P_{ref1} > P_{ref2}$

$$\dot{m}_{12} = \rho_1 k A_{vert} \left(P_{ref_1} - P_{ref_2}\right)^n \tag{3.31}$$

$$\dot{m}_{21} = 0 \tag{3.32}$$

Where A_{vert} is the area of the vertical boundary [m^2].

In Equations (3.17)-(4.6) pressure and density differences are manipulated to get always positive values. In this way, all the calculated mass flowrates are positive.

3.1.3 Modelling of the heat flows

The model is founded on some assumptions regarding energy exchanges:

- across normal boundaries heat is carried by interzonal airflows. Only dry air is considered.
- at wall surface boundaries, heat transfer is driven by convection. In particular, the overall heat exchange between indoor and outdoor air is evaluated, considering the global thermal transmittance of the envelope fabric.
- the presence of window is neglected, so no direct solar radiation enters the room.
- any radiative heat exchange is ignored.

Therefore, heat transfer is only related to mass flows and interaction with opaque structures. The mass airflows (calculated in §3.1.2) carry heat in terms of enthalpy. This energy transport can be modelled as:

$$q_{h_{ij}} = \dot{m}_{ij} c_{p_{air}} T_i \tag{3.33}$$

Where $q_{h,ij}$ represents the heat (or enthalpy) fluxes from zone i to zone j [W], $\dot{m}_{ij}$ is the mass flowrate from i to j [kg/s], $c_{p,air}$ is the specific heat of the air [J/(kg K)], and T_i is the air temperature in zone i [K]. Assuming dry air, $c_{p,air}$ is equal to 1005 J/(kg K).
Regarding the heat exchange between indoor air and the outdoor environment, it occurs through the building envelope structures. This heat transfer can be calculated as follows:

$$q_{h_{transm,i}} = U A_{exch} \left(T_i - T_{air,ext} \right) \tag{3.34}$$

Where $q_{h,transm,i}$ is the heat flux by transmission across the envelope in zone i [W], U is the thermal transmittance of the building structure [W/(m^2 K)], A_{exch} is the exchange area of the wall portion facing the zone i [m^2], T_i is the air temperature in zone i [K], and $T_{air,ext}$ is the external temperature [K]. The heat flux is considered as a removal term in the energy balance of the model (Equation (3.5)).
The thermal transmittance U incorporates all the thermal resistances of the building envelope. It can be defined in this way:

$$U = \frac{1}{R_{th,tot}} = \frac{1}{\frac{1}{R_{th,is}} + \frac{1}{R_{th,wall}} + \frac{1}{R_{th,es}}} \tag{3.35}$$

U is the reciprocal of the total thermal resistance $R_{th,tot}$ [(m^2 K)/W] between indoor and outdoor air. The latter is the sum of different terms: $R_{th,is}$ and $R_{th,es}$ are the liminar thermal resistances at the internal and external surfaces, respectively, associated with the boundary layers on both sides, and $R_{th,wall}$ is the thermal resistance of the fabric that includes the thermal properties of different layers composing the wall.

3.1.4 Equation system and resolution of the model

In the previous paragraphs, the modelling of mass flowrates and heat fluxes across the boundary surfaces separating adjacent zones, was provided. Now, the mass and energy conservation laws can be imposed for each *i*-th zone. For terms calculated by Equations (3.9)-(4.6) and (3.17)-(4.6) some conventions have been adopted, considering zone *i*:

- $\dot{m}_{ij}$ is an airflow leaving zone *i* and entering zone *j*, so, it is a negative term
- $\dot{m}_{ji}$ is an airflow coming from zone *j* into zone *i*, so, it is positive term.

As the heat exchange between indoor air and walls, given by Equation (3.34), is regarded, it is considered as a removal term, so it is a negative quantity.

The model is applied in steady-state conditions over n_{zon} cells. Equation (3.4) and (3.5) can be rewritten accordingly, with no mass and energy accumulation:

$$0 = \sum_{j=1}^{n_{zon}} \dot{m}_{ji} - \sum_{j=1}^{n_{zon}} \dot{m}_{ij} + \dot{m}_{sup} - \dot{m}_{rem} \tag{3.36}$$

$$0 = \sum_{j=1}^{n_{zon}} q_{h\,ji} - \sum_{j=1}^{n_{zon}} q_{h\,ij} - q_{h\,transm,i} + q_{h\,sup} - q_{h\,rem} \tag{3.37}$$

The symbols have the same meaning as in the original equations.

Each zone is characterized by three unknown thermophysical properties: air density (ρ), air temperature (T) and reference pressure (P_{ref}). A spatial discretization into n_{zon} implies $3n_{zon}$ unknown variables.

The mass flowrates across horizontal boundaries are function of density and reference pressure difference. The mass flows across vertical boundaries are function of densities and neutral planes, but the latter depend on density and reference pressure differences. Therefore, mass balances (Equation (3.36)) are function of reference pressures and densities. The dependency is based on the Power Law, so it is nonlinear. Similarly, energy balances (Equation (4.6)) are function of reference pressures, densities, and temperatures. Finally, the thermophysical parameters of air are linked by the perfect gas law (Equation (3.2)). From all these equations, a nonlinear equation system is generated, as shown in:

$$\begin{cases} n_{zon} \text{ mass balance equations} & \rightarrow f(P_{ref}, \rho, T) \\ n_{zon} \text{ energy balance equations} & \rightarrow f(P_{ref}, \rho, T) \\ n_{zon} \text{ ideal gas equations} & \rightarrow f(P_{ref}, \rho, T) \end{cases} \quad (3.38)$$

In this system, there are $3n_{zon}$ equations. However, it was demonstrated in [40] that only (n_{zon}-1) mass balances are linearly independent. Therefore, $3n_{zon}$-1 equations are linearly independent and $3n_{zon}$ are the unknown variables. It is necessary to fix as parameter one variable and substitute a mass balance. Since mass flowrates are function of the reference pressure difference, a basic reference pressure of one zone as a known value is assumed. The nonlinear system is reduced to $3n_{zon}$-1 independent equation with $3n_{zon}$-1 unknown properties, so it is resolvable.
The nonlinear equations can be written in their implicit form to get a system of this type:

$$\mathbf{F}(\mathbf{x}) = 0 \quad (3.39)$$

Where **F** represents the implicit function vector, while **x** is the unknown variable vector.
A numerical iterative method must be implemented to solve the nonlinear system. The final result is a vector containing the thermophysical properties (P_{ref}, T, ρ) of each zone. Thus, the mass flowrates can be explicitly computed reapplying Power Law equations: Equations (3.9)-(4.6) for horizontal and Equations (3.17)-(4.6) for vertical boundaries.
From the mass flowrates, the volumetric flowrates are easily determined through:

$$Q_{ij} = \frac{\dot{m}_{ij}}{\rho_i} * 3600 \quad (3.40)$$

Where Q_{ij} is the volumetric flowrate from zone i to zone j [m^3/h], $\dot{m}_{ij}$ is the corresponding mass flowrate [kg/s], and ρ_i is the air density [kg/m^3].
The volumetric flowrates Q represent the final output of the described zonal model, and they will be inserted as input parameters in the infection risk model.

The zonal model presented in this chapter was implemented in **MATLAB** environment. The main features of the compiled program regard the following instructions:

- ***if…else*** cycles have been generated to load each time the correct equations for the mass flowrates in the simulations. The single cycle selects one between the possible

flow configurations for horizontal (two possibilities) and vertical boundaries (eight possibilities), according to pressures and densities of adjacent zones.
- the default function ***fsolve*** has been employed to solve the nonlinear equation system resulting from the model construction.

For different case studies, presented in §4, the zonal model has been built as a MATLAB ***function***. Each ***function*** contains the instruction list.

3.2 The infection risk model

The infection risk model constitutes the second and final part of the global model. It is based on quanta of infection relative to COVID-19. It is coupled to the zonal model previously presented in order to exploit information about air movement between zones in determining the spread of infectious quanta over the room of concern. The final output of this risk model is the infection probability for a susceptible individual situated in one of the cells. The aim is evaluating whether the spatial discretization approach is effective in describing the link between risk degree and relative position of susceptibles, infected subjects and air vents. Moreover, understanding the connection between spatial distribution of risk, environment geometry and the characteristics of the ventilation system is also of concern.
A quanta balance equation is set to calculate quanta concentration for each zone. Natural removal rates by gravitational deposition and pathogen inactivation are neglected. This means that the number of airborne quanta will be overestimated as well as the resulting infection risk, reflecting the worst-case scenario. The relationship is identical to Equation (2.20), and it is reported here for the *i*-th zone:

$$V_i * \frac{\mathrm{d}C_i}{\mathrm{d}t} = q_i I_i - Q_{oi} C_i - \sum_{j=1}^{n_{zon}} Q_{ij} C_i + \sum_{j=1}^{n_{zon}} Q_{ji} C_j \tag{3.41}$$

Where V_i is the volume of the zone [m^3], C_i is quanta concentration [quanta/m^3], $q_i I_i$ is quanta generation rate [quanta/h], based on the number of infected people in the zone I_i, Q_{oi} is the exhaust airflow rate which removes quanta from the zone [m^3/h], Q_{ij} and Q_{ji} are the volume flow rates to and from adjacent zone *j* [m^3/h], respectively, and C_j is quanta concentration of the adjacent zone *j* [quanta/m^3]. The fresh air from diffusers is not considered in the balance, since it is assumed that outdoor air does not contain infectious quanta. The terms Q_{ij} and Q_{ji} represent the interzonal flowrates calculated from the zonal model.
Knowing the quanta concentration within a zone, the zonal infection risk can be calculated on the basis of intake doses through Equation (2.2), rewritten below to return a percentage:

$$P_{I_i} = \left(1 - \mathrm{e}^{-p \int_0^{t_{exp}} C_i(t)\mathrm{d}t}\right) * 100 \tag{3.42}$$

Where $P_{I,i}$ is the individual infection probability for susceptibles in zone *i* [%], *p* is the breathing flowrate [m^3/h], $C_i(t)$ is the zonal quanta concentration over time [quanta/m^3], and t_{exp} is the exposure time interval [h].
The infection risk is evaluated both under steady-state and transient conditions for the resolution of quanta concentration balance. Moreover, the use of masks is inserted in the problem. The following paragraphs describe how these aspects are developed in the model.

3.2.1 Infection risk under steady-state conditions

Considering quanta concentration balance under steady-state conditions, Equation (3.41) becomes for the *i*-th zone:

$$0 = q_i I_i - Q_{oi} C_i - \sum_{j=1}^{n_{zon}} Q_{ij} C_i + \sum_{j=1}^{n_{zon}} Q_{ji} C_j \tag{3.43}$$

Where symbols have the same meaning. In turn, Equation (4.6) can be reordered like this:

$$\left(-Q_{oi} - \sum_{j=1}^{n_{zon}} Q_{ij} \right) C_i + \sum_{j=1}^{n_{zon}} Q_{ji} C_j = -q_i I_i \tag{3.44}$$

Considering all zones, an equation system can be written in matrix form:

$$\mathbf{A} * \mathbf{C} = \mathbf{b} \tag{3.45}$$

Where **A** is the matrix of the volumetric flowrates, **C** is the column vector of the zonal quanta concentrations C_i, i.e., the unknown variables, and **b** is the column vector of the constant terms. Equation (4.6) represents a linear system, easily resolvable applying an iterative numerical method. The solutions C_i are the steady-state quanta concentrations of each zone, i.e., at saturation levels. These concentrations do not vary over the exposure time, so the infection risk will be:

$$P_{I_i} = (1 - \mathrm{e}^{-p C_{i,ss} t_{exp}}) * 100 \tag{3.46}$$

Where $C_{i,ss}$ pinpoints we are considering steady-state conditions. Although C_i remain constant, infection probability rises with increasing t_{exp} because the intake dose increases.

3.2.2 Infection risk under transient conditions

Under unsteady conditions, Equation (3.41) preserves its original shape. In this case, a system of ordinary differential equations (ODE) is obtained. It can be numerically solved, and the solutions are time-variable quanta concentrations $C_i(t)$ for each zone. In this case, values obtained are not constant, but concentration trends over the exposure time. Therefore, the integral in Equation (3.42) must be properly treated.
The ODE system is solved through a numerical method that divides the total exposure time into small time intervals, with a variable timestep. At these intervals, the integral can be computed resorting to *trapezoids method*. The area of each trapezoid, multiplied by the breathing flowrate, constitutes a portion of total intake dose, and it is calculated as follows:

$$dose_{i,\Delta t_k} = p * \left(\frac{(C_{i,k} + C_{i,k-1})}{2} * (t_k - t_{k-1}) \right) \tag{3.47}$$

Where $dose_{i,\Delta tk}$ is the portion of total dose inhaled by a susceptible individual in the *i*-th zone within the *k*-th time interval Δt_k [quanta]. $C_{i,k}$ and $C_{i,k-1}$ represent the quanta concentrations at time step *k* and *k-1*, respectively [quanta/m^3], ($t_k - t_{k-1}$) is the *k*-th time interval [h], and *p* is the breathing flowrate [m^3/h].
The total intake dose, over the whole exposure time, is:

$$dose_i = \sum_{k=1}^{t_{exp}} dose_{i,\Delta t_k} \tag{3.48}$$

Finally, the airborne infection risk is easily computed as:

$$P_{I_i} = (1 - \mathrm{e}^{-dose_i}) * 100 \tag{3.49}$$

Where $P_{I,i}$ is the infection probability for a susceptible person located in zone *i* [%].

3.2.3 Use of masks

The use of masks and respirators is included in the risk evaluation. Two types of personal protection devices are analysed: surgical masks and FFP2 respirators. Despite being typically medical devices, the COVID-19 pandemic has made them widely accessible for citizens. Conversely, homemade cloth masks are not considered.
As said in §2.1.4, each mask is characterized by a filtration efficiency *X* [%], and a leakage factor *Y* [%]. The former is related to the filtering material capability of intercepting noxious particles, the latter expresses the fit level to the wearer face. For a certain type of mask, X

could depend on the direction of the breathing flow, leading to different values for inhalation (X_{int}) and exhalation (X_{ext}). On the other hand, Y value does not change. Table 3.1 displays the parameters of surgical masks and FFP2 respirators, and the situation with no protection.

Table 3.1 Filtration efficiency and leakage factors for personal protection equipment.

TYPE OF PROTECTION	**Filtration efficiency [%]**		**Leakage factor [%]**
	$X_{int}^{(*)}$	$X_{ext}^{(*)}$	Y
No masks	*0*	*0*	*0*
Surgical mask	20	95	27
FFP2	94	94	11
(*)*Note*: Subscript "*int*" refers to a flow going towards the internal part of the mask (inhalation), while subscript "*ext*" refers to a flow going outside (exhalation).			

Technical specifications on the performance requirements for surgical masks are provided by standard UNI EN 14683:2019 [41]. The filtration efficiency for exhalation X_{ext} in Table 3.1 refers to the *bacterial filtration efficiency* (BFE) reported in the standard. Since no standard data are available for filtration efficiency during inalhation and leakages, these choices have been made:

- because of the proved inefficiency of surgical mask in protecting the wearer, a value of 20% for X_{int} is taken. Probably, this is an underestimation of the real performance, but it will constitute the worst-case scenario. Ad-hoc standard tests would be necessary to determine this parameter.
- a leakage factor of 27% is considered. This value is an estimation from results obtained by Mueller et al. (2020) [42]. In their work, they calculated the filtration efficiency of different masks when worn as designed and with a nylon overlayer to give a rough quantification to facial leakages due to poor fit.

Technical requirements for FFP2 respirators can be found in UNI EN 149:2009 [43]. In this case, both filtration efficiency and leakeges factor limit are established. The performance of these devices can be considered unvaried for inhalation and exhalation flows.
Combining filter efficiency X and fit factor Y, the global filtration efficiency Z [%], can be determined though Equation (2.12), considering both breathing regimes:

$$Z_{int/ext} = X_{int/ext} - \frac{X_{int/ext} * Y}{100} \tag{3.50}$$

In infection risk evaluation, the use of masks is modelled considering quanta emission term q and inhalation term p in Equation (3.41) and (3.42), respectively. An infected individual wearing mask is supposed to release fewer infectious quanta into the indoor environment. This reduction can be computed taking the filtration efficiency towards the external side:

$$q' = q * \left(1 - \frac{Z_{ext}}{100}\right) \quad (3.51)$$

Where q' is the reduced quanta production [quanta/h].
Similarly, a susceptible person wearing mask protects himself from inhaling all airborne quanta. In this case, the filtration efficiency towards the internal side must be taken and a reduction in the intake dose occurs. The corresponding calculation is done in terms of breathing flowrate decrease:

$$p' = p * \left(1 - \frac{Z_{int}}{100}\right) \quad (3.52)$$

Where p' is the reduced breathing rate [m^3/h].
In our model, only the situation with all present people wearing the same protective devices simultaneously is analysed.

The infection risk model was constructed in **MATLAB** environment. The main characteristics of the compiled program regard the following instructions:

- a ***switch…case*** cycle has been created for enabling the user to choose if masks are used and which type.
- a ***switch…case*** cycle has been created to run simulations for steady-state and transient regime, separately.
- the linear system for steady-state problem is solved through ***Jacobi*** or ***Seidel iterative method***. These are called in the main script by means of their own ***functions***.
- the default function ***ode45*** has been employed to solve the ODE system for transient regime.

The zonal model ***function*** is called into the risk model script to make the integration.
The infection risk model has been built as a MATLAB ***script*** for different case studies (see §4). Each ***script*** reports the instruction list.

Chapter 4

Model application and results

In the previous chapter, a detailed description of the construction of the zonal risk model was provided. The model has been applied to simulate the infection risk from COVID-19 within a test room. The analysed case-study is meant to represent a simplified real situation with a susceptible subject and an infected source sharing the same indoor environment. The considered space has the typical dimensions of an office room. Moreover, a simulation of a room with a fourfold volume compared to the original one was performed in order to observe the effect of a larger space on pathogens dilution and airborne infection risk.
The following paragraphs present model implementations and corresponding results. Several assumptions have been made to verify the correct operation of the developed model. These simplifications regard both the partition of the room and boundary conditions for the zonal model and infection risk calculations. Therefore, this application can be considered as the starting point for future improvements of the built code.

4.1 4-zone model for an office room case

The first implementation of the model concerns the calculation of the interzonal airflows and infection risk within a typical office room. The analysed space is mechanically ventilated, and the air distribution is achieved through a mixing ventilation system. The importance of the amount of outdoor air supplied to the environment has been investigated.

4.1.1 Geometrical domain and zonal discretization

The considered space in the model simulations is based on the "CORE-CARE test room" (*Controlled Room for Building Environmental Comfort Assessment and Subjective Human Response Evaluation*), which is situated at the third floor of the ex-Department of Technical Physics of the University of Padua. This test room is employed to carry out experimental studies on *indoor environmental quality* (IEQ), i.e., comfort evaluation in indoor environments, with particular attention to thermal comfort and indoor air quality (IAQ).
The considered office room presents similar dimensions and layout (i.e., fixtures arrangement) of those of CORE-CARE, but it does not replicate identical characteristics. The modelled room has a dimension of 4.0x4.0x2.7 m, so it occupies a floor area of 16 m^2 and a volume of 43.2 m^3. Figure 4.1 shows the orientation and the overall size of the office room, along with fixtures and ventilation system terminals layout.

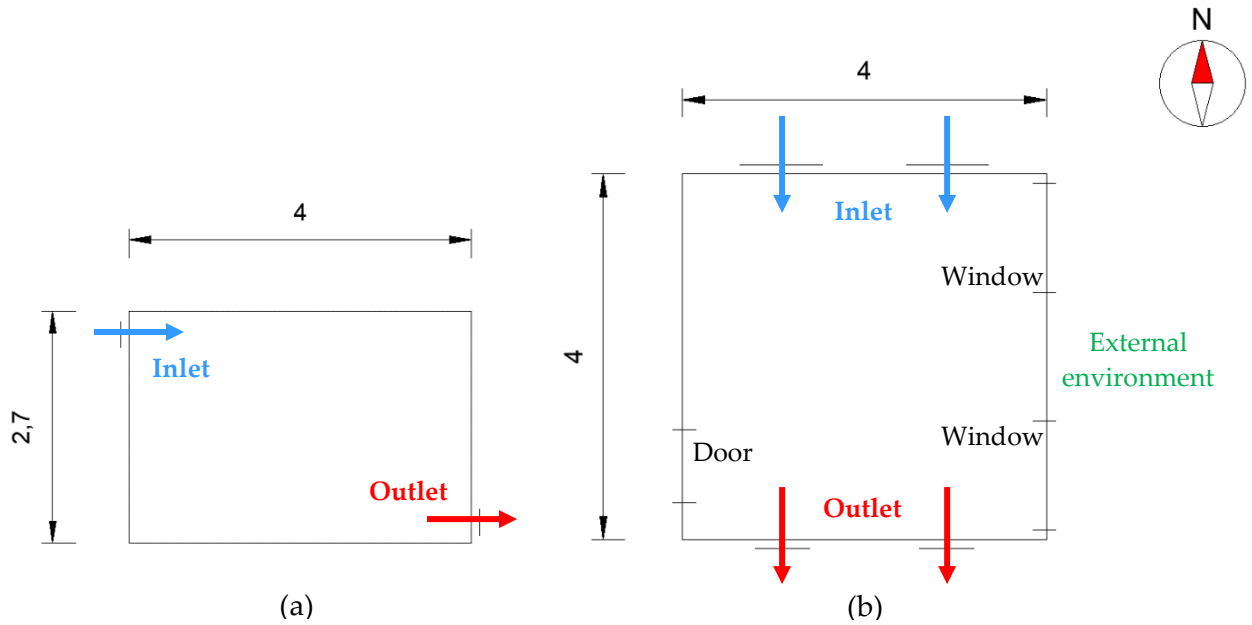

Figure 4.1 Dimensions and orientation of the office room. Front view with indication of air vents layout (a). Top view with fixtures position and air vents layout (b).

As shown in front (Figure 4.1(a)) and top view (Figure 4.1(b)) of the room, there are two windows located on the East wall, and a door on the West wall. Each window has a dimension of 1.2x1.4m, covering an area of 1.68 m^2, whereas the door is a 0.8x2.1 m opening. The East wall constitutes the external façade of the room, so it separates the indoors from the outdoors. Conversely, the other structures are internal partitions: the office room is adjacent to a corridor through the West wall, and to other building spaces through the North wall, South wall, floor slab and ceiling. The dimensions of the main room elements are reported in Table 4.1.

Table 4.1 Dimensions of room elements.

Room element	Dimensions(*) [m]			Area [m^2]	Volume [m^3]
	l	***w***	***h***		
Entire office room	4	4	2.7	-	43.20
East wall	4	-	2.7	10.80	-
West wall	4	-	2.7	10.80	-
North wall	-	4	2.7	10.80	-
South wall	-	4	2.7	10.80	-
Floor	4	4	-	16.00	-
Ceiling	4	4	-	16.00	-
Window (x2)	1.2	-	1.4	1.68	-
Door	0.8	-	2.1	1.68	-
(*)*Note*: *l* = length refers to the North-South direction; *w* = width is related to East-West direction; *h* = height.					

Concerning the mechanical ventilation and air distribution system, outdoor air is supplied by means of two linear diffusers located at the top of the North wall, while the exhaust air is extracted through two opposite outlets placed at the bottom of the South wall (see Figure 4.1). The air diffusers are positioned 12 cm below the ceiling level and at 64 cm from the East and West wall, symmetrically. The exhaust grilles are located 9 cm above the floor and at a distance of 80 cm from the East and West wall, symmetrically.
The geometrical domain has been divided into **4 identical zones** with a cross section on the plan view. Therefore, a **4-zone risk model** is applied to examine the infection probability inside the analysed office room. The performed spatial macro-discretization is shown in Figure 4.2, along with the chosen zone numeration.

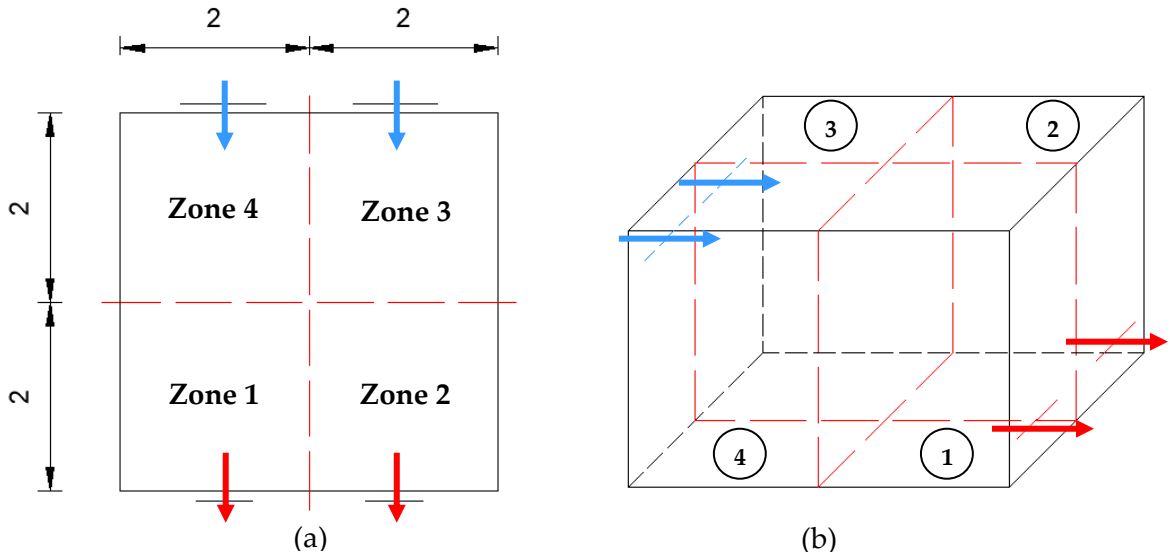

Figure 4.2 Zonal subdivision of the room and numeration. Top view (a). 3D view (b).

The figure above shows that each zone is a parallelepiped with dimensions of 2x2x2.7 m, since the crossed planes section the space along its axes of symmetry. Zone 1 and Zone 2 contain the air outlets, whereas air is supplied in Zone 3 and Zone 4. The simplified partitioning proposed in this work does not provide an assessment of thermal stratification inside the considered volume due to buoyancy effects.

4.1.2 Zonal model assumptions

As said in §3, the first step of the analysis consists of the calculation of the interzonal airflows for the chosen spatial partition (see Figure 4.2) by applying the described zonal model.
The nonlinear system obtained with mass and energy balance equations in steady-state conditions for each zone (see §3.1.4), is solved under the following assumptions:

- each cell is well-mixed with uniform temperature and density.
- the flow coefficient k is set to 0.83 m/(s Pa^n).

- turbulent airflows are considered leading to a flow exponent *n* equal to 0.5.
- the basic static reference pressure of Zone 1 is fixed as a known variable in order to write a system of linearly independent equations (as explained in §3.1.4). It is chosen equal to the atmospheric pressure, that is $\boldsymbol{P_{ref,1}}$**=1 atm=101325 Pa**.

The previous simplifications are related to the modelling approach and mathematical resolution, whereas the single mass and heat flows are function of the interactions between adjacent zones and external environment for the analysed situation. As the mass and heat transfers are concerned, the following boundary conditions are set:

- dry air is considered, so the heat carried by the mass airflows is calculated with a specific heat $c_{p,air}$ equal to 1005 J/(kg K).
- the room is perfectly sealed, therefore there are no infiltrations from the outdoors.
- only the East wall faces the outdoor weather conditions, the other walls, including the West wall adjacent to the corridor, are considered adiabatic.
- windows presence is neglected, therefore there is no solar radiation entering the room from outside.
- radiative heat exchanges involving the internal surfaces are neglected.
- for the outdoor environment, winter design conditions for Padua are assumed, which means an external temperature of -5 °C ($T_{air,ext}$). In this case, the effect of the solar radiation on the opaque building components is absent, so the sol-air temperature ($T_{sol-air}$) is equal to the external air temperature.
- the East wall is characterized by a thermal transmittance *U* of 0.3 W/(m^2 K).
- cooling and heating system terminals are not operative in this case-study room.
- any type of internal heat gain is neglected (people, electrical devices, lights, etc.). As to subjects sharing the indoor space, they are not considered as heat sources, but only quanta emitters if they are infected from COVID-19.
- the linear diffusers convey air jets into the room at a temperature of 20 °C and a corresponding density of 1.204 kg/m^3.

The abovementioned fixed parameters are summarized in Table 4.2.

Table 4.2 Fixed parameters in the 4-zone model for the office room.

PARAMETER	SYMBOL	VALUE	U.M.
Flow coefficient	k	0.83	m/(s Pa^n)
Flow exponent for turbulent regime	n	0.5	-
Reference pressure of Zone 1	$P_{ref,1}$	101325	Pa
External air temperature (winter design)	$T_{air,ext}$	-5	°C
Specific heat of dry air	$c_{p,air}$	1005	J/(kg K)
Air jet temperature	T_{jet}	20	°C
Air jet density	ρ_{jet}	1.204	kg/m^3
East wall thermal transmittance	U	0.3	W/(m^2 K)

Observing Figure 4.2 and the third assumption of the above list, it is clear that only Zones 2 and 3 are interested by heat transmission between indoor and outdoor environment. Moreover, the heat transfer is considered to occur only across the wall structure, neglecting the presence of windows in the conductive and convective exchange. In the other zones, there are only heat fluxes connected to mass transfer through the boundary surfaces.
Concerning the supplied outdoor air, each linear diffuser contributes to half of the total flowrate. Similarly, the same flowrate is extracted equally divided into the two exhaust grilles. Therefore, the air jets and exhaust mass flowrates have been modelled through the following expression:

$$\dot{m}_{in} = \dot{m}_{out} = 0.5\rho_{\text{jet}} \frac{ACH * V}{3600} \tag{4.1}$$

Where $\dot{m}_{in}$ is the mass flowrate supplied by one linear diffuser [kg/s], $\dot{m}_{out}$ is the mass flowrate extracted by one exhaust grille [kg/s], ρ_{jet} is the air jet density [kg/m^3], *ACH* represents the air changes per hour [h^{-1}], and *V* is the office room volume [m^3]. The corresponding volumetric flowrate are simply given by:

$$Q_{in} = Q_{out} = ACH * V \tag{4.2}$$

Where Q_{in} and Q_{out} are the supply and exhaust volumetric flowrate, respectively [m^3/h].

4.1.3 Simulation parameters

As the infection risk final calculation is concerned, the model simulation has been run under some assumptions intended to depict a real everyday situation in the analysed office room. These fixed conditions regard the activity level of the bystanders and the operation of the ventilation system. They are shown below:

- **1 infected person** and **1 susceptible person** share the office. Different situations are analysed depending on the position of the infected subject within the room. Since the space has been divided into four cells, he can be located in each of them, leading to four possible configurations. Conversely, the infection risk is calculated for all the possible positions of the susceptible subject (the infection probability is a function of the zonal quanta concentration, that does not depend on the susceptible individual). Figure 4.3 presents these considered possibilities.
- both individuals perform typical office tasks, thus a sedentary/standing activity level can be considered. For the susceptible person, an inhalation rate of 0.54 m^3/h has been chosen, accordingly. Similarly, for the infected person, a quanta generation rate ranging from 10 to 70 quanta/h has been taken (see Table 2.3). In this second case,

however, larger margins for q have been considered compared to those reported in Table 2.3 for SARS-CoV-2 for standing activity. In fact, Buonanno et al. calculated a value of 61 quanta/h for the restaurant outbreak in Guangzhou [23], where the activity level was presumably similar to that of offices (see §2.1.1.2), therefore, adopting a wider range seems reasonable. This choice is also justified by the fact that those authors provide probability density functions for q, not definite values.

- when the model integrates the use of masks, both individuals wear the same type of protection presented in §3.2.3. In this way three simple scenarios are generated: no masks, use of surgical masks, and use of FFP2 (for corresponding parameters, see Table 3.1).
- a typical workday of 8 hours is considered. For the sake of simplicity, there are not intermediate breaks. Therefore, the susceptible person undergoes an exposure time of 8 continuous hours, which is also the simulation interval.
- the ventilation system works continuously during the day, providing a fresh air flowrate corresponding to 1, 1.5 and 2 h^{-1} (*ACH*).

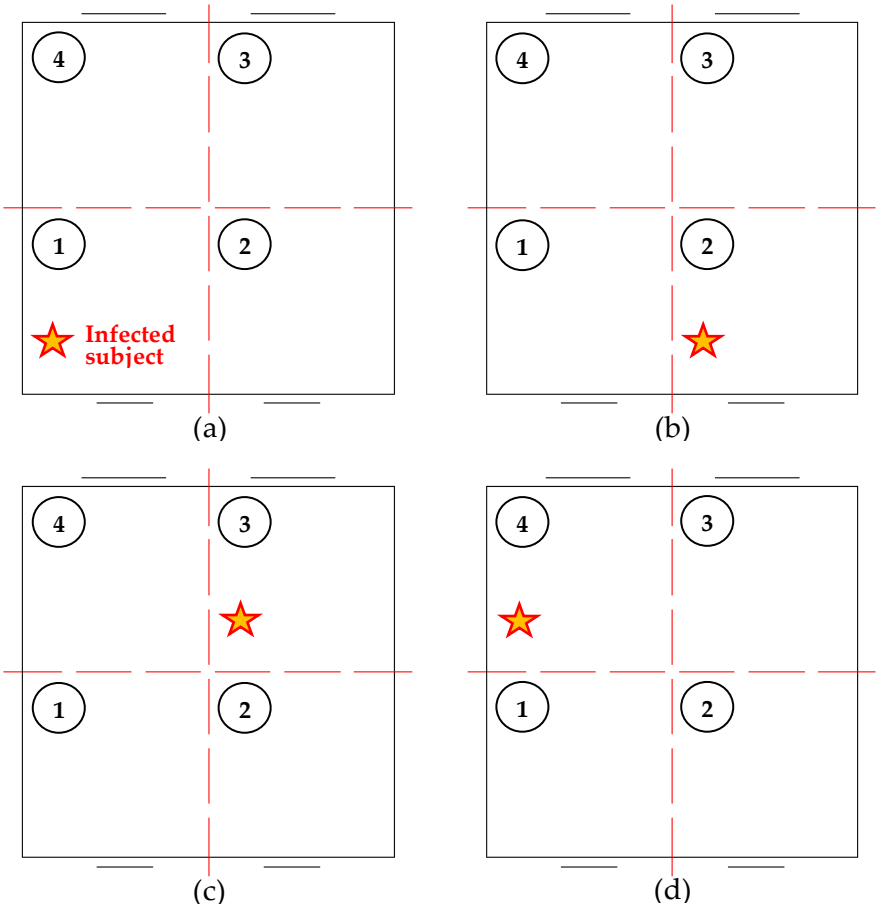

Figure 4.3 Simulation scenarios for different positions of the infected subject. Infected source in Zone 1 (a). Infected source in Zone 2 (b). Infected source in Zone 3 (c). Infected source in Zone 4 (d).

For each position of the infected person shown in Figure 4.3, the simulation parameters are summarized in Table 4.3.

Table 4.3 Model simulation parameters.

SIMULATION PARAMETER	SYMBOL	VALUES	U.M.
Breathing rate	p	0.54	m^3/h
Quanta generation rate	q	10	quanta/h
		20	quanta/h
		30	quanta/h
		40	quanta/h
		50	quanta/h
		60	quanta/h
		70	quanta/h
Exposure time	t_{exp}	8	h
Air changes per hour	ACH	1.0	h^{-1}
		1.5	h^{-1}
		2.0	h^{-1}

For this 4-zone infection risk model assessing the probability of contracting COVID-19 within an office room, the infected person can be at four different positions and the outdoor air flowrate can assume three values, leading to twelve simulated situations. In the following paragraph, the main results are presented.

4.1.4 Model results

The main results from the model simulations refer to interzonal flowrates and zonal infection probabilities. The former are the final output of the zonal ventilation model constituting the first step of the analysis, whereas the latter are the final outcome of the risk evaluation.

4.1.4.1 Interzonal mass and volumetric flowrates

The implementation of the zonal ventilation model, described in §3.1, enables the definition of the interzonal airflows crossing the boundary surfaces between two adjacent zones. These airflows assume different values according to the outdoor air flowrate, which is an input parameter for the mass and energy balance equations. For the case-study of interest, three values for *ACH* are considered (see Table 4.3), so the 4-zone model leads to three different sets of interzonal airflows. The outcomes are reported in terms of mass flowrates for each situation in Table 4.4, Table 4.5, and Table 4.6. For each boundary surface, the net mass flowrate is calculated. Conversely Table 4.7, Table 4.8, and Table 4.9 show the volumetric flowrates, which constitute an input parameter in the successive infection risk evaluation. In each table, the flowrate across a single diffuser and a single exhaust grille is reported.

Table 4.4 Interzonal mass flowrates in the case of *ACH*=1.0 h^{-1}.

ACH=1.0 h^{-1}				
INTERFACE	$\dot{m}_{ij}$	**[kg/h]**	**Net $\dot{m}$ [kg/h]**	**Direction**
Zones 1 and 2	$\dot{m}_{12}$	523	0	-
	$\dot{m}_{21}$	523		
Zones 2 and 3	$\dot{m}_{23}$	507	26	*From 3 to 2*
	$\dot{m}_{32}$	533		
Zones 3 and 4	$\dot{m}_{34}$	521	0	-
	$\dot{m}_{43}$	521		
Zones 4 and 1	$\dot{m}_{41}$	532	26	*From 4 to 1*
	$\dot{m}_{14}$	506		
Air diffuser/Exhaust grille	$\dot{m}_{in} = \dot{m}_{out}$	26	26	Inlet/Outlet

Table 4.5 Interzonal mass flowrates in the case of *ACH*=1.5 h^{-1}.

ACH=1.5 h^{-1}				
INTERFACE	$\dot{m}_{ij}$	**[kg/h]**	**Net $\dot{m}$ [kg/h]**	**Direction**
Zones 1 and 2	$\dot{m}_{12}$	530	0	-
	$\dot{m}_{21}$	530		
Zones 2 and 3	$\dot{m}_{23}$	507	39	*From 3 to 2*
	$\dot{m}_{32}$	546		
Zones 3 and 4	$\dot{m}_{34}$	527	0	-
	$\dot{m}_{43}$	527		
Zones 4 and 1	$\dot{m}_{41}$	543	39	*From 4 to 1*
	$\dot{m}_{14}$	504		
Air diffuser/ Exhaust grille	$\dot{m}_{in} = \dot{m}_{out}$	39	39	Inlet/Outlet

Table 4.6 Interzonal mass flowrates in the case of *ACH*=2.0 h^{-1}.

ACH=2.0 h^{-1}				
INTERFACE	$\dot{m}_{ij}$	**[kg/h]**	**Net $\dot{m}$ [kg/h]**	**Direction**
Zones 1 and 2	$\dot{m}_{12}$	534	0	-
	$\dot{m}_{21}$	534		
Zones 2 and 3	$\dot{m}_{23}$	503	52	*From 3 to 2*
	$\dot{m}_{32}$	555		
Zones 3 and 4	$\dot{m}_{34}$	530	0	-
	$\dot{m}_{43}$	530		
Zones 4 and 1	$\dot{m}_{41}$	551	52	*From 4 to 1*
	$\dot{m}_{14}$	499		
Air diffuser/ Exhaust grille	$\dot{m}_{in} = \dot{m}_{out}$	52	52	Inlet/Outlet

Table 4.7 Interzonal volumetric flowrates in the case of *ACH*=1.0 h^{-1}.

ACH=1.0 h^{-1}		
INTERFACE	**VOLUMETRIC FLOWRATES**	**VALUES [m^3/h]**
Zones 1 and 2	Q_{12}	427.7
	Q_{21}	427.5
Zones 2 and 3	Q_{23}	414.8
	Q_{32}	436.2
Zones 3 and 4	Q_{34}	426.1
	Q_{43}	426.2
Zones 4 and 1	Q_{41}	434.8
	Q_{14}	413.3
Air diffuser/Exhaust grille	$Q_{in}=Q_{out}$	21.6

Table 4.8 Interzonal volumetric flowrates in the case of *ACH*=1.5 h^{-1}.

ACH=1.5 h^{-1}		
INTERFACE	**VOLUMETRIC FLOWRATES**	**VALUES [m^3/h]**
Zones 1 and 2	Q_{12}	435.7
	Q_{21}	435.4
Zones 2 and 3	Q_{23}	416.5
	Q_{32}	448.7
Zones 3 and 4	Q_{34}	433.1
	Q_{43}	433.3
Zones 4 and 1	Q_{41}	446.4
	Q_{14}	414.1
Air diffuser/ Exhaust grille	$Q_{in}=Q_{out}$	32.4

Table 4.9 Interzonal volumetric flowrates in the case of *ACH*=2.0 h^{-1}.

ACH=2.0 h^{-1}		
INTERFACE	**VOLUMETRIC FLOWRATES**	**VALUES [m^3/h]**
Zones 1 and 2	Q_{12}	439.7
	Q_{21}	439.4
Zones 2 and 3	Q_{23}	414.4
	Q_{32}	457.3
Zones 3 and 4	Q_{34}	436.3
	Q_{43}	436.4
Zones 4 and 1	Q_{41}	454.1
	Q_{14}	411.0
Air diffuser/ Exhaust grille	$Q_{in}=Q_{out}$	43.2

As an example, Figure 4.4 shows the situation depicted in Table 4.4 and Table 4.7, with an air exchange rate of 1.0 h^{-1}. Figure 4.4(a) reports the net mass flowrates, whereas Figure 4.4(b) illustrates the bidirectional volumetric flowrates for each interface.

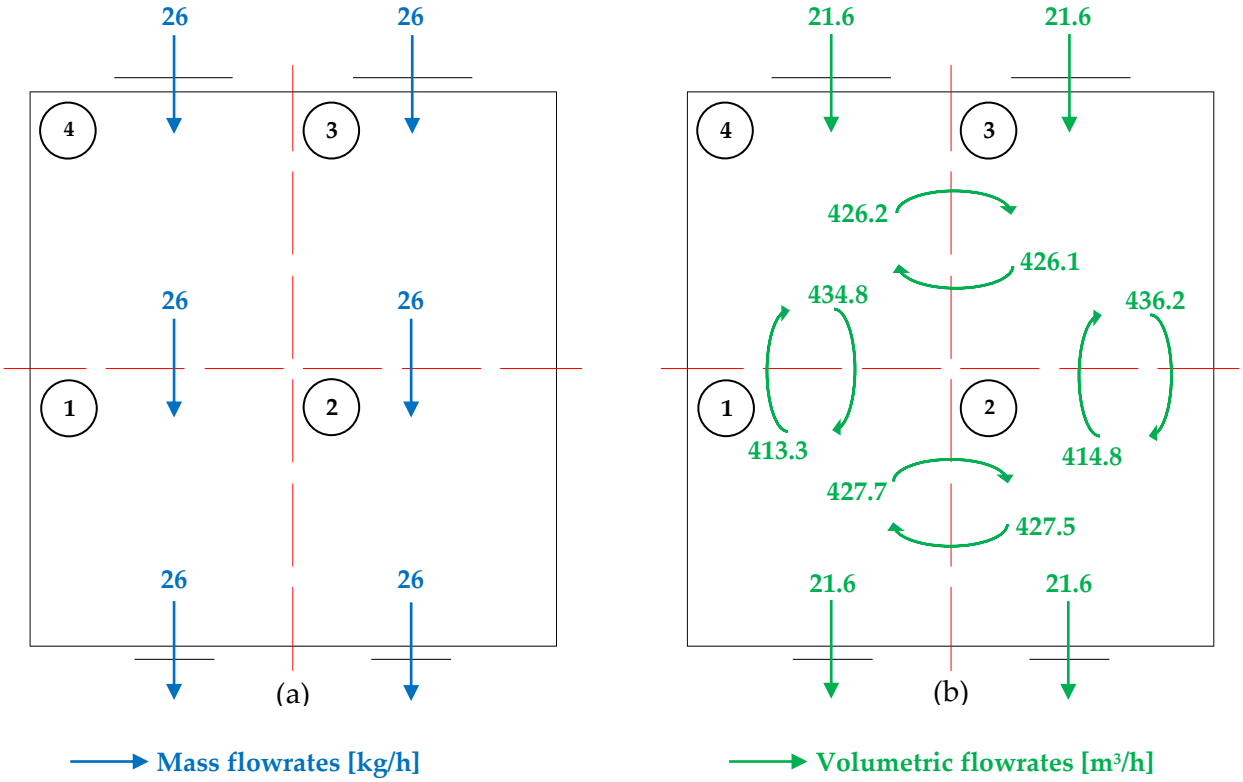

Figure 4.4 Interzonal airflows with *ACH*=1.0 h^{-1}. Net mass flowrates [kg/h] (a). Volumetric flowrates [m^3/h] (b).

From the tables above, it can be seen that the obtained interzonal flowrates are higher than the ventilation air flowrate by about an order of magnitude. Moreover, it can be noticed that *ACH* value has only a very slight influence on the interzonal air movements. It would be necessary verifying if these resulting values are mainly determined by the adopted partitioning approach, i.e., the chosen number of cells. In any case, these considerable airflows entail a significant mixing effect within the room volume, producing a high internal recirculation of airborne material. In fact, the interzonal volumetric flowrates are the vehicles transporting the infectious particles from one zone to the other, and the spatial distribution of risk strongly depends on their extent.

4.1.4.2 Zonal probabilities of infection

The infection risk assessment has been carried out solving the quanta concentration balance under both steady-state and transient conditions (see §3.2), within each zone. In this subparagraph, only the results under the latter case are reported, taking into consideration a time-varying quanta concentration. As said at the end §3.2, the MATLAB function ***ode45*** has been exploited for the transient regime. This function automatically establishes the

simulation timesteps. The infection risk has been calculated through Equations (3.47)-(3.49) at each timestep. However, only the zonal infection probabilities at the end of the total exposure time (8 h) are shown in the tables below. For briefness, only the outcomes for a quanta emission of 20 quanta/h are taken, but similar risk trends are obtained for the other generation rates. The chosen q value is in agreement with those reported in Table 2.3 for standing activity. Since this 4-zone model presents twelve simulation situations (as said in §4.1.3), the final results are grouped into four tables, from Table 4.10 to Table 4.13, referring to the position of the infected source. In this case, subjects do not use masks.

Table 4.10 Zonal infection probability after 8 h with infected source in Zone 1 and q=20 quanta/h (no mask).

***q*=20 quanta/h**	**INFECTED SOURCE IN ZONE 1**			
***ACH* [h^{-1}]**	**Zonal infection probability P_I [%]**			
	Zone 1	**Zone 2**	**Zone 3**	**Zone 4**
1.0	83.36	82.08	80.84	81.28
1.5	71.71	69.57	67.47	68.19
2.0	62.34	59.52	56.74	57.68

Table 4.11 Zonal infection probability after 8 h with infected source in Zone 2 and q=20 quanta/h (no mask).

***q*=20 quanta/h**	**INFECTED SOURCE IN ZONE 2**			
***ACH* [h^{-1}]**	**Zonal infection probability P_I [%]**			
	Zone 1	**Zone 2**	**Zone 3**	**Zone 4**
1.0	82.07	83.37	81.30	80.83
1.5	69.56	71.72	68.22	67.45
2.0	59.51	62.34	57.71	56.73

Table 4.12 Zonal infection probability after 8 h with infected source in Zone 3 and q=20 quanta/h (no mask).

***q*=20 quanta/h**	**INFECTED SOURCE IN ZONE 3**			
***ACH* [h^{-1}]**	**Zonal infection probability P_I [%]**			
	Zone 1	**Zone 2**	**Zone 3**	**Zone 4**
1.0	82.40	82.85	83.38	82.08
1.5	70.16	70.91	71.74	69.57
2.0	60.34	61.33	62.37	59.52

Table 4.13 Zonal infection probability after 8 h with infected source in Zone 4 and q=20 quanta/h (no mask).

***q*=20 quanta/h**	**INFECTED SOURCE IN ZONE 4**			
***ACH* [h^{-1}]**	**Zonal infection probability P_I [%]**			
	Zone 1	**Zone 2**	**Zone 3**	**Zone 4**
1.0	82.84	82.41	82.09	83.37
1.5	70.90	70.18	69.59	71.73
2.0	61.31	60.36	59.54	62.36

From the tables above, some considerations can be made:

- the airborne infection risk reaches high values up to almost 85% after an exposure time of 8 h, even for a quanta emission rate of 20 quanta/h. This means that for higher *q*, the probability to contract COVID-19 for the susceptible person can rise up to almost 100%. The obtained results highlight the importance of adopting suitable control measures to reduce the airborne transmission of COVID-19.
- increasing the ventilation rate proves to be a very effective control strategy against airborne transmission. In every situation displayed by the tables, going from *ACH* of 1.0 h^{-1} to 2.0 h^{-1} leads to a reduction in infection probability of approximately 20% in each zone of the room. Thus, the ventilation flowrate conveys a remarkable dilution and cleaning effect on the infectious particles released by the infected individual.
- the relative position of the susceptible subject and the infected source does not seem to be so influential on the infection probability. A slight reduction in P_I can be noticed from the zone where the infected person is located to the others, but the difference consists of just few percentage points. However, this small decrease becomes more substantial with increasing ventilation rates. Taking as example Table 4.10 with infected source in Zone 1, the higher difference in infection probability occurs between Zone 3 and Zone 1 itself, which are those not affecting each other through interzonal air movements, reaching almost 2.5% with 1.0 h^{-1}, 4% with 1.5 h^{-1}, and 5.5% with 2 h^{-1}. For the other cases, the trend is similar.
- the relative position of the infected source in regard to air diffusers and exhaust outlets is not a so crucial aspect in this case-study, as well. Nevertheless, the difference between zonal infection probabilities is higher when the infected source is close to the exhaust grilles (Table 4.10 and Table 4.11) than to the linear diffusers (Table 4.12 and Table 4.13). In the second case, the infection risk is even more uniform within the whole volume. This discrepancy can be justified by the cleaning effect of the ventilation flowrate crossing the office room from the North wall to the South one. Observing the result in §4.1.4.1, all situations present a net flowrate from Zone 3 to Zone 2, and from Zone 4 to Zone 1, therefore, if the infected source is in Zone 1, the general ventilation direction guides the infectious quanta towards the exhaust vents; on the other hand, if the infected source is in Zone 4, the air distribution promotes the spread of virus towards Zone 1 and the other zones, leading to a homogenous infection risk within the entire space.

The last two points suggest that the zonal approach does not give great answers in terms of spatial distribution of the infection risk, since it turns out to be uniform within the entire volume, more or less. Probably, the reason of this result lies in the small number of cells for the case-study: the calculated interzonal flowrates assume high values (see §4.1.4.1) and the resulting flow field configuration is almost equivalent to a perfectly mixed space. Therefore, four zones do not produce an adequate spatial discretization and the outcomes are not enough

meaningful. In any case, as stated above, slight differences between zonal infection probabilities can be observed, underlining that the zonal approach is effective.
From the tables, it emerges that different positions of the infected person do not produce relevant variations in absolute values of the infection risk. For this reason, hereinafter, the focus will be centred on a single configuration, with the infected source standing in Zone 1. Table 4.14 gives a complete overview with all simulation results for this situation, after an exposure time of 8 h and without masks.

Table 4.14 Zonal infection probability after 8 h with infected source in Zone 1 (no mask).

INFECTED SOURCE IN ZONE 1					
ACH **[h^{-1}]**	***q*** **[quanta/h]**	**Zonal infection probability P_I [%]**			
		Zone 1	**Zone 2**	**Zone 3**	**Zone 4**
1.0	10	59.21	57.66	56.23	56.73
	20	83.36	82.08	80.84	81.28
	30	93.21	92.41	91.61	91.90
	40	97.23	96.79	96.33	96.50
	50	98.87	98.64	98.39	98.48
	60	99.54	99.42	99.30	99.34
	70	99.81	99.76	99.69	99.72
1.5	10	46.81	44.84	42.81	43.60
	20	71.71	69.57	67.47	68.19
	30	84.95	83.21	81.44	82.06
	40	92.00	90.74	89.42	89.88
	50	95.74	94.89	93.96	94.29
	60	97.74	97.18	96.56	96.78
	70	98.80	98.45	98.04	98.19
2.0	10	38.63	36.38	34.23	34.95
	20	62.34	59.52	56.74	57.68
	30	76.89	74.25	71.55	72.47
	40	85.82	83.62	81.29	82.09
	50	91.29	89.56	87.69	88.35
	60	94.66	93.37	91.91	92.42
	70	96.72	95.78	94.68	95.07

It can be observed that for higher quanta emission rates, the infection probability remains above 95% even if the ventilation rate increases up to 2.0 h^{-1}. Furthermore, the zonal infection probabilities are even more uniform than for lower *q* values, and slight differences are flattened. Conversely, the effect of higher *ACH*, is evident for lower quanta generation

rates. These aspects can be easily quantified by calculating the relative variation in zonal infection risk with the different ventilation rates through this equation:

$$\Delta P_{I,\%} = \left(\frac{P_{I,1\ h^{-1}} - P_{I,1.5\ h^{-1}}}{P_{I,1\ h^{-1}}} \right) * 100 \tag{4.3}$$

Where $\Delta P_{I,\%}$ is the percentage relative change in infection probability between the considered situations [%], $P_{I,1\ h^{-1}}$ is the infection probability related to a ventilation rate of 1 h^{-1} [%], whereas $P_{I,1.5\ h^{-1}}$ is that related to 1.5 [%]. $P_{I,2\ h^{-1}}$ [%] must be used for percentage difference between 1 h^{-1} and 2 h^{-1}. The results are reported in Table 4.15.

Table 4.15 Percentage relative variation in zonal infection risk increasing the ventilation rate.

INFECTED SOURCE IN ZONE 1					
***ACH* [h^{-1}]**	***q* [quanta/h]**	**Percentage relative variation of risk $\Delta P_{I,\%}$ [%]**			
		Zone 1	**Zone 2**	**Zone 3**	**Zone 4**
1.5 vs 1.0	10	20.9	22.2	23.9	23.1
	20	14.0	15.2	16.5	16.1
	30	8.9	10.0	11.1	10.7
	40	5.4	6.3	7.2	6.9
	50	3.2	3.8	4.5	4.3
	60	1.8	2.3	2.8	2.6
	70	1.0	1.3	1.7	1.5
2.0 vs 1.0	10	34.8	36.9	39.1	38.4
	20	25.2	27.5	29.8	29.0
	30	17.5	19.7	21.9	21.1
	40	11.7	13.6	15.6	14.9
	50	7.7	9.2	10.9	10.3
	60	4.9	6.1	7.4	7.0
	70	3.1	4.0	5.0	4.7

From the table above, the major effect of the ventilation rate on situations with lower *q*, can be noticed, with a relative reduction in infection risk up to 40% in the case of 2.0 h^{-1} and a generation of 10 quanta/h. Effective dilution and removal of quanta for higher release rates can be achieved only further increasing *ACH* or through other strategies.
The zonal infection risk trend over exposure time can be represented through the characteristic risk graphs. Figure 4.5, Figure 4.6, and Figure 4.7 illustrate the infection risk exponential curves concerning the same situation of Table 4.15, i.e., with infected source in Zone 1.

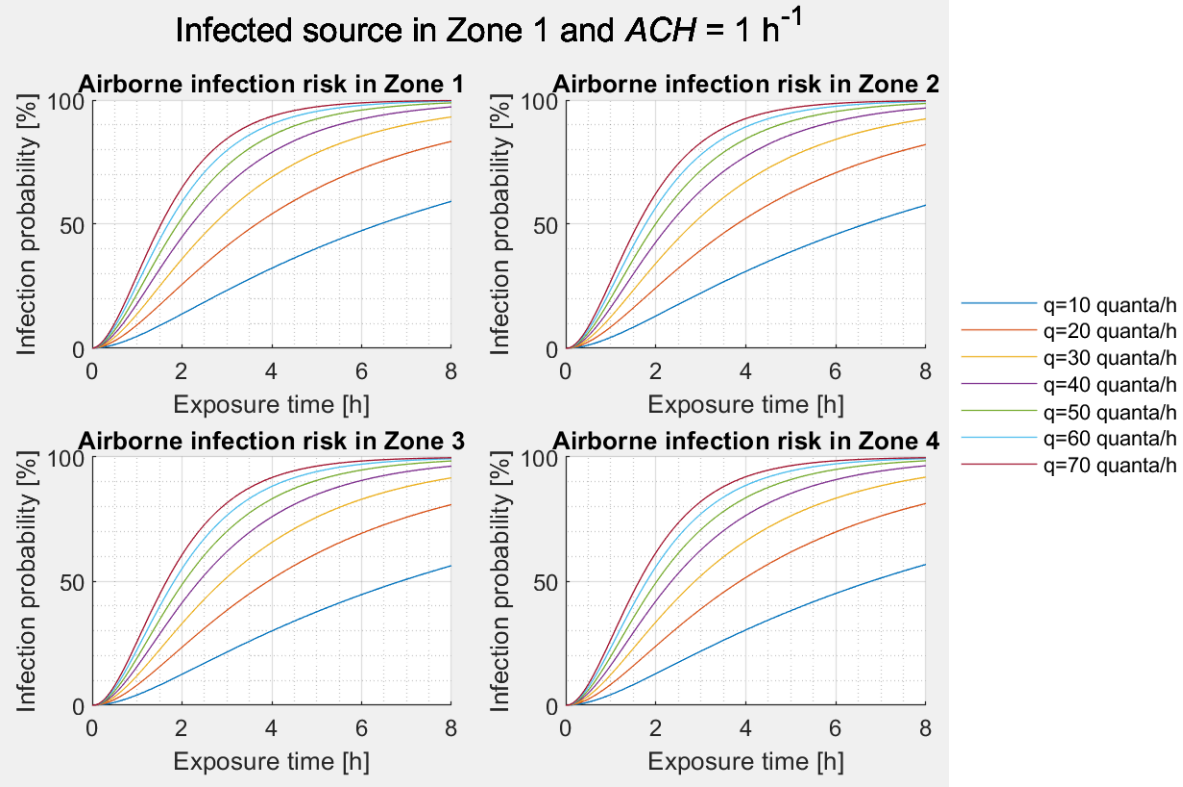

Figure 4.5 Infected source in Zone 1 and *ACH*=1 h^{-1} (no masks): zonal infection risk trends.

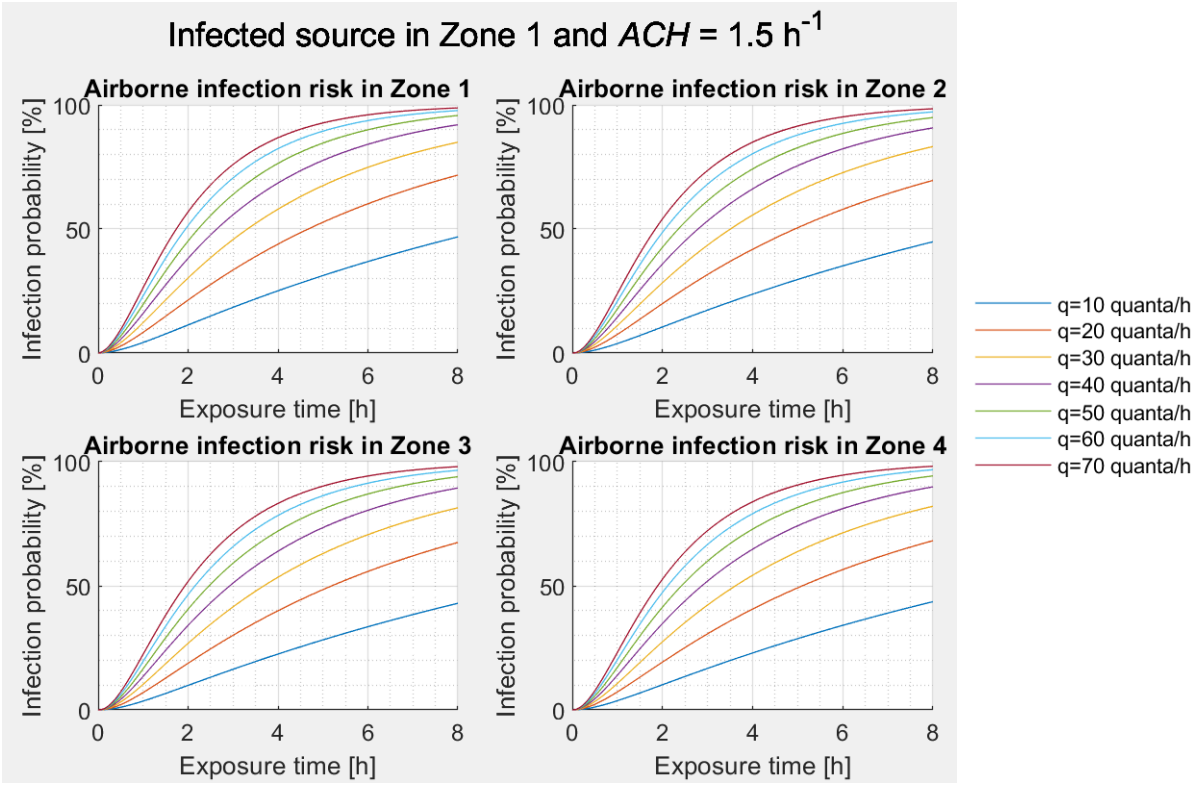

Figure 4.6 Infected source in Zone 1 and *ACH*=1.5 h^{-1} (no masks): zonal infection risk trends.

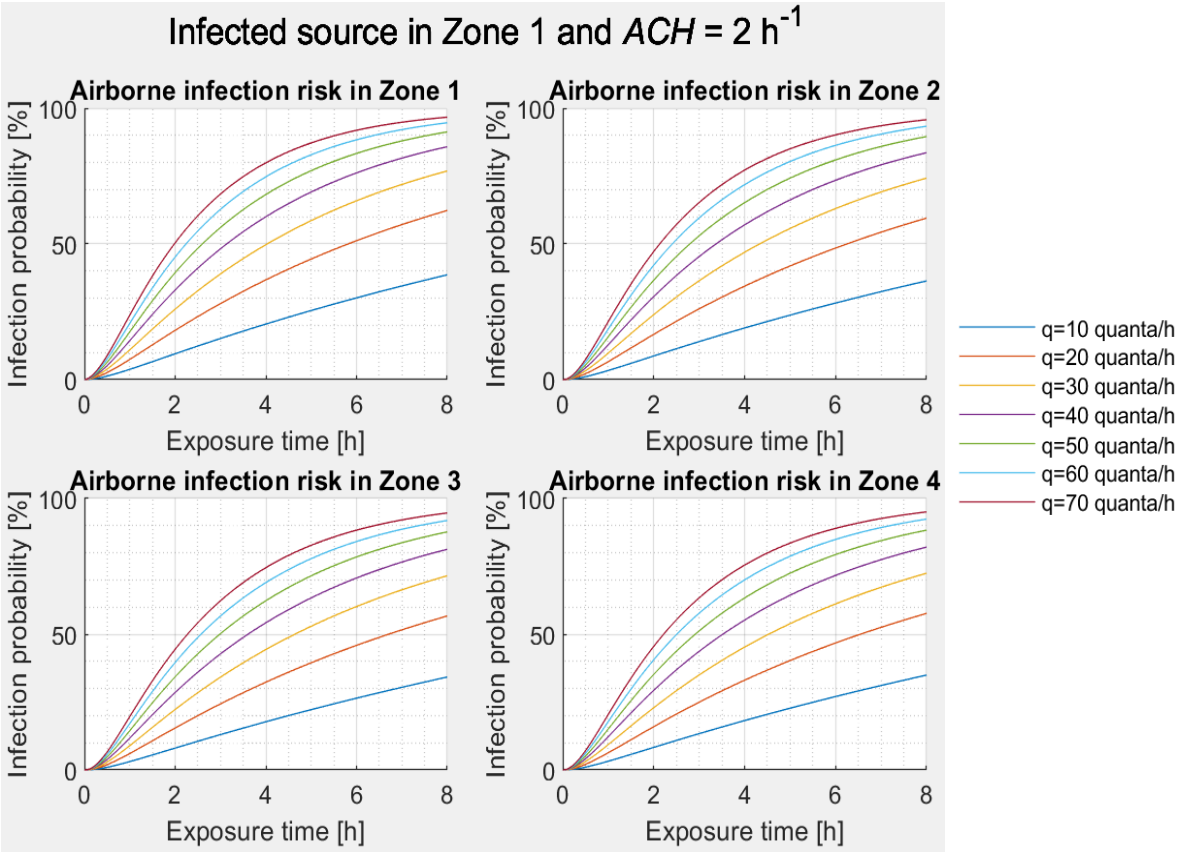

Figure 4.7 Infected source in Zone 1 and *ACH*=2 h^{-1} (no masks): zonal infection risk trends.

As we can see from these figures, considering the worst-case scenario with a production of 70 quanta/h, it would be necessary to spend less than 1.5÷2 hours close to the infected source to keep the infection probability below 50%, which remains an unacceptable threshold.
To sum up, the adopted approach subdividing the office room into four zones, gives some preliminary information about the spatial distribution of the infection risk within the volume, although differences among cells are small. From the obtained results, two main conclusions can be inferred:

- increasing *ACH* to a technically achievable value is an optimal choice to dilute the airborne pathogens and replace infectious air. This effect is much more evident for low quanta emission rates, which are typical of office tasks where the employee is sitting and not speaking. However, other strategies could be necessary to lower the infection risk below an acceptable level for the susceptible individuals.
- it is necessary to employ a discretization grid with a higher number of cells to investigate the importance of the relative position of infected subject, susceptible subject, air diffusers and exhaust grilles with more reliable results. The 4-zone model constitutes a starting point to give a spatial resolution to infection risk assessment problems.

The following two subparagraphs deal with the bystanders wearing masks and the discrepancy between results under steady-state and transient conditions. Both of them treat the situation shown at the end of this section, with the infected source located in Zone 1, in order to make a comparison with original outcomes.

4.1.4.3 Addition of mask use by individuals

From §4.1.4.2, the obtained risk values are unacceptable to guarantee a safe workplace for individuals, even for a ventilation rate of 2.0 h^{-1}. Wearing masks becomes imperative for trying to contain the COVID-19 airborne transmission. All original situations have been simulated also with the use of surgical masks and FFP2 respirators, but, in this section, only the case with the infected source in Zone 1 is considered. For the sake of simplicity, the results are reported for a quanta emission rate of 20, 40 and 60 quanta/h, just to give a qualitative image of the influence of protective devices on infection risk reduction.
Table 4.16, Table 4.17, and Table 4.18 show the zonal infection risk probabilities related to the type of used facial protection, with 1, 1.5, and 2 h^{-1}, respectively. The effect of wearing masks is clear: surgical masks help to reduce infection risk by approximately 20÷50 % compared to the initial value without protections. Obviously, the absolute values of probabilities are also function of q and remain still substantial, but the decrease is noteworthy. On the other hand, FFP2 respirators prove to be an exceptional control measure against airborne transmission, since they enable to keep the infection risk under a value of 10%, except for the case with ACH=1 h^{-1} and q=60 quanta/h (see Table 4.16). With FFP2, the infection probability starts to assume acceptable values over the whole working time, so the employees will be safer. Observing the tables, the combination of masks and adequate ventilation rates contribute to a significant risk reduction.

Table 4.16 Zonal infection probability after 8 h with infected source in Zone 1, ACH=1 h^{-1} and mask use.

***ACH*=1 h^{-1}**	**INFECTED SOURCE IN ZONE 1**				
MASK	***q*** **[quanta/h]**	**Zonal infection probability P_I [%]**			
		Zone 1	**Zone 2**	**Zone 3**	**Zone 4**
No masks	20	83.36	82.08	80.84	81.28
	40	97.23	96.79	96.33	96.50
	60	99.54	99.42	99.30	99.34
Surgical masks	20	37.46	36.23	35.11	35.51
	40	60.89	59.34	57.89	58.40
	60	75.54	74.07	72.68	73.17
FFP2	20	4.67	4.49	4.32	4.38
	40	9.13	8.77	8.45	8.56
	60	13.38	12.86	12.40	12.56

Table 4.17 Zonal infection probability after 8 h with infected source in Zone 1, *ACH*=1.5 h^{-1} and mask use.

***ACH*=1.5 h^{-1}**	**INFECTED SOURCE IN ZONE 1**				
MASK	***q*** **[quanta/h]**	**Zonal infection probability P_I [%]**			
		Zone 1	**Zone 2**	**Zone 3**	**Zone 4**
No masks	20	71.71	69.57	67.47	68.19
	40	92.00	90.74	89.42	89.88
	60	97.74	97.18	96.56	96.78
Surgical masks	20	28.14	26.76	25.47	25.91
	40	48.37	46.36	44.45	45.10
	60	62.90	60.71	58.59	59.32
FFP2	20	3.32	3.13	2.95	3.01
	40	6.52	6.16	5.82	5.93
	60	9.62	9.09	8.60	8.77

Table 4.18 Zonal infection probability after 8 h with infected source in Zone 1, *ACH*=2 h^{-1} and mask use.

***ACH*=2 h^{-1}**	**INFECTED SOURCE IN ZONE 1**				
MASK	***q*** **[quanta/h]**	**Zonal infection probability P_I [%]**			
		Zone 1	**Zone 2**	**Zone 3**	**Zone 4**
No masks	20	62.34	59.52	56.74	57.68
	40	85.82	83.62	81.29	82.09
	60	94.66	93.37	91.91	92.42
Surgical masks	20	22.55	21.08	19.70	20.15
	40	40.02	37.72	35.51	36.25
	60	53.55	50.84	48.21	49.10
FFP2	20	2.57	2.39	2.21	2.27
	40	5.08	4.72	4.38	4.49
	60	7.52	6.99	6.49	6.66

In order to highlight in a more understandable way the reduction extent in infection probabilities, the relative variation in zonal risk with the different devices can be calculated through the following equation:

$$\Delta P_{I,\%} = \left(\frac{P_{I,no\ mask} - P_{I,surgical}}{P_{I,no\ mask}} \right) * 100 \qquad (4.4)$$

Where $\Delta P_{I,\%}$ is the percentage relative change in infection probability between the considered situations [%], $P_{I,no\ mask}$ is the infection probability without protection devices [%], whereas $P_{I,surgical}$ is that with surgical masks [%]. For FFP2, $P_{I,FFP2}$ must be used [%].

The relative variations are calculated for each situation shown from Table 4.16 to Table 4.18, and are reported in Table 4.19, Table 4.20, and Table 4.21.

Table 4.19 Percentage relative variation in zonal infection risk using protection devices with ACH=1 h^{-1}.

***ACH*=1 h^{-1}**	**INFECTED SOURCE IN ZONE 1**				
MASK	***q*** **[quanta/h]**	**Percentage relative variation of risk $\Delta P_{I,\%}$ [%]**			
		Zone 1	**Zone 2**	**Zone 3**	**Zone 4**
Surgical	20	55.1	55.9	56.6	56.3
vs	40	37.4	38.7	39.9	39.5
No masks	60	24.1	25.5	26.8	26.3
FFP2	20	94.4	94.5	94.7	94.6
vs	40	90.6	90.9	91.2	91.1
No masks	60	86.6	87.1	87.5	87.4

Table 4.20 Percentage relative variation in zonal infection risk using protection devices with ACH=1.5 h^{-1}.

***ACH*=1.5 h^{-1}**	**INFECTED SOURCE IN ZONE 1**				
MASK	***q*** **[quanta/h]**	**Percentage relative variation of risk $\Delta P_{I,\%}$ [%]**			
		Zone 1	**Zone 2**	**Zone 3**	**Zone 4**
Surgical	20	60.8	61.5	62.2	62.0
vs	40	47.4	48.9	50.3	49.8
No masks	60	35.6	37.5	39.3	38.7
FFP2	20	95.4	95.5	95.6	95.6
vs	40	92.9	93.2	93.5	93.4
No masks	60	90.2	90.6	91.1	90.9

Table 4.21 Percentage relative variation in zonal infection risk using protection devices with ACH=2 h^{-1}.

***ACH*=2 h^{-1}**	**INFECTED SOURCE IN ZONE 1**				
MASK	***q*** **[quanta/h]**	**Percentage relative variation of risk $\Delta P_{I,\%}$ [%]**			
		Zone 1	**Zone 2**	**Zone 3**	**Zone 4**
Surgical	20	63.8	64.6	65.3	65.1
vs	40	53.4	54.9	56.3	55.8
No masks	60	43.4	45.5	47.5	46.9
FFP2	20	95.9	96.0	96.1	96.1
vs	40	94.1	94.4	94.6	94.5
No masks	60	92.1	92.5	92.9	92.8

The tables above show the effectiveness of surgical masks and FFP2 in decreasing the infection risk. Surgical masks provide an intermediate protection to the susceptible subjects

and their efficacy rises if they are coupled with higher ventilation rates. As to FFP2 respirators, they reduce the infection risk by a magnitude of 85 to 95%, more or less.
Comparing the worst-case scenario, with ACH=1 h^{-1} and no masks, to the best-case scenario, with ACH=2 h^{-1} and FFP2, the importance of these strategies for airborne transmission mitigation can be observed. This comparison is illustrated by Table 4.22 for the absolute value of zonal risk, and Table 4.23 for the relative variations.

Table 4.22 Zonal infection probability after 8 h for worst and best scenario, with infected source in Zone 1.

INFECTED SOURCE IN ZONE 1					
Scenario	***q*** **[quanta/h]**	**Zonal infection probability P_I [%]**			
		Zone 1	**Zone 2**	**Zone 3**	**Zone 4**
ACH= 1 h^{-1}	20	83.36	82.08	80.84	81.28
and	40	97.23	96.79	96.33	96.50
No masks	60	99.54	99.42	99.30	99.34
ACH=2 h^{-1}	20	2.57	2.39	2.21	2.27
and	40	5.08	4.72	4.38	4.49
FFP2	60	7.52	6.99	6.49	6.66

Table 4.23 Percentage relative variation in zonal infection risk between worst and best scenario.

INFECTED SOURCE IN ZONE 1					
Comparison	***q*** **[quanta/h]**	**Percentage relative variation of risk $\Delta P_{I,\%}$ [%]**			
		Zone 1	**Zone 2**	**Zone 3**	**Zone 4**
Worst-case	20	96.9	97.1	97.3	97.2
vs	40	94.8	95.1	95.5	95.3
Best-case	60	92.4	93.0	93.5	93.3

The combination of higher ACH with use of FFP2 leads to a reduction of about 92÷97 % in infection risk compared to the worst scenario.
In an office room the employees must wear masks for all the duration of the workday, in order to reduce the airborne transmission of COVID-19, especially in a small space as in the analysed case-study. Asymptomatic workers would decrease the release of infectious quanta into the indoor environment, whereas the susceptible individuals would safeguard themselves from inhaling high doses of pathogens. So, the advantage is bidirectional, and this is the reason for those considerable risk reductions reported in the tables.
To conclude, Figure 4.8, Figure 4.9, and Figure 4.10 give a graphic representation to the importance of wearing surgical masks or FFP2. To obtain understandable diagrams, the specific situation with the infected source in Zone 1 and a quanta generation rate of 20 quanta/h has been chosen. The curves for other q values present a similar trend.

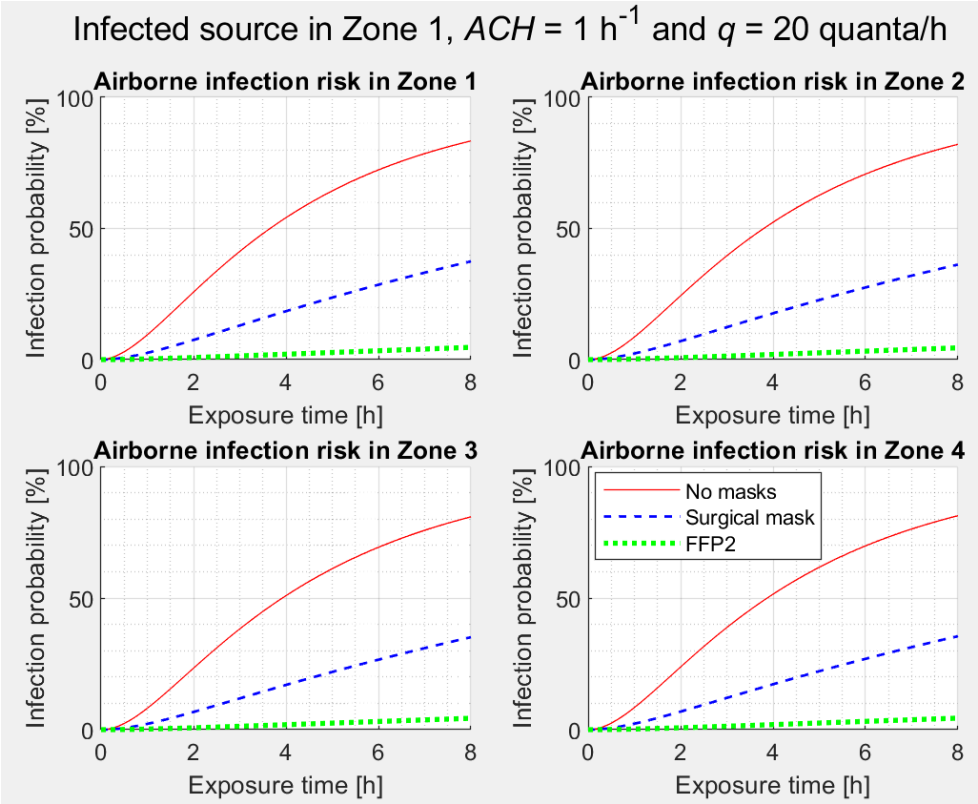

Figure 4.8 Zonal infection risk trend with and without masks (*ACH*=1 h^{-1}, *q*=20 quanta/h).

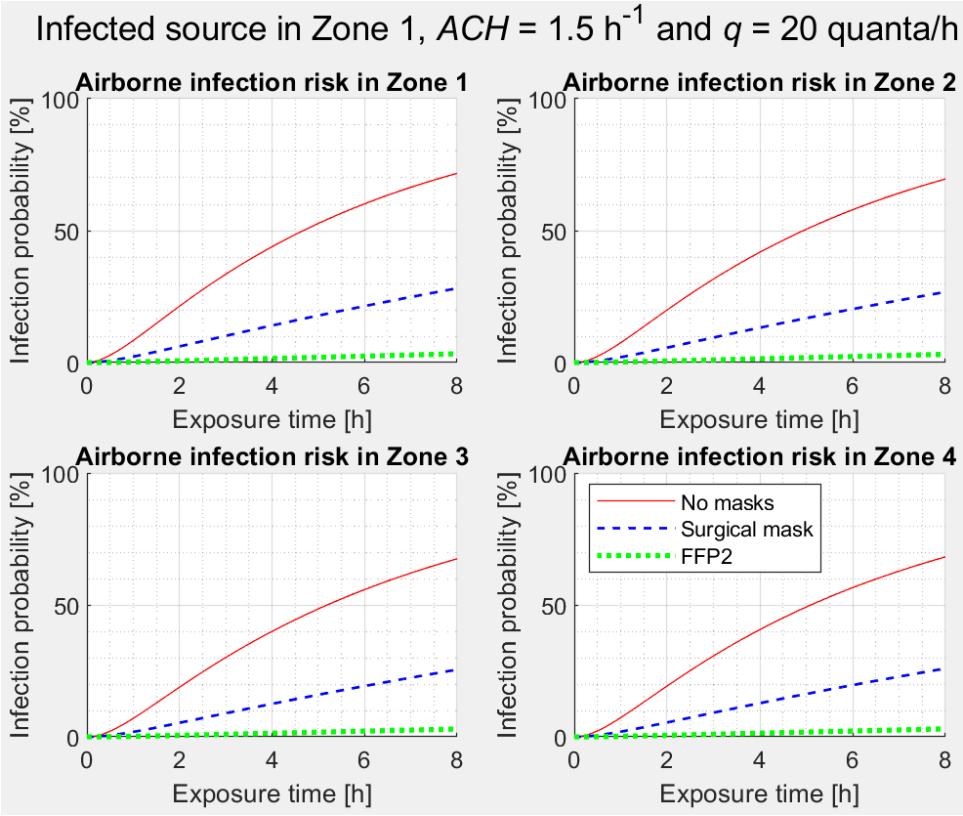

Figure 4.9 Zonal infection risk trend with and without masks (*ACH*=1.5 h^{-1}, *q*=20 quanta/h).

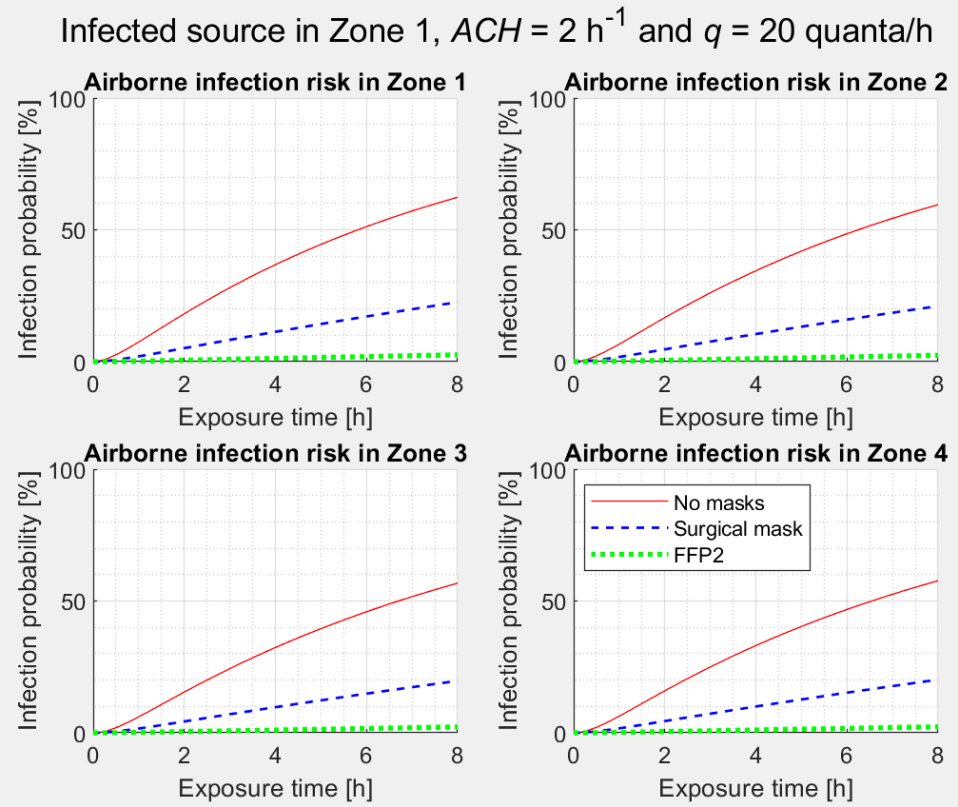

Figure 4.10 Zonal infection risk trend with and without masks (*ACH*=2 h^{-1}, *q*=20 quanta/h).

The figures above are qualitative images and confirm the effect of masks on the reduction of infection risk as shown quantitively in the previous tables.

To conclude, the use of masks is strongly recommended whenever individuals share the same indoor environment. Surgical masks provide a good protection against airborne transmission of SARS-CoV-2. FFP2 respirators are even better, since they strongly reduce the infection probability to levels below 10% and coupling them with high ventilation rates is an optimal mitigation strategy.

4.1.4.4 Infection risk evaluation: steady-state vs transient regime

While the interzonal flowrates are always defined under steady-state conditions, the quanta concentration and infection risk calculations are performed under both steady-state and transient conditions. In the previous subparagraphs, the results refer to the transient state. In this section, a comparison between these two regimes is carried out and differences are presented both in quanta concentration levels and risk extent. A specific simulation case is considered:

- the infected source is located in Zone 1 releasing pathogens at a rate of 20 quanta/h.
- two ventilation rates are compared: 1.0 and 2.0 h^{-1}.
- individuals do not wear masks.

For other *q* and *ACH* values, the same considerations can be done.

As quanta concentration is concerned, Figure 4.11 and Figure 4.12 report the results for *ACH* equal to 1.0 h^{-1} and 2.0 h^{-1}, respectively.

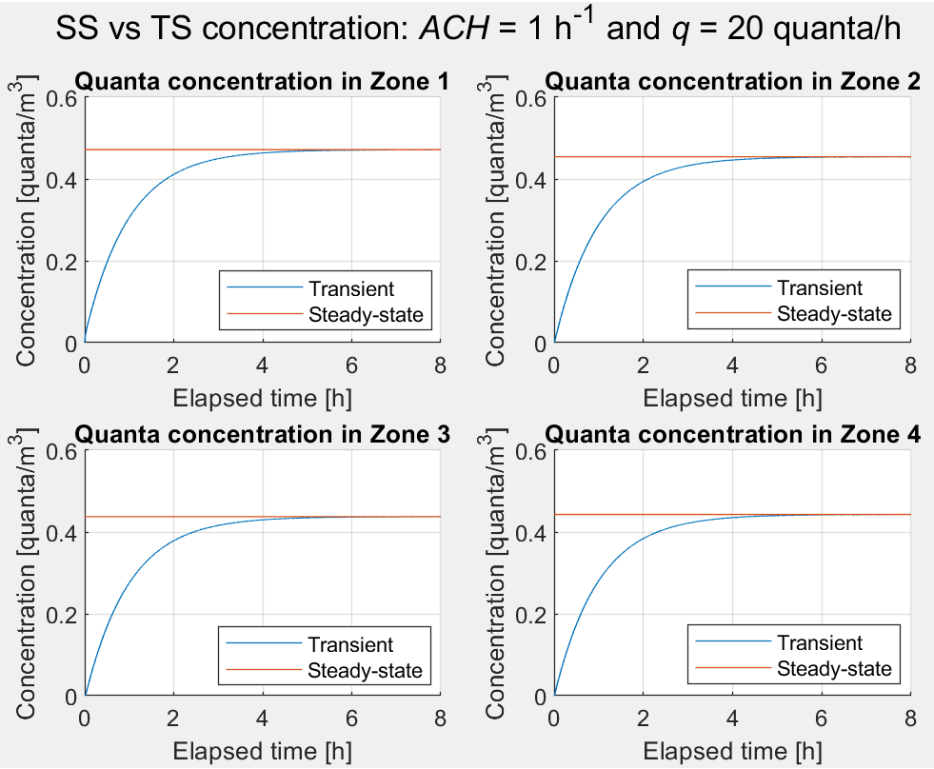

Figure 4.11 SS vs TS quanta concentration (*ACH*=1 h^{-1}, *q*=20 quanta/h, no masks).

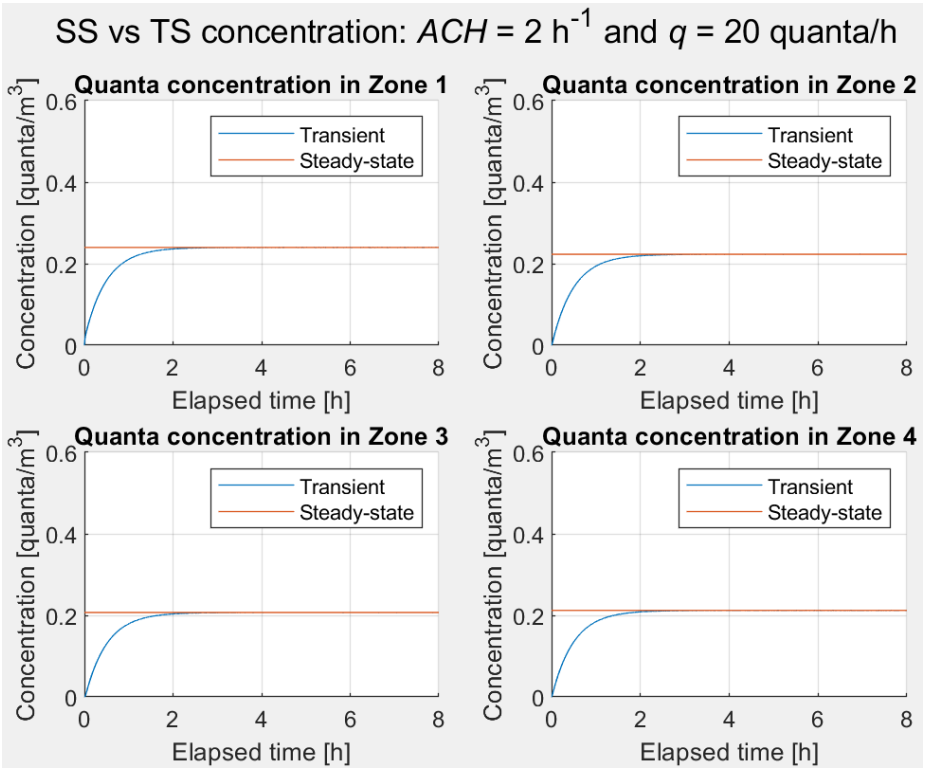

Figure 4.12 SS vs TS quanta concentration (*ACH*=2 h^{-1}, *q*=20 quanta/h, no masks).

The time-variable quanta concentration starts from zero and asymptotically reaches the saturation level, i.e., the steady-state quanta concentration C_{ss}. That trend for C_{ts} (transient state concentration) is obtained through the dynamic resolution of quanta concentration balance for each zone. Some important observations derive from examination of figures:

- increasing *ACH* enhances the dilution of quanta in the indoor environment, thus their concentration is lowered leading to a reduction in intake dose and infection probability.
- with higher *ACH* values, it takes less time to quanta concentration reaching the steady-state level. The dynamic trend of C_i (*i*-th zone) matches saturation after 4÷5 h with *ACH*=1 h^{-1}, after 2 h with *ACH*=2 h^{-1}.
- some effects of zonal approach are visible, since quanta concentration decreases moving from Zone 1, where the infected source is positioned. An interesting operation is quantifying these concentration differences for both the adopted ventilation rates, as shown in Table 4.24.

Table 4.24 Zonal quanta concentration variation compared to Zone 1 (*q*=20 quanta/h, no masks).

***q*=20 quanta/h**	**INFECTED SOURCE IN ZONE 1**			
***ACH* [h^{-1}]**	**Zonal quanta concentration [quanta/m^3]**			
	Zone 1	**Zone 2**	**Zone 3**	**Zone 4**
1.0	0.4716	0.4544	0.4375	0.4429
2.0	0.2398	0.2231	0.2071	0.2122
***ACH* [h^{-1}]**	**Concentration ratios $C_{ss,i}/C_{ss,1}$ [-]**			
1.0	1	0.964	0.928	0.939
2.0	1	0.930	0.864	0.885

In the table above, the concentration ratios point out that quanta spread more uniformly within the space with 1 h^{-1} than with 2 h^{-1}. Therefore, the higher ventilation rate presents a better cleaning effect, although the interzonal flowrates are slightly higher (compare Table 4.7 with Table 4.9). This findings on the concentration deviations, however, are coherent with the infection probability deviations observed in Table 4.10 for the same cases. Anyway, the room can be almost considered as a well-mixed environment.

The difference of quanta concentration over time between the two regimes, affects the inhaled dose by the susceptible person and his infection risk, consequently. The risk diagrams corresponding to the same situations are illustrated by Figure 4.13 and Figure 4.14. It can be clearly noticed that:

- analysing the problem under steady-state conditions causes an overestimation of quanta concentration and, thus, of infection risk. This overevaluation arises especially during the initial exposure hours, when the discrepancy between the actual concentration and the saturation level is larger (see Figure 4.11 and Figure 4.12).

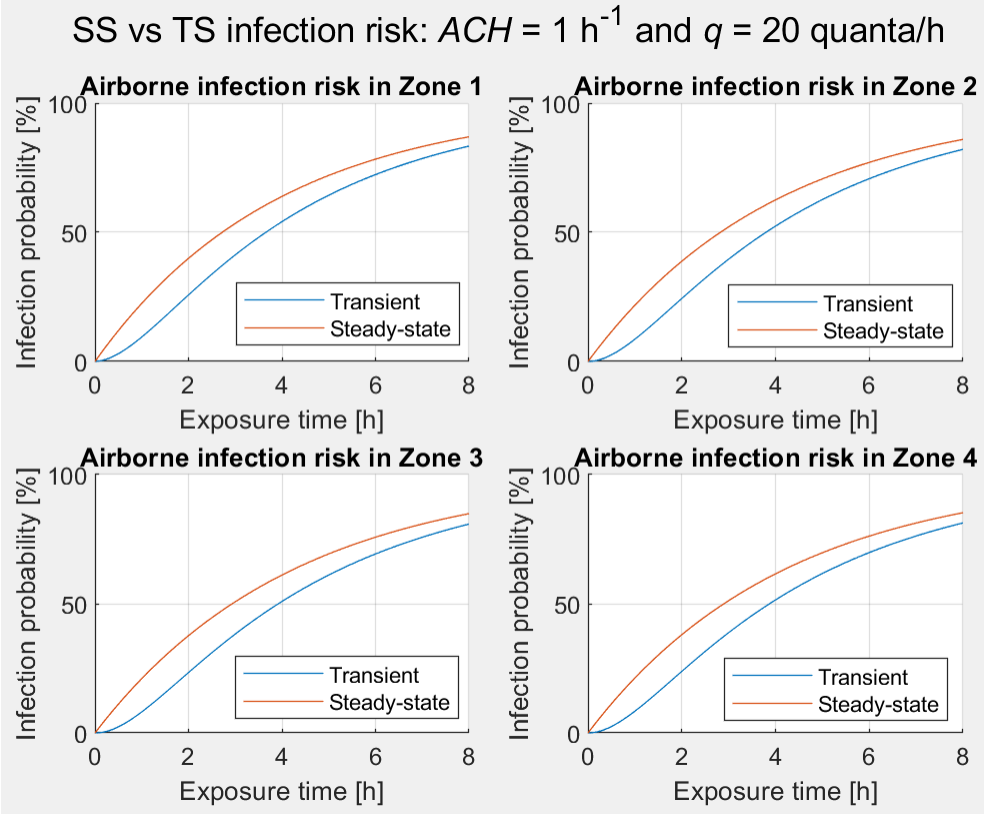

Figure 4.13 SS vs TS infection risk (*ACH*=1 h^{-1}, *q*=20 quanta/h, no masks).

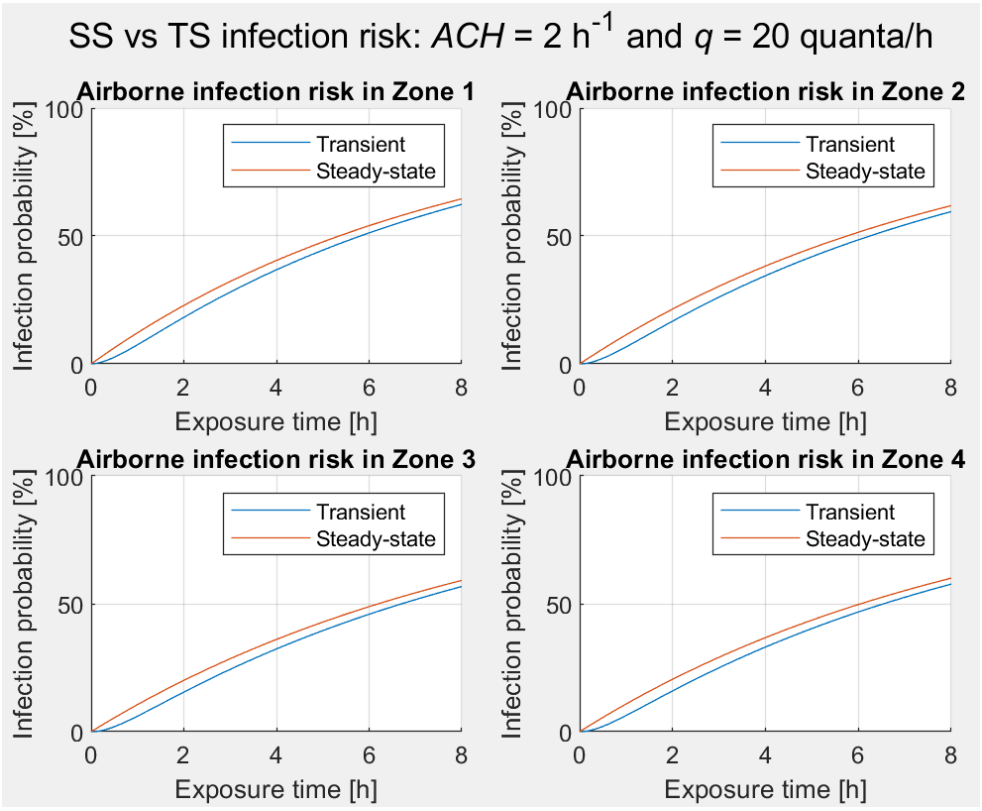

Figure 4.14 SS vs TS infection risk (*ACH*=2 h^{-1}, *q*=20 quanta/h, no masks).

- as the elapsed time approaches the total working hours, the distance between probability curves decreases .
- the overestimation of the infection risk is larger for lower ventilation rates. The trend is consistent with previous considerations, since for lower *ACH* it takes more time for concentration to reach the steady-state threshold, so, the difference between the regimes is accentuated.

Since the steady-state resolution of quanta concentration balance mainly overestimates the risk during the first exposure period, this difference is quantified for the simulated cases at 2 hours. The calculation is performed by the following equation, for each zone:

$$\Delta P_{I,\%} = \left(\frac{P_{I,ss} - P_{I,ts}}{P_{I,ts}} \right) * 100 \tag{4.5}$$

Where $\Delta P_{I,\%}$ is the percentage overestimation of infection probability [%], $P_{I,ss}$ is the infection probability under steady-state conditions [%], whereas $P_{I,ts}$ is that under dynamic conditions [%].

The results are shown by Table 4.25.

Table 4.25 Overestimation of infection probability under SS conditions after exposure of 2 hours (q= 20 quanta/h, no masks).

***q*=20 quanta/h**		**INFECTED SOURCE IN ZONE 1**			
***ACH* [h^{-1}]**	**Regime**	**Zonal infection probability P_I [%] after 2 h**			
		Zone 1	**Zone 2**	**Zone 3**	**Zone 4**
1.0	*Steady state*	39.91	38.78	37.65	38.02
	Transient	25.79	24.40	23.41	23.86
2.0	*Steady state*	22.82	21.41	20.04	20.48
	Transient	18.16	16.68	15.46	15.92
***ACH* [h^{-1}]**		**Overestimation $\Delta P_{I,\%}$ [%]**			
1.0		54.75	58.93	60.83	59.35
2.0		25.66	28.36	29.62	28.64

The overestimation is larger in the case of lower ventilation rate, reaching 60%, whereas, for higher *ACH* the deviation is kept under 30%.

The last comparison has been made running the simulation for the same situations with individuals wearing surgical masks or FFP2 respirators. Concerning surgical masks, Figure 4.15 and Figure 4.16 depict quanta concentration curves and infection risk trends, respectively. Similarly, for FFP2, Figure 4.17 shows quanta concentration, whereas Figure 4.18 the infection probability. For the sake of simplicity, only the graphs regarding Zone 1 and Zone 2 are reported for both ventilation rates.

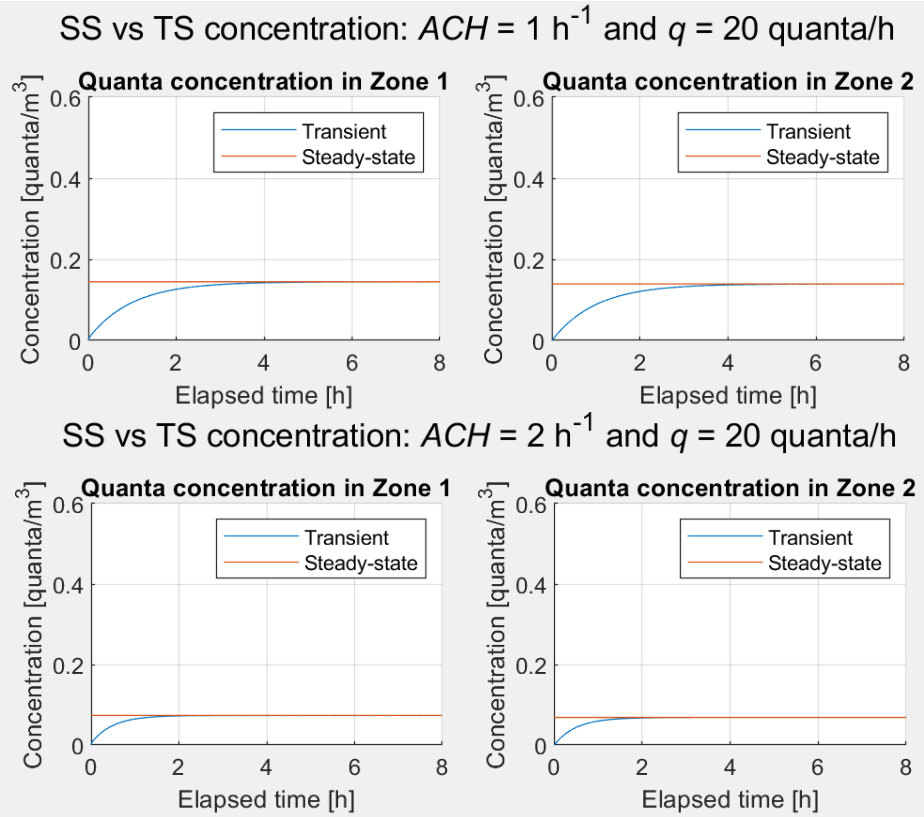

Figure 4.15 SS vs TS quanta concentration Zone 1 and 2 (q=20 quanta/h, surgical mask).

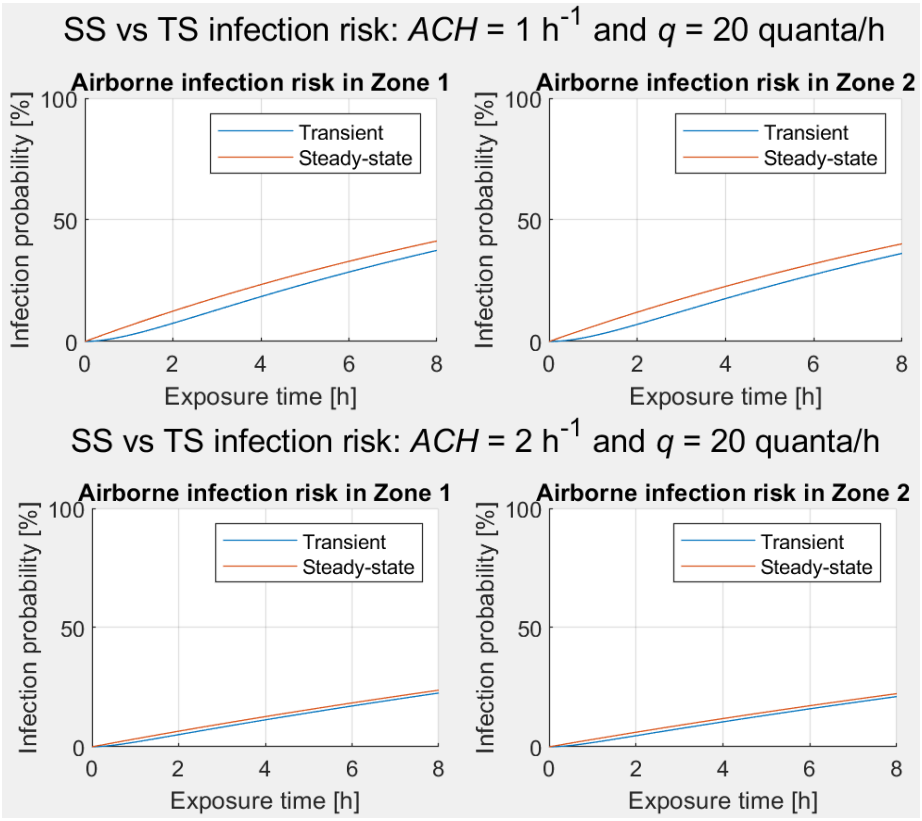

Figure 4.16 SS vs TS infection risk Zone 1 and 2 (q=20 quanta/h, surgical mask).

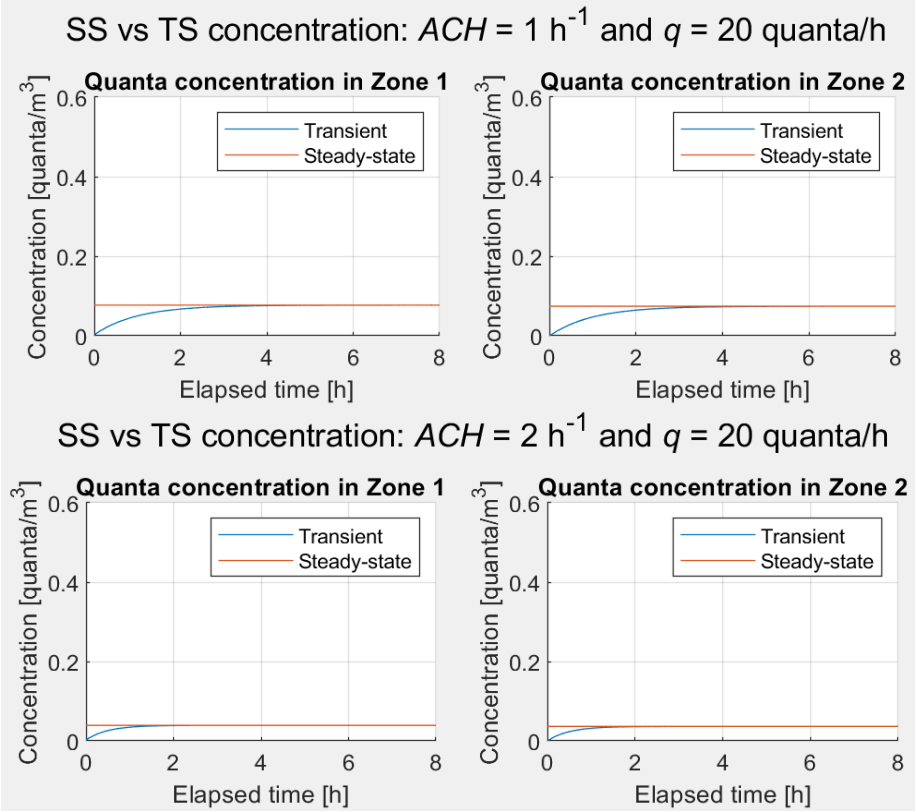

Figure 4.17 SS vs TS quanta concentration Zone 1 and 2 (q=20 quanta/h, FFP2).

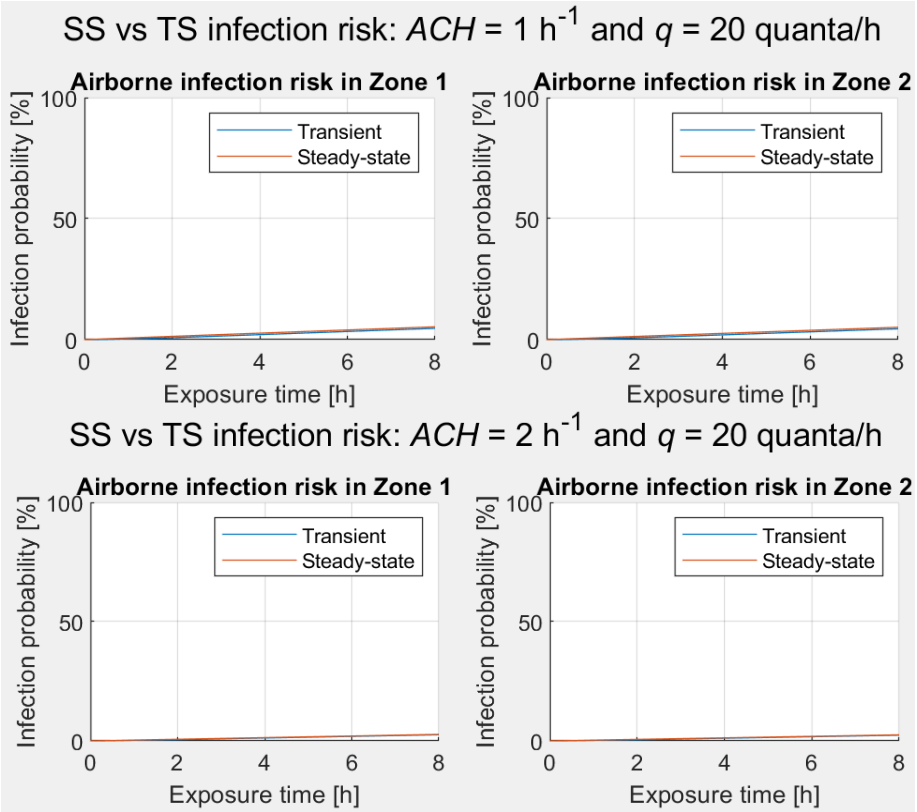

Figure 4.18 SS vs TS infection risk Zone 1 and 2 (q=20 quanta/h, FFP2).

Observing the images, masks prove to be a powerful instrument for reducing the quanta concentration in the indoor environment. As the parallelism between steady-state and transient conditions is concerned, these aspects can be detectes:

- the deviation between the two regimes is flattened compared to the case with no masks. For FFP2 there is almost no difference in the final results.
- the first point derives from the fact that the saturation level is very low, and the system takes less time to asympotically reach the steady-state threshold than before.

To sum up, the outcomes on infection risk differ if they are obtained under steady-state or transient conditions, and this deviation decreases with higher *ACH* and use of masks because these measures lower the saturation level of quanta in the room. Anyway, a risk assessor can perform the simulation considering the operational regime according to his objectives:

- transient state calculations should be carried out for situations characterized by a short exposure time for a susceptible subject, in order to obtain more precise results and to avoid overestimations.
- steady-state simplicity can be exploited for long exposure scenarios, or to maintain a margin of safety for example in design activities.

4.2 4-zone model for a fourfold office room

In this section, some results are reported concerning simulations of an office room with a fourfold volume compared to that described in §4.1. It is essentially an open space office. The assumptions and simulation parameters are identical to those of the original case-study both for the zonal modelling part and the final infection risk assessment (see §4.1.2 and §4.1.3). The only difference regards the dimensions of the geometrical domain. The following subparagraphs illustrate the case-study geometry, the obtained interzonal volumetric flowrates and infection risk probabilities; in this way, the comparison with results shown in §4.1 enables investigating the influence of volume on risk extent.

4.2.1 Geometrical domain and zonal discretization

The room of concern has a dimension of 8.0x8.0x2.7 m, so it occupies a floor area of 64 m^2 and a volume of 172.8 m^3. The zonal partitioning and cell numeration has been made in the same way as in the previous case: the open space office has been divided into **4 identical zones** with a cross section on the plan view. Therefore, a **4-zone risk model** is applied in this second case-study, as well. The orientation and the overall size of the room along with the performed spatial macro-discretization are shown in Figure 4.19Figure 4.1. The arrangement of the ventilation system terminals is specified, whereas windows and door are not shown in the figure, since they are neglected in the model. Room dimensions have been chosen so that a single zone correspond exactly to the original office room (based on a real room, i.e., Core-Care of the University of Padua) in terms of volume. This aspect is shown in Figure 4.19.

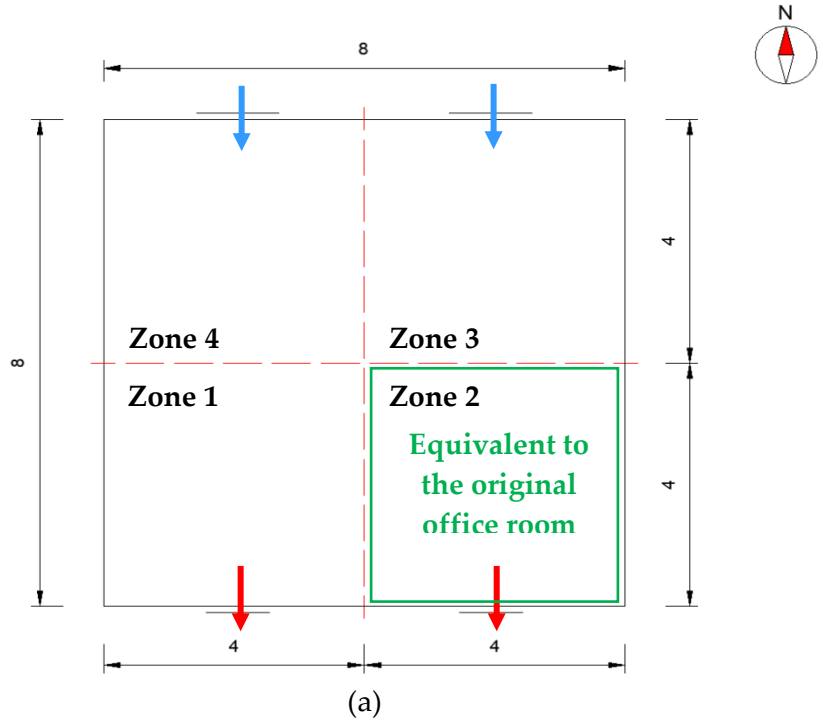

Figure 4.19 Zonal subdivision and numeration of the geometrical domain representing an open space office. Top view (a). 3D view (b).

As it can be seen, each zone is a parallelepiped with dimensions of 4x4x2.7 m. Air is supplied in Zone 3 and Zone 4 and is extracted by Zone 1 and Zone 2. No thermal stratification is taken into consideration, like the previous case-study.

4.2.2 Model results

The main results from the model simulations refer to interzonal flowrates and zonal infection probabilities. They are compared to those obtained for the first case-study, in order to verify the coherence in the orders of magnitude and in the risk trends.

4.2.2.1 Interzonal volumetric flowrates

Even for this case-study, three values for *ACH* are considered, i.e., 1, 1.5 and 2 h^{-1}. Therefore, the implementation of the zonal model defines three configurations for the air movement within the interested room. Table 4.26, Table 4.27, and Table 4.28 show the volumetric flowrates that are calculated for each given ventilation rate. The mass flowrates are not reported in this case; however, the bidirectional volumetric flowrates themselves permit to also visualize the net flows across the boundary surfaces. For each situation, the resulting motion field is similar to that illustrated by Figure 4.4.

Table 4.26 Interzonal volumetric flowrates in the case of *ACH*=1.0 h^{-1} (open space office).

ACH=1.0 h^{-1}		
INTERFACE	**VOLUMETRIC FLOWRATES**	**VALUES [m^3/h]**
Zones 1 and 2	Q_{12}	879.3
	Q_{21}	878.8
Zones 2 and 3	Q_{23}	828.7
	Q_{32}	914.5
Zones 3 and 4	Q_{34}	872.5
	Q_{43}	872.7
Zones 4 and 1	Q_{41}	908.2
	Q_{14}	822.0
Single air diffuser	Q_{in}	86.4
Single exhaust grille	Q_{out}	86.4

Table 4.27 Interzonal volumetric flowrates in the case of *ACH*=1.5 h^{-1} (open space office).

ACH=1.5 h^{-1}		
INTERFACE	**VOLUMETRIC FLOWRATES**	**VALUES [m^3/h]**
Zones 1 and 2	Q_{12}	886.9
	Q_{21}	886.2
Zones 2 and 3	Q_{23}	811.7
	Q_{32}	940.4
Zones 3 and 4	Q_{34}	876.6
	Q_{43}	876.6
Zones 4 and 1	Q_{41}	930.7
	Q_{14}	801.2
Single air diffuser	Q_{in}	129.6
Single exhaust grille	Q_{out}	129.6

Table 4.28 Interzonal volumetric flowrates in the case of *ACH*=2.0 h^{-1} (open space office).

ACH=2.0 h^{-1}		
INTERFACE	**VOLUMETRIC FLOWRATES**	**VALUES [m^3/h]**
Zones 1 and 2	Q_{12}	890.1
	Q_{21}	889.0
Zones 2 and 3	Q_{23}	790.4
	Q_{32}	962.0
Zones 3 and 4	Q_{34}	876.1
	Q_{43}	875.8
Zones 4 and 1	Q_{41}	949.0
	Q_{14}	775.9
Single air diffuser	Q_{in}	172.8
Single exhaust grille	Q_{out}	172.8

The interzonal volumetric flowrates calculated by the zonal model are very high and overcome the ventilation flowrates by about an order of magnitude, as for the small room. Moreover, *ACH* value does not significantly affect these airflows. Probably, this high recirculation rates still lie in the small spatial resolution given by the chosen discretization grid with four cells.
Having said that, the obtained results are consistent with those for the previous case-study. In fact, the volumetric flowrates within this larger office room are double of those within the smaller one and it seems coherent with the relative scale between the two geometrical domains. This aspect constitutes a first rough validation element on the reliability of the model outcomes.

4.2.2.2 Zonal probabilities of infection

Infection risk assessment has been carried out for all possible configurations discussed in §4.1.3. However, here only some results are shown to compare this case-study with the original one. The interested situation presents the following features: a single infected source stands in Zone 1, individuals do not wear masks and quanta concentration balance is solved under dynamic conditions (i.e., transient state). Table 4.29 reports the zonal infection probabilities after an exposure time of 8 h (i.e., the complete workday), for all imposed ventilation rates (i.e., 1, 1.5, and 2 h^{-1}) and for the entire considered *q* range (i.e., from 10 to 70 quanta/h). Therefore, this table exactly depicts the same situation of Table 4.14.
It can be clearly seen from the table that the infection risk is significantly lower than the original office room. This is due the enhanced dilution caused by a larger volume, as quanta spread over a wider space leading to an overall lower concentration (as only one infected source is considered). Interestingly, the zonal approach seems to be more effective in this case, since higher deviations between zonal infection probabilities can be observed.

Table 4.29 Zonal infection probability after 8 h with infected source in Zone 1 and no masks (opens space office).

INFECTED SOURCE IN ZONE 1					
***ACH* [h^{-1}]**	***q* [quanta/h]**	**Zonal infection probability P_I [%]**			
		Zone 1	**Zone 2**	**Zone 3**	**Zone 4**
1.0	10	20.49	19.04	17.75	18.19
	20	36.78	34.46	32.34	33.08
	30	49.73	46.94	44.35	45.25
	40	60.03	57.04	54.04	55.22
	50	68.22	65.22	62.35	63.36
	60	74.73	71.84	69.03	70.03
	70	79.90	77.20	74.53	75.48
1.5	10	15.01	13.49	12.11	12.56
	20	27.76	25.15	22.75	23.55
	30	38.60	35.25	32.10	33.15
	40	47.82	43.98	40.32	41.55
	50	55.65	51.54	47.55	48.89
	60	62.31	58.07	53.90	55.31
	70	67.96	63.73	59.48	60.93
2.0	10	11.90	10.34	8.93	9.38
	20	22.38	19.61	17.06	17.88
	30	31.61	27.92	24.47	25.58
	40	39.75	35.37	31.21	32.56
	50	46.92	42.05	37.36	38.88
	60	53.23	48.04	42.95	44.61
	70	58.80	53.41	48.04	49.80

In order to quantify the influence of a fourfold volume on the infection risk, the relative difference between the infection probabilities of this case and the previous one can be calculated through the following relationship:

$$\Delta P_{I,\%} = \left(\frac{P_{I,smaller\ room} - P_{I,larger\ room}}{P_{I,smaller\ room}} \right) * 100 \tag{4.6}$$

Where $\Delta P_{I,\%}$ is the percentage relative change in infection probability between the two considered case-studies [%], $P_{I,smaller\ room}$ is the infection probability related to the first case-study about the smaller office room [%], whereas $P_{I,larger\ room}$ is that related to the second case study about the open space office [%].
The percentage relative differences are shown in Table 4.30.

Table 4.30 Percentage relative difference in zonal infection risk between the two analysed case-studies.

Comparison between the original case-study and a fourfold volume room					
INFECTED SOURCE IN ZONE 1					
***ACH* [h^{-1}]**	***q* [quanta/h]**	**Percentage relative difference of risk $\Delta P_{I,\%}$ [%]**			
		Zone 1	**Zone 2**	**Zone 3**	**Zone 4**
1.0	10	65.39	66.98	68.43	67.94
	20	55.88	58.02	60.00	59.30
	30	46.65	49.20	51.59	50.76
	40	38.26	41.07	43.90	42.78
	50	31.00	33.88	36.63	35.66
	60	24.92	27.74	30.48	29.50
	70	19.95	22.61	25.24	24.31
1.5	10	67.93	69.92	71.71	71.19
	20	61.29	63.85	66.28	65.46
	30	54.56	57.64	60.58	59.60
	40	48.02	51.53	54.91	53.77
	50	41.87	45.68	49.39	48.15
	60	36.25	40.24	44.18	42.85
	70	31.21	35.27	39.33	37.95
2.0	10	69.19	71.58	73.91	73.16
	20	64.10	67.05	69.93	69.00
	30	58.89	62.40	65.80	64.70
	40	53.68	57.70	61.61	60.34
	50	48.60	53.05	57.40	55.99
	60	43.77	48.55	53.27	51.73
	70	39.21	44.24	49.26	47.62

The dilution effect of a larger volume is evident, especially for low quanta emissions whose relative reduction exceeds 65%. Moreover, increasing the ventilation rate, the differences become more pronounced, even in the case of higher quanta generation rates reaching almost 50%. Despite the positive decrease of risk, infection probabilities shown in Table 4.29 are still unacceptable to get a safe environment, so, wearing masks always remains the best choice.

Like the first case-study, the zonal infection risk trend over exposure time can be represented through the characteristic risk graphs. Figure 4.20, Figure 4.21, and Figure 4.22 illustrate the infection risk exponential curves concerning the same situation of Table 4.29. Comparing these figures with the corresponding situation represented by Figure 4.5, Figure 4.6, and Figure 4.7, the risk reduction can be easily detected. The figures clearly show the effect of dilution on infection probability, and the use of masks can further lower those risk curves.

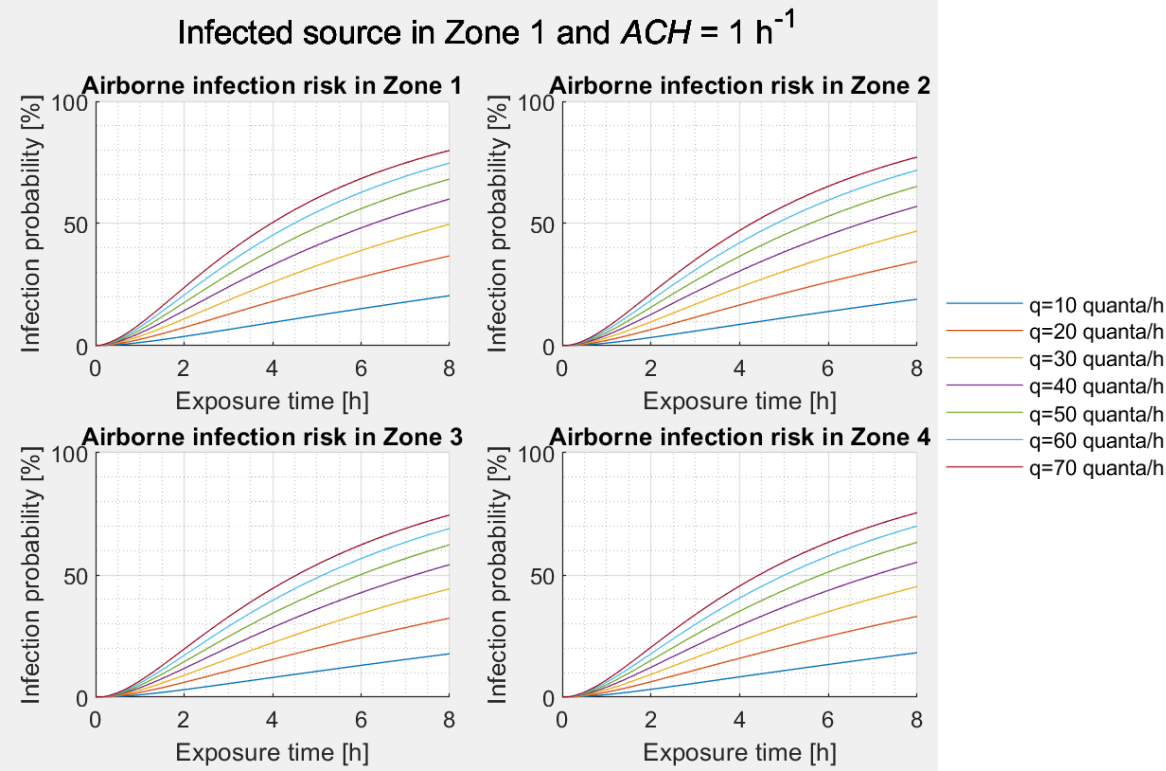

Figure 4.20 Infected source in Zone 1 and *ACH*=1 h^{-1} (no masks): zonal infection risk trends (open space office).

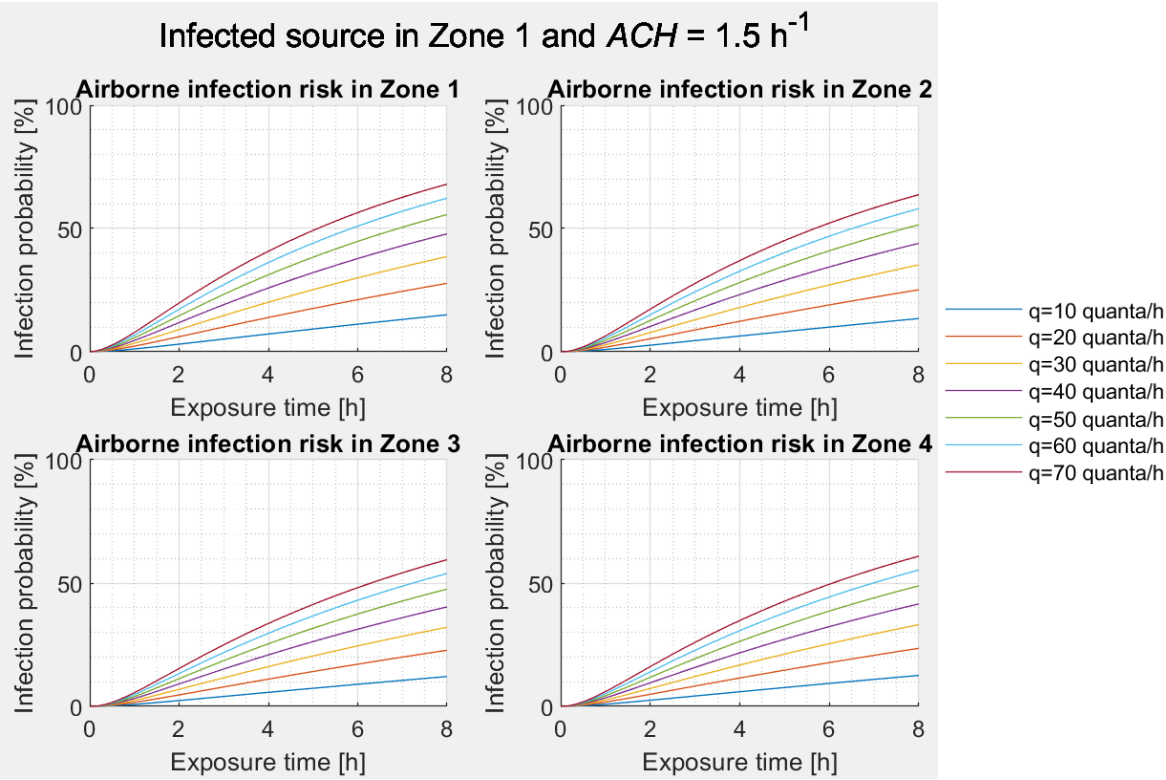

Figure 4.21 Infected source in Zone 1 and *ACH*=1.5 h^{-1} (no masks): zonal infection risk trends (open space office).

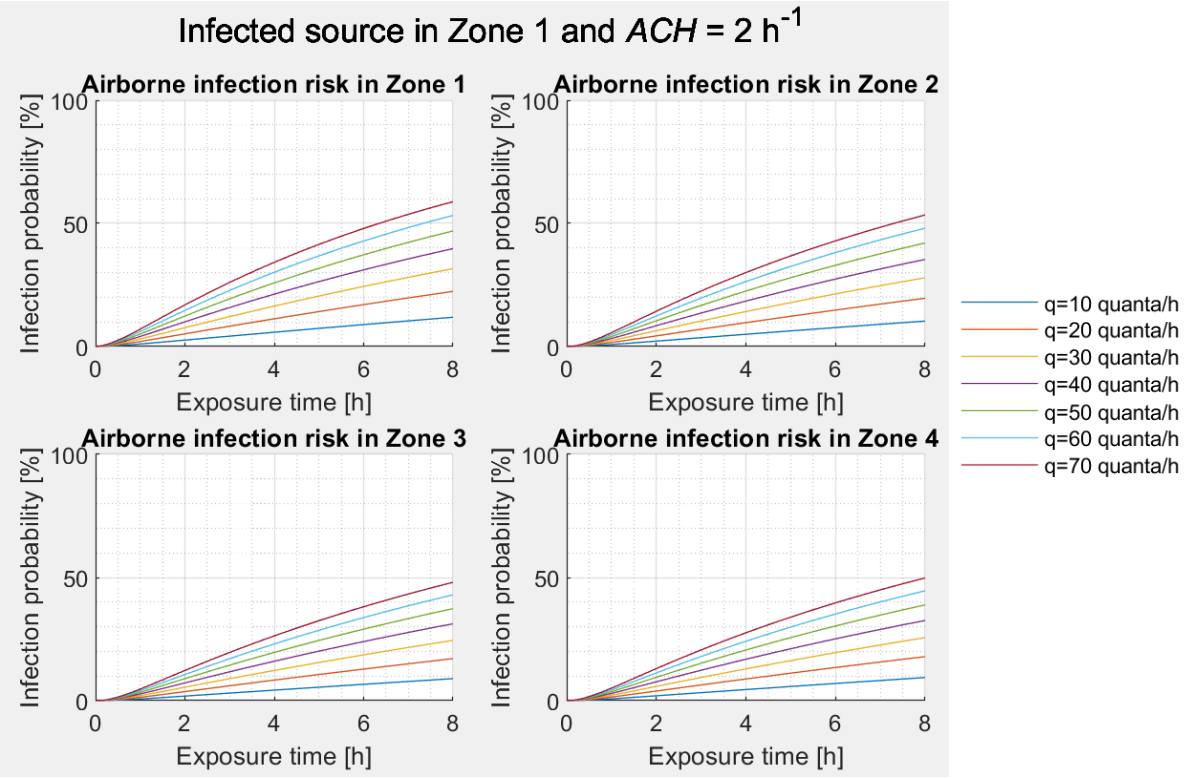

Figure 4.22 Infected source in Zone 1 and *ACH*=2 h^{-1} (no masks): zonal infection risk trends (open space office).

In this chapter the model results have been shown for two case-studies, namely a typical office room and an open space office with a fourfold volume compared to the former. The capacity of the zonal model to define the indoor air motion field has been tested, as well as how the infection risk is affected by specific parameters, such as *ACH*, use of masks, room volume, and relative position between individuals and ventilation terminals. The main conclusions coming from the model implementation can be briefly summarized:

- the four-cell discretization grid determines a motion field with high interzonal airflows, which define a remarkable recirculation rate within the space.
- the obtained infection risk is almost uniform within the entire space, so, the relative position between individuals does not seem so important.
- the position of infected source in relation to air diffuser slightly influences the overall homogeneity of infection risk.
- increasing *ACH* proves to be the first mitigation strategy, as it causes risk reductions up to 40% in the smaller room, and even higher in the larger one.
- wearing masks has an outstanding importance in decreasing risk, and a great improvement is observed moving from surgical masks to FFP2 respirators.
- combination of FFP2 with 2.0 h^{-1} is the best control measure among those considered, and it involves risk reduction of about 92÷97 % in the first case-study.
- model resolution under steady-state conditions significantly overestimates the risk.
- a fourfold volume involves higher dilution of quanta and lowers risk up to 74%.

Conclusions and future developments

In this thesis work, the problem of pandemic caused by SARS-CoV-2-19 has been briefly illustrated and the importance of mitigating the airborne infection risk of the disease has been highlighted. Based on the peculiarities of this transmission route, a zonal risk model has been developed and implemented to evaluate the infection probability for a susceptible person sharing an enclosed space with an asymptomatic infected source. This model consists of a subdivision of the considered domain into perfectly mixed cells, in order to define interzonal air movements and successive spread of infectious material.

In this analysis, a four-zone discretization grid has been chosen to observe risk trend for two case-studies: a typical single office room with dimensions of 4.0x4.0x2.7 m and an open space office with dimensions of 8.0x8.0x2.7 m. For both situations, the outdoor air is supplied and distributed by means of a mixing ventilation system. The objective of the simulations is evaluating the relevance of relative position between susceptible subjects and infected source on risk level and how specific parameters such as ventilation flowrate, room volume, and use of face masks could affect the infection probability.

The following results emerge from the model implementations:

- the adopted partitioning grid basically defines a well-mixed environment, as the room is characterized by high interzonal flowrates. These flows create a significant recirculation of airborne pathogens, so, the final infection risk is almost uniform within the space. For both case-studies, the interzonal volumetric flowrates are larger than ventilation flowrates by about an order of magnitude.
- in the case of the smaller office room, the relative position between susceptible and infected source has a limited effect, given the uniformity in infection risk level. This outcome is reasonable considering that for a such small volume, the indoor environment easily achieved a perfect mixing.
- for the open space office, interestingly, the zonal approach seems to be more effective, since higher deviations between zonal infection probabilities can be observed compared to the first case.
- increasing the air exchange rate (*ACH*) promote dilution and subsequent removal of pathogens, proving to be an effective mitigation strategy against airborne transmission. Considering low quanta emission rates (10÷20 quanta/h), typical of office tasks, a reduction up to almost 50% can be achieved going from 1 to 2 h^{-1}, for both case-studies.
- with the infected source close to the air diffusers, released pathogens homogeneously spread across the whole volume, leading to uniform risk. This aspect highlights that ventilation systems have certainly a role in dispersing the infectious material, but this

negative effect is irrelevant compared to the risk reduction obtained through higher ventilation rates.

- wearing masks is strongly recommended: surgical masks guarantee a risk percentage reduction up to 65% for low quanta emissions and ACH=2 h^{-1}; FFP2 are even better, with a risk decrease up to 95% for low quanta generation rates and ACH=2 h^{-1}.
- among those simulated situations, a risk reduction by 92÷97 % is obtained coupling high ventilation rates with the use of FFP2. This combination proves to be the best mitigation strategy among those analysed.
- larger volume implies higher dilution of the infectious material, lowering the overall infection probability. In the open space office, the risk level is lower than that in the smaller room by about 70% in the case of low quanta emissions and ACH=2 h^{-1}.
- calculating the infection risk under steady-state conditions leads to an overestimation of its value, especially in the initial exposure hours.

Considering the whole previous presentation, it clearly emerges that the developed model constitutes a starting point for future more complete risk assessment for different real situations. It still presents some limitations and critical issues arising from simplifications and assumptions adopted for its definition, and future improvements are necessary to guarantee more reliable, consistent results.

Regarding the weak points of the model, the main ones are summarized hereinafter:

- the analysis has been carried out considering isothermal jets for the supply air. The buoyancy effect driven by non-isothermal jets entering the room during heating or cooling season has not been investigated. Since the primary objective is evaluating the importance of ventilation rate on infection risk extent, this choice is justified. However, for future works, especially in the case of all-air conditioning system, the influence of non-isothermal jets providing heating or cooling to the room should be examined.
- the ACH range for the model simulations (from 1 to 2 h^{-1}) is limited, as higher ventilation flowrates could be reached through an all-air system. Anyway, as this work constitutes a first phase of assessment on the correct operation of the model, the adopted values are reasonable.
- contrary to FFP2, the properties of surgical masks are not standard values, because there are not specific standard experimental tests to quantify filtration efficiency for inhalation phase (X_{int}) and leakage factor (Y). In the future, standards should be revised to provide these data.
- concerning the zonal modelling, four cells are too few to give a suitable spatial resolution in defining the air movements within the room. A denser discretization mesh should be employed to investigate the imperfect mixing of the indoor space.
- some elements such as thermal plumes from internal heat sources, air jets from diffusers and boundary layer caused by the drag force at the wall surfaces, were not modelled in the simulations.

- human subjects have been considered only as potential quanta emitters, but not as heat sources.
- solar radiation and radiative heat transfer from internal devices and surfaces have been neglected.
- windows and doors are not considered in the zonal model both in mass balance (i.e., no air infiltrations from the outdoors or adjacent spaces) and energy balance (i.e., no solar radiation and no convection and conduction trough glasses and frames).

The model needs to be improved trying to adjust the critical points listed above. Besides that, future developments and application of this zonal risk model can be planned as below:

- along with increasing the number of cells of the spatial grid, the thermal stratification must be investigated to detect air recirculation along walls and corresponding ascending and descending airflows.
- a validation for the zonal model could be provided and it can be achieved through CFD modelling or experimental studies. This will make the model reliable, consistent and will broaden its feasibility.
- once the model has been improved, the final objective is applying it to a real situation concerning larger indoor spaces than those examined here, e.g., fair stands, academic classrooms, meeting rooms, atria, and so on. This is the real purpose of the model, since it would provide a risk assessment for these wide domains employing less time and less computational efforts than a CFD analysis.

Nomenclature

SYMBOL	MEANING	U.M.
A	surface area	[m^2]
ACH	air change per hours	[h^{-1}]
C	quanta concentration	[quanta/m^3]
$\bar{C}$	average quanta concentration	[quanta/m^3]
C_0	initial quanta concentration	[quanta/m^3]
C_a	volumetric fraction of the exhaled CO_2	[ppm]
C_{co_2}	volumetric fraction of CO_2	[ppm]
$c_{p,air}$	specific heat of air	[J/(kg K)]
D	intake dose	[number of pathogens]
$dose$	intake dose of quanta	[quanta]
E	energy	[J]
F	rebreathed fraction	[-]
$\bar{f}$	averaged rebreathed fraction	[-]
f_{mask}	corrective factor for masks	[%] or [-]
G	gravitational acceleration	[m/s^2]
H	zone height	[m]
h	room height	[m]
I	number of infected people	[-]
ID_{50}	50% infectious dose	[number of pathogens]
IF	intake fraction	[-]
k	flow coefficient	[m/(s Pa^n)]
L	zone width	[m]
l	room length	[m]
M	mass	[kg]
$\dot{m}$	mass flowrate	[kg/s] or [kg/h]
MM_{air}	molar mass of air	[kg/kmol]
N	total number of people	[-]
N_{br}	breathing frequency	[breaths/s]
n	flow exponent	[-]
n_{zon}	number of zones	[-]
NC	number of new infection cases	[-]
P	static pressure	[Pa]
ΔP	pressure difference	[Pa]
P_I	probability of infection	[%] or [-]
p	breathing flowrate	[m^3/h]

SYMBOL	MEANING	U.M.
p'	reduced breathing rate due to mask	[m^3/h]
pdf	probability density function	[-]
Q	ventilation rate	[m^3/s] or [m^3/h]
Q_0	exhaust airflow rate	[m^3/s] or [m^3/h]
q	quanta generation rate	[quanta/h]
q'	reduced quanta emission rate due to mask	[quanta/h]
q_h	heat flux	[W]
R	ideal gas constant	[J/(kmol K)]
R_{air}	gas constant for air	[J/(kg K)]
R_{A0}	reproductive number	[-]
R_{th}	thermal resistance	[(m^2 K)/W]
r	Infectivity fitting parameter (exponential dose-response model)	[-]
RH	relative humidity	[%]
S	number of susceptible people	[-]
T	temperature	[K] or [°C]
t	time	[s] or [h]
Δt	time interval	[s] or [h]
t_{exp}	exposure time	[s] or [h]
U	thermal transmittance	[W/(m^2 K)]
V	volume	[m^3]
V_{br}	tidal volume	[m^3] or [cm^3]
V_e	equivalent volume of expired air in a room	[m^3]
w	room width	[m]
X	filtration efficiency of mask	[%]
Y	leakage factor of mask	[%]
y	mass fraction	[-]
Z	global efficiency of mask	[%]
Z_n	neutral plane height	[m]
z	coordinate for zone height	[m]

VECTORS AND MATRIXEX

SYMBOL	MEANING	U.M. of elements
A	matrix of volumetric flowrates	[m^3/h]
b	column vector of known terms	[quanta/h]
C	column vector of quanta concentrations	[quanta/m^3]
F	vector of functions (nonlinear system)	-
x	vector of unknown variables	-

GREEK SYMBOLS

SYMBOL	MEANING	U.M. of elements
α	fitting parameter (Beta-Poisson dose-response model)	[-]
β	fitting parameter (Beta-Poisson dose-response model)	[-]
η	efficiency (filters and UV lamps)	[%] or [-]
λ	quanta removal rate	[h^{-1}]
ρ	air density	[kg/m^3]
$\Delta\rho$	density difference	[kg/m^3]
ϕ	aerodynamic diameter of droplets	[μm] or [m]

Subscripts

SUBSCRIPT	MEANING
0	initial value
air, ext	external/outdoor air
CO_2	carbon dioxide CO_2
dep	deposition
es	external surface (for liminar resistance)
exh	exhaled
ext	mask efficiency towards external side (exhalation)
filt	filtration
G-N	Gammaitoni-Nucci
horiz	horizontal
i	i-th zone
in	supply air
ind	indoor environment
inh	inhaled
int	mask efficiency towards internal side (inhalation)
is	internal surface (for liminar resistance)
j	j-th zone
jet	jet
k	k-th zone or k-th time interval
out	exhaust air
outd	outdoor environment
R-M	Rudnick-Milton
ref	reference

SUBSCRIPT	MEANING
rem	removed
ss	steady state
sup	supplied
transm	heat dissipation by transmission
ts	transient state
UV	UV
vent	ventilation
vert	vertical
viab	viability loss
W-R	Wells-Riley
wall	wall (thermal resistance)
$0\text{-}Z_n$	from 0 to Z_n
$Z_n\text{-}H$	from Z_n to H
z	height coordinate

References

[1] L. Morawska and J. Cao, “Airborne transmission of SARS-CoV-2: The world should face the reality,” *Environ. Int.*, vol. 139, no. April, p. 105730, 2020, doi: 10.1016/j.envint.2020.105730.

[2] L. Morawska *et al.*, “How can airborne transmission of COVID-19 indoors be minimised?,” *Environ. Int.*, vol. 142, no. April, 2020, doi: 10.1016/j.envint.2020.105832.

[3] A. A. Aliabadi, S. N. Rogak, K. H. Bartlett, and S. I. Green, “Preventing Airborne Disease Transmission: Review of Methods for Ventilation Design in Health Care Facilities,” *Adv. Prev. Med.*, vol. 2011, pp. 1–21, 2011, doi: 10.4061/2011/124064.

[4] E. Y. C. Shiu, N. H. L. Leung, and B. J. Cowling, “Controversy around airborne versus droplet transmission of respiratory viruses: implication for infection prevention,” *Curr. Opin. Infect. Dis.*, vol. 32, no. 4, pp. 372–379, 2019, doi: 10.1097/QCO.0000000000000563.

[5] J. W. Tang, “Investigating the airborne transmission pathway - different approaches with the same objectives,” *Indoor Air*, vol. 25, no. 2, pp. 119–124, 2015, doi: 10.1111/ina.12175.

[6] AiCARR, “Gli impianti e la diffusione del SARS-CoV-2-19 nei luoghi di lavoro,” 2020. http://www.aicarr.org/Documents/Normativa/COVID19/200313_AICARR_SARSCOV2_19.pdf (accessed Jan. 20, 2021).

[7] Z. T. Ai and A. K. Melikov, “Airborne spread of expiratory droplet nuclei between the occupants of indoor environments: A review,” *Indoor Air*, vol. 28, no. 4, pp. 500–524, 2018, doi: 10.1111/ina.12465.

[8] J. Wei and Y. Li, “Airborne spread of infectious agents in the indoor environment,” *Am. J. Infect. Control*, vol. 44, no. 9, pp. S102–S108, 2016, doi: 10.1016/j.ajic.2016.06.003.

[9] ASHRAE, “ASHRAE Position Document on Infectious Aerosols,” 2020. https://www.ashrae.org/file library/about/position documents/pd_infectiousaerosols_2020.pdf (accessed Jan. 20, 2021).

[10] S. Herfst *et al.*, “Drivers of airborne human-to-human pathogen transmission,” *Curr. Opin. Virol.*, vol. 22, pp. 22–29, 2017, doi: 10.1016/j.coviro.2016.11.006.

[11] I. Eames, J. W. Tang, Y. Li, and P. Wilson, “Airborne transmission of disease in hospitals,” *J. R. Soc. Interface*, vol. 6, no. SUPPL. 6, pp. S697–S702, 2009, doi: 10.1098/rsif.2009.0407.focus.

[12] W. H. Seto, “Airborne transmission and precautions: Facts and myths,” *J. Hosp. Infect.*, vol. 89, no. 4, pp. 225–228, 2015, doi: 10.1016/j.jhin.2014.11.005.

[13] X. Xie, Y. Li, A. T. Y. Chwang, P. L. Ho, and W. H. Seto, “How far droplets can move in indoor environments - revisiting the Wells evaporation-falling curve,” *Indoor Air*, vol. 17, no. 3, pp. 211–225, 2007, doi: 10.1111/j.1600-0668.2007.00469.x.

[14] A. Nalca and D. K. Nichols, “Rabbitpox: A model of airborne transmission of smallpox,” *J. Gen. Virol.*, vol. 92, no. 1, pp. 31–35, 2011, doi: 10.1099/vir.0.026237-0.

[15] Jonix S.r.l, “JONIX duct Non Thermal Plasma Technology. Dispositivi per la sanitizzazione e decontaminazione delle condotte aerauliche.” https://jonixair.com/pdf/prodotti/duct/jonix_brochure_duct_it.pdf (accessed Feb. 08, 2021).

[16] Jonix S.r.l, “JONIX duct: Modulo ionizzante canalizzabile. Manuale d’uso,” 2016. https://jonixair.com/pdf/prodotti/duct/jonix_manuale_uso_e_manutenzione_duct.pdf.
[17] AiCARR, “Protocollo per la riduzione del rischio da diffusione del del SARS-CoV2-19 mediante gli impianti di climatizzazione e ventilazione esistenti,” 2020. http://www.aicarr.org/Documents/Normativa/COVID19/200318_SCHEMA_GESTIONE_HVAC_SARSCoV219_DEF.pdf (accessed Jan. 20, 2021).
[18] AiCARR, “Posizione di AiCARR sul funzionamento degli impianti di climatizzazione durante l’emergenza SARS-CoV-2-19,” 2020. http://www.aicarr.org/Documents/Normativa/COVID19/200406_PP_AICARR_COVID-19.pdf (accessed Jan. 20, 2021).
[19] AiCARR, “Prontuario sul ruolo degli impianti di climatizzazione invernale ed estiva nella riduzione della diffusione della COVID-19,” 2020. http://www.aicarr.org/Documents/Normativa/COVID19/200411_Prontuario AiCARR_ Ruolo_impianti_HVAC.pdf (accessed Jan. 20, 2021).
[20] L. Mazzarella, “Coronavirus e climatizzazione Quando , come e perché accendere l ’ aria condizionata Sommario,” 2020. http://www.aicarr.org/Documents/Normativa/COVID19/200615_CLIMATIZZAZIONE_COVID.pdf (accessed Jan. 20, 2021).
[21] AiCARR, “Protocollo per la riduzione del rischio da diffusione del SARS-CoV-2 nelle operazioni di gestione e manutenzione degli impianti di climatizzazione e ventilazione esistenti,” 2020. http://www.aicarr.org/Documents/Normativa/COVID19/200727_PROTOCOLLO MANUTENZIONE_COVID-19.pdf (accessed Jan. 20, 2021).
[22] L. D. Knibbs and P. D. Sly, “Airborne transmission of viral respiratory pathogens don’t stand so close to me?,” *Am. J. Respir. Crit. Care Med.*, vol. 194, no. 3, pp. 253–254, 2016, doi: 10.1164/rccm.201602-0432ED.
[23] G. Buonanno, L. Morawska, and L. Stabile, “Quantitative assessment of the risk of airborne transmission of SARS-CoV-2 infection: Prospective and retrospective applications,” *Environ. Int.*, vol. 145, no. September, p. 106112, 2020, doi: 10.1016/j.envint.2020.106112.
[24] S. L. Miller *et al.*, “Transmission of SARS-CoV-2 by inhalation of respiratory aerosol in the Skagit Valley Chorale superspreading event,” *Indoor Air*, no. September, pp. 1–10, 2020, doi: 10.1111/ina.12751.
[25] G. N. Sze To and C. Y. H. Chao, “Review and comparison between the Wells-Riley and dose-response approaches to risk assessment of infectious respiratory diseases,” *Indoor Air*, vol. 20, no. 1, pp. 2–16, 2010, doi: 10.1111/j.1600-0668.2009.00621.x.
[26] E. A. Nardell, “Wells Revisited: Infectious Particles vs. Quanta of Mycobacterium tuberculosis Infection–Don’t Get Them Confused,” *Mycobact. Dis.*, vol. 06, no. 05, pp. 5–7, 2016, doi: 10.4172/2161-1068.1000231.
[27] L. Gammaitoni and M. C. Nucci, “Using a Mathematical Model to Evaluate the Efficacy of TB Control Measures,” *Emerg. Infect. Dis.*, vol. 3, no. 3, pp. 335–342, 1997, doi: 10.3201/eid0303.970310.
[28] S. N. Rudnick and D. K. Milton, “Risk of indoor airborne infection transmission estimated from carbon dioxide concentration,” *Indoor Air*, vol. 13, no. 3, pp. 237–245, 2003, doi: 10.1034/j.1600-0668.2003.00189.x.
[29] G. Buonanno, L. Stabile, and L. Morawska, “Estimation of airborne viral emission: Quanta emission rate of SARS-CoV-2 for infection risk assessment,” *Environ. Int.*, vol. 141, no. May, p. 105794, 2020, doi: 10.1016/j.envint.2020.105794.

[30] A. Mikszewski, G. Buonanno, L. Stabile, and A. Pacitto, “Airborne Infection Risk Calculator User’s Manual Version 2.1 October 2020,” 2020. https://research.qut.edu.au/ilaqh/wp-content/uploads/sites/174/2020/10/AIRC-v2.1-Users-Manual.pdf (accessed Mar. 04, 2021).
[31] L. D. Knibbs, L. Morawska, S. C. Bell, and P. Grzybowski, “Room ventilation and the risk of airborne infection transmission in 3 health care settings within a large teaching hospital,” *Am. J. Infect. Control*, vol. 39, no. 10, pp. 866–872, 2011, doi: 10.1016/j.ajic.2011.02.014.
[32] G. Cammarata, “Probabilità di contagio a grande distanza per via aerea da SARS-CoV-2 nelle scuole italiane,” *AiCARR J.*, vol. 63, no. 4, pp. 37–49, 2020, doi: 10.36164/AiCARRJ.63.04.02.
[33] J. M. Villafruela, I. Olmedo, F. A. Berlanga, and M. Ruiz de Adana, “Assessment of displacement ventilation systems in airborne infection risk in hospital rooms,” *PLoS One*, vol. 14, no. 1, pp. 1–18, 2019, doi: 10.1371/journal.pone.0211390.
[34] S. Zhu, J. Srebric, J. D. Spengler, and P. Demokritou, “An advanced numerical model for the assessment of airborne transmission of influenza in bus microenvironments,” *Build. Environ.*, vol. 47, no. 1, pp. 67–75, 2012, doi: 10.1016/j.buildenv.2011.05.003.
[35] E. A. Hathway, C. J. Noakes, P. A. Sleigh, and L. A. Fletcher, “CFD simulation of airborne pathogen transport due to human activities,” *Build. Environ.*, vol. 46, no. 12, pp. 2500–2511, 2011, doi: 10.1016/j.buildenv.2011.06.001.
[36] A. Cavallini, F. Busato, and F. Pregliasco, “Remarks on the air recirculation in HVAC systems during the SARS-CoV-2 outbreak : the case of all-air ducted plants,” *AiCARR J.*, vol. 63, no. 4, pp. 50–55, 2020, doi: 10.36164/AiCARRJ.63.04.03.
[37] C. J. Noakes and P. Andrew Sleigh, “Mathematical models for assessing the role of airflow on the risk of airborne infection in hospital wards,” *J. R. Soc. Interface*, vol. 6, no. SUPPL. 6, 2009, doi: 10.1098/rsif.2009.0305.focus.
[38] Y. Lu, J. Dong, and J. Liu, “Zonal modelling for thermal and energy performance of large space buildings: A review,” *Renew. Sustain. Energy Rev.*, vol. 133, no. 73, p. 110241, 2020, doi: 10.1016/j.rser.2020.110241.
[39] F. Haghighat, Y. Li, and A. C. Megri, “Development and validation of a zonal model - POMA,” *Build. Environ.*, vol. 36, no. 9, pp. 1039–1047, 2001, doi: 10.1016/S0360-1323(00)00073-1.
[40] Y. Lin, “POMA - A Zonal Model for Airflow and Temperature Distribution Analysis,” Concordia University Montreal, Quebec, Canada, 1999.
[41] Ente Nazionale Italiano di Unificazione UNI, *UNI EN 14683:2019, Maschere facciali ad uso medico - Requisiti e metodi di prova*, CEN, Brussels, Belgium, 2009.
[42] A. V. Mueller, M. J. Eden, J. M. Oakes, C. Bellini, and L. A. Fernandez, “Quantitative Method for Comparative Assessment of Particle Removal Efficiency of Fabric Masks as Alternatives to Standard Surgical Masks for PPE,” *Matter*, vol. 3, no. 3, pp. 950–962, 2020, doi: 10.1016/j.matt.2020.07.006.
[43] Ente Nazionale Italiano di Unificazione UNI, *UNI EN 149:2009, Dispositivi di protezione delle vie respiratorie. Semimaschere filtranti antipolvere. Requisiti, prove, marcatura*, CEN, Brussels, Belgium, 2009.

Acknowledgments

I would like to express my gratitude to my supervisors, Prof. M. De Carli and Prof. A. Zarrella, for their helpfulness during the entire development of this theses work. Their support has been relevant for the most crucial phases of the research.

Special thanks go to the PhD student Marco for his guidance during the work and for being an important reference figure for both the writing and the modelling part. Our continuous interaction allowed me to understand complexity and methods of the research field. His suggestions contributed to my overall personal growth.

My deepest appreciation to my whole family for the encouragements it give me during these six months. Special thanks to my mother and my father for the economic support they provided and because they always believe in me. Thanks to my sisters and my brother, who make my days livelier and show everyday their esteem towards me.

Finally, but not least, thanks to all my friends. To those I knew during my academic studies because I shared unforgettable moments with them. To those of my party for the recreation time we spent together in this satisfactory, but stressful, period.

Padua, April 2021 **Giacomo Tognon**